Fall 2019

Salt Marsh Health and Biomass Responses to a Changing Environment

Gwen Joelle Miller

SALT MARSH HEALTH AND BIOMASS RESPONSES TO A CHANGING ENVIRONMENT

by

Gwen Joelle Miller

Bachelor of Science
University of California Davis, 2010

Master of Science
California State University Monterey Bay, 2014

Submitted in Partial Fulfillment of the Requirements

For the Degree of Doctor of Philosophy in

Marine Science

College of Arts and Sciences

University of South Carolina

2019

Accepted by:

James T. Morris, Major Professor

Susan Lang, Committee Member

Jean Ellis, Committee Member

Cuizhen Wang, Committee Member

Cheryl L. Addy, Vice Provost and Dean of the Graduate School

DEDICATION

I dedicate this to my amazing grandfather, David Woodin, from whom I get a large portion of my personality and I will forever miss. And to my niece Frances Weber-Miller who holds the future.

.

ACKNOWLEDGEMENTS

I would like to thank my family for their continued support and encouragement. My grandma Terry Woodin, for always helping me and being marvelous. My sisters Morgan and Nickole for being my best friends. My parents for getting me interested in the environment at a young age. Paul Béguelin for helping me destress and maintain my sanity. Thanks to Rohan Dhall for always making me laugh. And all my cycling friends, for helping me take science breaks.

None of this work could have been done without the help of my advisor Jim Morris. He has taken me to gorgeous marshes, and we have had countless hours of fun doing fieldwork in the steamy pluff mud. I am also extremely grateful for Karen Sundberg and Warren Hankinson who helped me tremendously throughout my time at UofSC and for their friendship. I am grateful for the help with lab work from Dr. Susan Lang and Bryan Benitez-Nelson, and the help with remote sensing work from Cuizhen Wang. I am also grateful for the help from Jean Ellis, for her advice, edits, and donation of time. I loved the opportunities provided to me by both the Baruch Institute/North Inlet Winyah Bay NERR and Plum Island Ecosystems-LTER, these are amazing places to conduct research and are breathtakingly gorgeous.

I would like to thank Earl Davey, Cathy Wigand and Troy Hill for teaching me how to use computed tomography to analyze belowground biomass. I am also extremely thankful for Dr. Shane Boylan and Albert Georgia for letting me use the CT scanner at the Charleston aquarium. Dr. Boylan spent several days of his valuable time to help me run mud through the CT scanner.

This work was supported by various grants including; the National Science Foundation Division of Environmental Biology under grant number 1052636, the South Carolina Sea Grant Consortium/NOAA grant number 13540-FB33, Carolinas Integrated Sciences & Assessments (CISA) program, National Oceanic and Atmospheric Administration (NOAA) Climate Program Office, NOAA Award # NA11OAR4310148, Slocum-Lunz foundation grant, SPARC Graduate Research Grant, John Vernberg Bicentennial Fellowship in Marine Science, and the School of the Earth Ocean and Environment Travel Grant.

ABSTRACT

Coastal salt marshes are important ecosystems not only for their aesthetic beauty but also for their ecosystem services that they provide including improving water quality, providing protection from storm surges and hurricanes, and carbon sequestration. With climate change, including drought, warmer temperatures and sea-level rise, these systems are going to be impacted. Understanding how salt marshes will respond, or already have responded, to climate change will help us be better prepared for the future. By scripting a model to project how marshes may migrate with sea-level rise, I discover that salt marshes within Beaufort and Jasper counties, South Carolina will largely keep pace with sea-level rise. However, there are portions of the marsh area within these counties that will likely drown and development will impede areas of projected marsh migration.

Additionally, I explored how above and belowground biomass changes with elevation above sea level, which are important relationships for modeling efforts. Using high-resolution satellite data, I mapped aboveground biomass across the entire marsh. Pairing this with elevation data, I created a growth curve of biomass versus elevation. The established growth curve is particularly useful as an input for biogeomorphic models of marsh development. Through computed tomography analysis, I analyzed belowground biomass. I found that belowground biomass is also a function of elevation, but there can be significant inter-site

variability regardless of elevation. Looking at fall/spring variability, biomass abundance does not largely change, which indicates that belowground biomass is more likely longer lived.

In the last part of this dissertation I looked at a past marsh dieback event to better understand drivers that lead to decline in marsh health. Using Landsat data, I created a map of change in salt marsh health by using differences in Normalized Difference Vegetation Indices. It is likely that the vegetation within higher elevations experienced stress due to hypersalinity, while vegetation within the lower marsh experienced stress from hypoxia leading to increased rates of vegetation decline in these zones. Overall this dissertation improves our understanding of drivers of marsh health and increases awareness of how salt marshes may respond under a changing climate.

TABLE OF CONTENTS

LIST OF TABLES

LIST OF FIGURES

CHAPTER 1

INTRODUCTION

Coastal salt marshes are important ecosystems not only for their aesthetic beauty but also for their ecosystem services that they provide including improving water quality, providing protection from storm surges and hurricanes, and carbon sequestration (Fisher and Acreman, 2004; Möller et al., 2014; Mulholland et al., 2009; Whiting and Chanton, 2001). The southeastern United States contains the majority of coastal wetlands within the continental United States, and states such as South Carolina rely on the aesthetic beauty of coastal wetlands to draw crowds of tourists for economic revenue (Faulkenberry et al., 2000; Osland et al., 2016). However, marshes are not immune to the effects of climate change. Drought conditions and warm temperatures influence biomass production and if sea level rises quicker than a marsh can build elevation, the wetland will be lost (Kirwan et al., 2012; Miller et al., 2017; Morris et al., 2002).

The Marsh Equilibrium Model (MEM) predicts how salt marshes may respond to projected sea-level rise (Morris et al., 2002). MEM relies on the idea that marshes either increase or decrease biomass production in relation to changes in sea-level. The combination of biomass and inundation time influences the settling of suspended inorganic sediment which in turn influences changes in marsh

elevation (Morris et al., 2002). In theory marshes can migrate upland, but due to development, this may not always be possible. In addition, climate change will bring more frequent occurrences of drought and warmer temperatures, which will likely have further impacts within salt marshes (Karl et al., 2009; Miller et al., 2017). The effects of drought are compounded by warmer temperatures since higher temperatures result in higher rates of evapotranspiration. The accumulation of salts and reduced rainfall results in stressful conditions for plant growth, which can negatively impact growing conditions (McKee et al., 2004; Miller et al., 2017).

This dissertation furthers the understanding of how climate change will influence coastal marshes within South Carolina, by looking into the future, present, and past. Chapter 2 increases modelling capabilities within marshes by developing an improved landscape scale Marsh Equilibrium Model. Within this chapter I apply MEM to Jasper and Beaufort Counties, which are tourist destination impart due to the beauty of their expanse marshes (Faulkenberry et al., 2000; Osland et al., 2016). Chapter 3, moves to improve our understanding of aboveground biomass across a marsh. In this chapter I use a newer satellite system, PlanetScope, to estimate aboveground biomass within an entire marsh. I then am able to observe how aboveground biomass changes throughout the marsh, and its dependency on elevation. Chapter 3 also explains how the relationship between elevation and aboveground biomass can be established. Belowground biomass is another parameter for MEM and is less understood due to its decreased visibility. Chapter 4 explores the role elevation, fertilizer application, and location plays in

belowground biomass production. By utilizing Computed Tomography, root and rhizome structure is maintained, and can be quantified. Chapter 5 looks at past events, which can better inform us about the future. In this chapter I utilize satellite data to look at a marsh dieback event, and compare how marsh health fluctuates throughout the system. By using aboveground biomass production as a proxy for marsh health, I am able to look as climate data, and elevation data to help explain a noted marsh dieback event. Together these chapters increase our ability to understand how climate change will impact survival of coastal marshes.

CHAPTER 2

MODELING ELEVATION CHANGE IN RELATION TO SEA-LEVEL RISE WITHIN BEAUFORT AND JASPER COUNTY SOUTH CAROLINA SALT MARSHES

Introduction

The Carolinas are home to the largest extent of salt marshes along the eastern seaboard. To survive sea-level rise, these marshes must either migrate inland or increase their elevation through biomass and sediment accumulation (Nyman et al., 2006; Redfield, 1972). Beaufort and Jasper counties are of particular interest to stakeholders such as the South Carolina Nature Conservancy. One of the goals of this study is to provide the South Carolina Nature Conservancy valuable insight on how these marshes are projected to change in relation to sea-level rise. I postulate that overall, within the study area, there will be a negative trend of total upland and marsh areas while water and mudflat areas will exhibit an increasing trend.

The Marsh Equilibrium Model (MEM) is a hybrid analytical numerical model which predicts how salt marshes may respond to projected sea-level rise (Morris et al., 2002). MEM relies on the idea that: 1. marshes either increase or decrease biomass production in relation to changes in sea-level, 2. a combination of biomass and inundation time influences the settling of suspended inorganic sediment and 3. these two factors influence changes in marsh elevation (Morris et al., 2002). MEM takes into account variables such as plant biomass, suspendered sediment, elevation, and tidal constituents. It can provide a more robust model of marsh migration than the "bathtub" modeling approach (Hinkel et al., 2014). A “bathtub” modelling approach considers mainly elevation effects and pays little or no attention to such factors as environmental feedback. The current version of

a landscape-scale based MEM (MEM 3-D) uses ArcPy for modelling purposes, which requires the user to also purchase ArcGIS (Edwards, 2016). ArcPy provides an easy to use interface; but, due to file size limitations and its slowness, it is impractical to use MEM 3-D for modelling large marsh areas distributed across counties. For example, the wetland area used by Edwards was relatively small and had an input file of 58 megabytes while the Jasper and Beaufort County input file exceeds 1.58 gigabytes. Therefore, another goal of this study is to explore the possibility of transcribing the MEM 3-D code into a Python script so it could be used to model the movements of large areas of salt marsh and then applying this strategy as a tool for modelling the behavior of the Jasper and Beaufort counties salt marshes.

Methods

Study Area

The study area includes salt marshes within Beaufort and Jasper counties (Figure 2.1). This wetland area is within the Port Royal Sound Watershed and was selected based on interest from the South Carolina Nature Conservancy. The Port Royal Sound Watershed is valued both economically and environmentally. The region is frequented by tourism bringing outside revenue to the region. The region also has experienced impacts from sea-level rise, tropical storm systems, and winter storms making it even more vital to maintain or restore wetland health.

Marsh Equilibrium Model

The main components of MEM include elevation, tidal range, and plant biomass. For elevation data, I obtained a 2013 bare earth Lidar digital elevation model (DEM) from the South Carolina Department of Health and Environmental Control (Figure 2.1). The DEM had a 3-meter resolution and included Jasper and Beaufort Counties. I extracted the Port Royal Sound Watershed area from the DEM, then selected estuary and marsh areas using classifications from the National Wetland Inventory and the National Gap Analysis Program layers (USFWS, 2015). The total area categorized as estuarine or marsh was 1167.0484 km^2. The watershed was large and had variable tidal ranges. Therefore, I split the DEM into seven zones (Figure 2.2). I found the mean sea level and tidal amplitude within each zone using a total of 19 tide gauges (Figure 2.3). Each of the 19 tide gauges have mean sea level and tidal amplitude data associated with them, which are provided by NOAA (National Oceanic and Atmospheric Administration, 2012). Table 2.1 shows the tidal variables used in each zone. Based on Morris et al. (2002), I estimated plant biomass using the following equation:

$$B = aD + bD^2 + c \quad (1)$$

where B is biomass ($g/m^2 \times yr^1$), D is depth (cm) and a, b, c are model coefficients. To solve the equation, zero biomass was assumed at mean sea level minus 10 cm (Z_{min}) and mean high water plus 30 centimeters (Z_{max}). Biomass was maximized at the mean elevation between Z_{max} and Z_{min}. Maximum biomass was 1400 g/m^2 based on a study conducted by Jensen et al. (2002). Since the model coefficients a,

b, and *c*, are dependent on tidal constituents, they are different for each of the seven modelled DEM zones (Table 2.2). Depth is calculated by:

$$D = \frac{MHW - Z}{Trange} \quad (2)$$

MWH is mean high water (cm), Z is elevation (cm) and *Trange* is the tidal range (cm). The rate of elevation change within the marsh was estimated by applying the Marsh Equilibrium Model (Morris et al., 2002, 2013) :

$$\frac{\Delta Z}{\Delta T} = \left(\frac{1}{k2} * q * m * f * absD * 0.5 * D\right) + \left(\frac{1}{k1} * kr * RSR * BGTR * B\right) \quad (3)$$

where Z is elevation, T is time (year), *k2* the self-packing density for mineral sediments (g/cm^3), *k1* is the self-packing density for organic sediments (g/cm^3), q is trapping efficiency (g/g), *m* is the suspended sediment concentration (g/cm^3), f is the frequency for semi-diurnal tides, *absD* (cm) is the absolute depth, *kr* is the refractory fraction of organic matter, *RSR* is the root to shoot ratio, *BGTR* is the belowground turnover rate (years), and *B* is biomass (g/cm^2). Organic and mineral sediments packing densities, q, *kr*, *RSR*, and *BGTR* were obtained from Morris (personal communication) and Edwards (2016). The United States Geological Survey and United States National Water Quality Monitoring Council have suspended sediment concentrations found within Beaufort and Jasper Counties, I found the average suspended sediment concentration based on the available data for the two counties (Conlon and Journey, 2008; National Water Quality Monitoring Council, 2017). A summary of these values is found in Table 2.3. Absolute depth was calculated by:

$$absD = MHW - Z \quad (4)$$

MHW is mean high water (cm), and Z is elevation (cm) found in the DEM. To incorporate sea-level rise and determine if the marsh is keeping up with sea-level rise a final equation is needed;

$$Z = Z_i + \frac{\Delta Z}{\Delta T} - slr \quad (5)$$

the modeled elevation (Z) is equal to the initial elevation (Z_i) plus the change in elevation $\frac{\Delta Z}{\Delta T}$ minus the estimated rise in sea level (*slr*). Lastly, since sea-level rise is not estimated to rise linearly, I estimated sea-level rise by applying

$$slr = A \times i + sB \times i^2 \quad (6)$$

A is the current rate of sea-level rise for Fort Pulaski Georgia (0.317 cm/year), *i* is the time iteration (years) and *sB* is an accelerating term for sea-level rise (0.00683). Total sea-level rise was predicted to be 1 m/100 years, which is the median estimated rate of global sea-level rise (Sweet et al., 2017).

Model coding

In order to model the elevational change within the large study area I wrote MEM into a Python script based on Edwards (2016). I used the Python libraries gdal and rasterio to extract metadata from the georeferenced DEM data, and then used numpy to create an empty array with the same dimensions as the input file. The Python script was programmed to compute the annual elevation change within the region over 100 years and export the data into a georeferenced tiff file, which can be used in GIS software such as ArcGIS or QGIS. An example of the

written Python can be found in Appendix A. Lastly, based on elevations definitions, the area was classified into land types and a time line (every 10 years over the course of the modelling period) set of maps of land types was developed (Table 2.4). This allowed for easy determination of which parts of the marsh are keeping pace with sea-level rise.

Results and Discussion

Modelled results indicate that wetland areas in the Port Royal Watershed are largely able to keep pace with sea-level rise but will decline in extent over time (Figure 2.4). The predicted changes in land type start out small, then ramp up after about 60 years. This is the time when wetland losses are predicted to become more noticeable (Figure 2.4). The northeast region will likely experience the largest loss of wetland marsh area. However, the model used does not consider the effects of developed areas or other barriers to marsh migration, so the extent of marsh migration will likely be smaller than the model predicts.

To better facilitate the determination of marsh presence/absence, I classified 2013 versus 2113 model outputs into "Never Marsh," "No Longer Marsh," "New Marsh," and "Still Marsh" (Figure 2.5). This map illustrates that the eastern portion of the study area is losing the largest extent of marsh area, and all of the upland area in this study is converted to marsh. Future work should be conducted to incorporate consideration of the effects of developed areas or other impediments to marsh migration.

Python was particularly useful for developing code because it did not have data size limitations and greatly facilitated my ability to successfully estimate marsh migration and change over the 100-year period. I also found that use of the Marsh Equilibrium Model, because it takes into account so many variables (plant biomass, suspendered sediment, elevation, and tidal constituents), provides a more robust model of change than the more limited "bathtub" modelling approach, an approach that provides limited or no opportunities for consideration of environmental feedback loops. Furthermore, as noted elsewhere in this section, Python is an open-sourced software, available on both PCs and Macs; this broadens its scope of use as compared to software such as ArcGIS and ArcPy, both available only on PCs. Using Python coding to analyze the results from MEM, Coastal Zone Managers can assess salt marsh regions that are particularly vulnerable to sea-level rise and therefore, can implement better focused sustainable development or restoration projects. This should help promote ongoing healthy interactions between humans and salt marsh ecosystems.

I provided the results to the South Carolina Nature Conservancy. They are using the model outputs to better determine which lands to purchase for restoration or conservation easements. Future work can be done throughout the southeastern United States to predict marsh vulnerability and to anticipate changes in salt marsh elevations over time spans as long as 100 years.

Furthermore, I found using Python, a large capacity open-sourced software program available on Mac and PC computers, considerably broadens the scope of

use of MEM; particularly when compared to using expensive software, such as ArcGIS and ArcPy, tools that are only available on PCs.

Conclusions

Because of its capacity to handle analyses with large data bases, Python is a practical, freely available scripting tool to use when applying MEM to model migration of large areas of marsh.

I used this approach to provide requested information to The South Carolina Nature Conservancy concerning a large (a total marsh and mud flat area of approximately 1167.0484 km^2) tract of salty marsh land in Jasper and Beaufort counties of South Carolina. The Nature Conservancy is currently using the data I provided to help them pinpoint possible land parcel purchases for marsh conservation purposes, in light of the effects of current rates of sea water rise.

I found that marshes within the study area are generally predicted to be able to keep pace with sea-level rise over the course of the 100 year time span, with some wetland loss in the north-eastern region. All the upland area is predicted to be eventually converted into marsh; however, as a caveat, the model did not include consideration of the effects of potential development of adjacent areas within the parameters studied.

Table 2.1. Summary of tidal constituents used within each of the DEM zones for the Marsh Equilibrium Model.

DEM Zone	MSL (m)	Tidal Amplitude (m)
DEM 0	0.088	1.604
DEM 1	-0.013	1.098
DEM 2	-0.005	1.171
DEM 3	-0.005	0.998
DEM 4	-0.051	0.886
DEM 5	-0.038	1.116
DEM 6	-0.070	1.078

Table 2.2. Model coefficients used to estimate biomass within each of the DEM zones.

DEM Zone	a	b	c
DEM 0	2718.8531	-2610.9253	692.1894
DEM 1	2813.3715	-3277.3334	796.2272
DEM 2	2224.7049	-2268.5584	854.5752
DEM 3	2315.4096	-2204.9672	792.1540
DEM 4	2675.1962	-3387.7823	871.8761
DEM 5	2416.9314	-2437.2089	800.7944
DEM 6	2606.9711	-2562.9448	737.0616

Table 2.3. Model Variables used in the Marsh Equilibrium Model. K2 the self-packing density for mineral sediments (g/cm^3), k1 is the self-packing density for organic sediments (g/cm^3), q is trapping efficiency (g/g), m is the suspended sediment concentration (g/cm^3), f is the frequency for semi-diurnal tides, kr is the refractory fraction of organic matter, RSR is the root to shoot ratio, and RGTR is belowground turnover rate (years).

Variable	Value
k1	0.085
k2	1.99
q	2.8
m	3.35e-5
f	704
kr	0.1
RSR	2
BGTR	1

Table 2.4. Classification table for defining land type based on elevation.

Classification	Definition
Water	Below mean low water (MLW)
Mudflat	Minimum elevation for vegetation (MLW – 10 cm)
Marsh	Between minimum elevation for vegetation and maximum elevation for vegetation (MHW + 10 cm)
Upland/Scrub	Above maximum elevation for vegetation

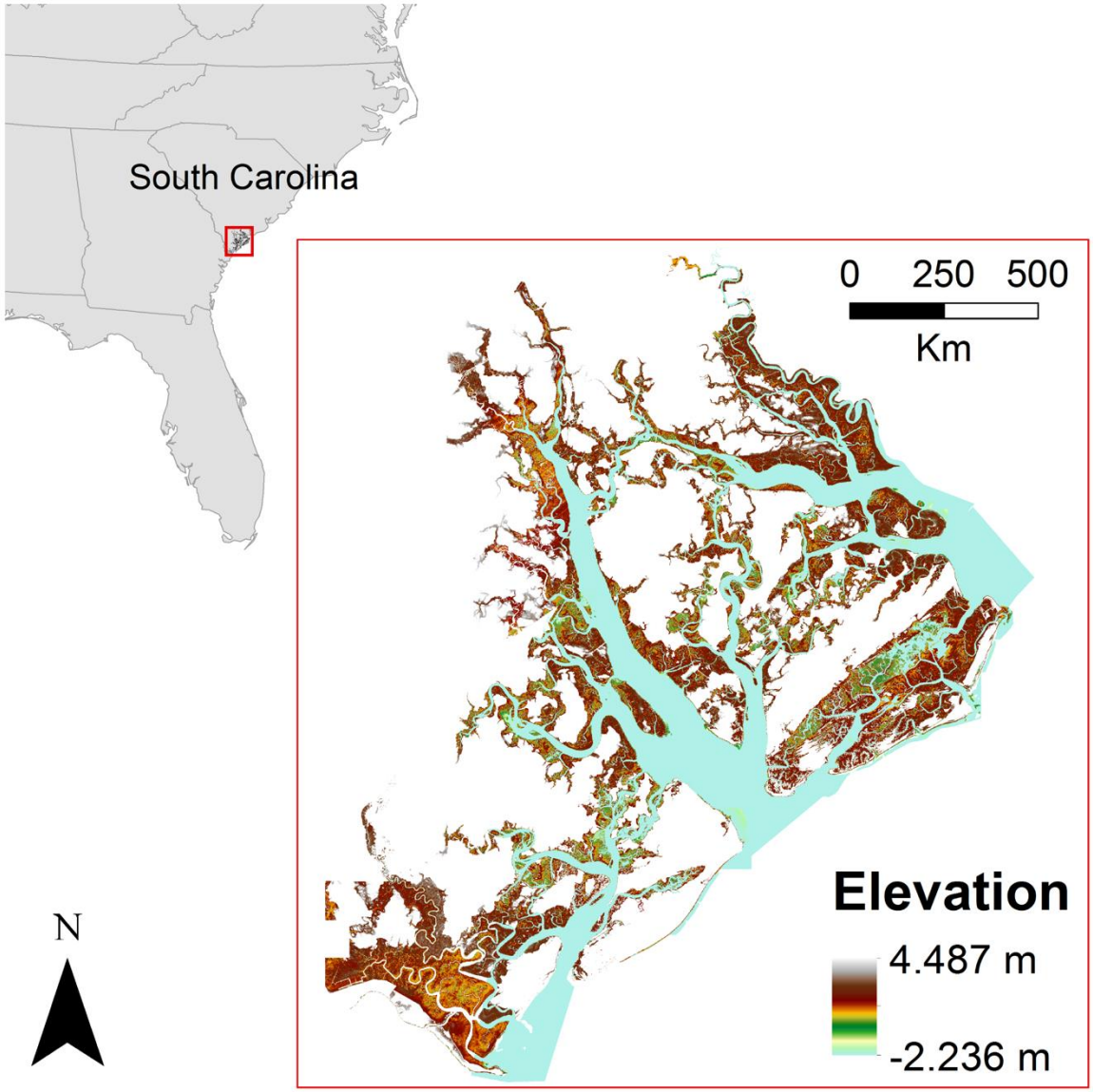

Figure 2.1. Elevation layer within Beaufort and Jasper marsh and estuarine areas.

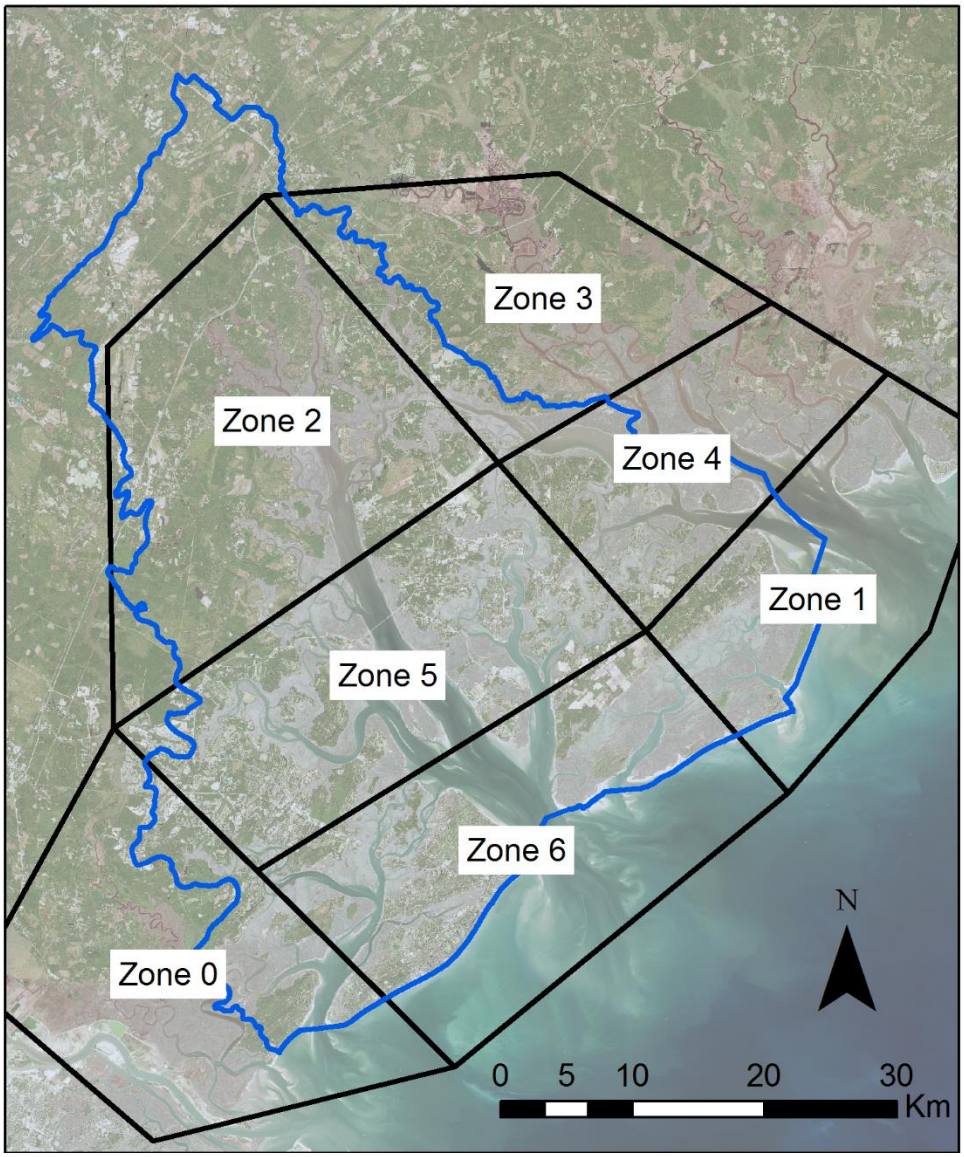

Figure 2.2. Port Royal Sound Watershed area used in this study is shown in blue. The tidal zones 0-6 are defined as the areas inside each of the black polygons.

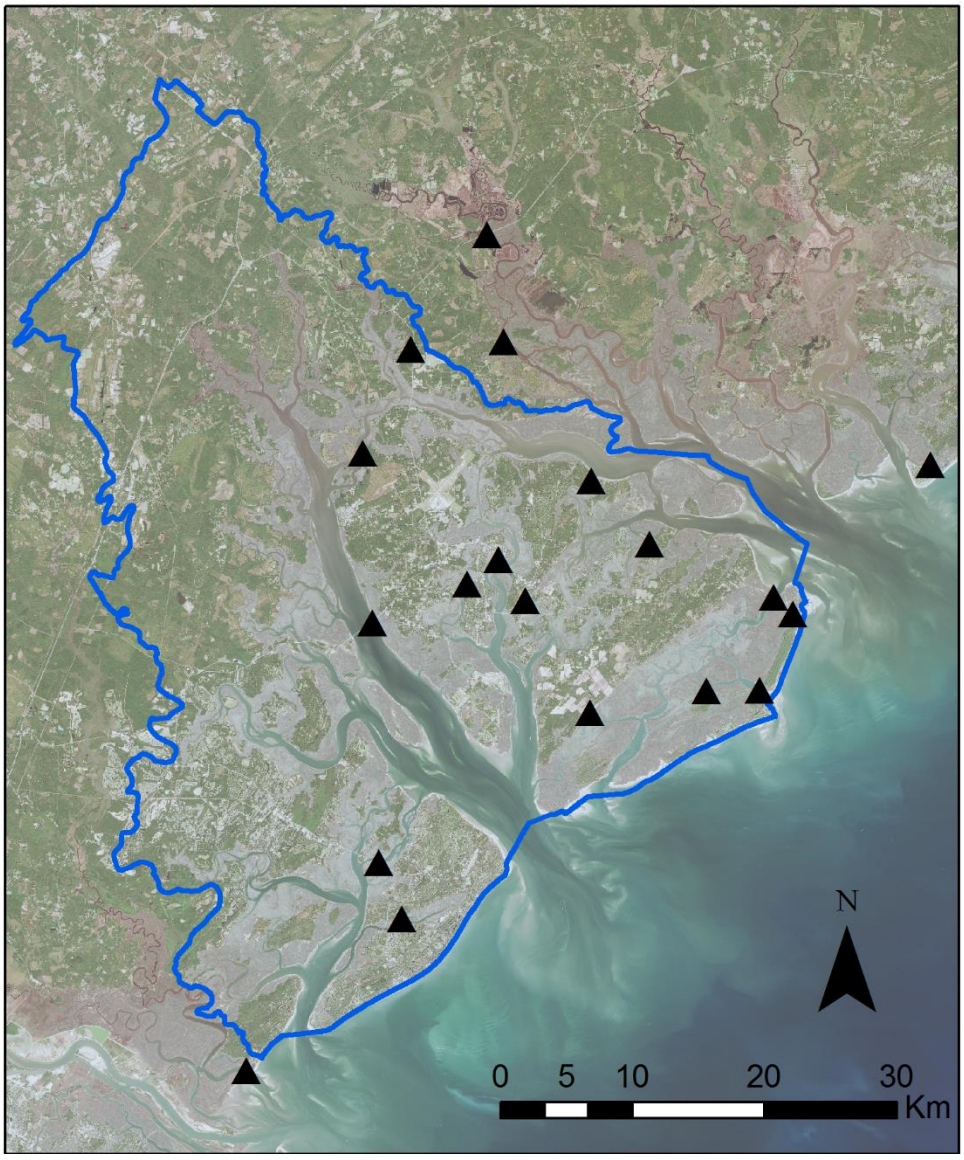

Figure 2.3. Location of tide gauges used to determine tidal constituents for the Marsh Equilibrium Model. Tide gauge locations are shown with triangles. The blue outline indicates the Port Royal Round Watershed boundaries used in this study.

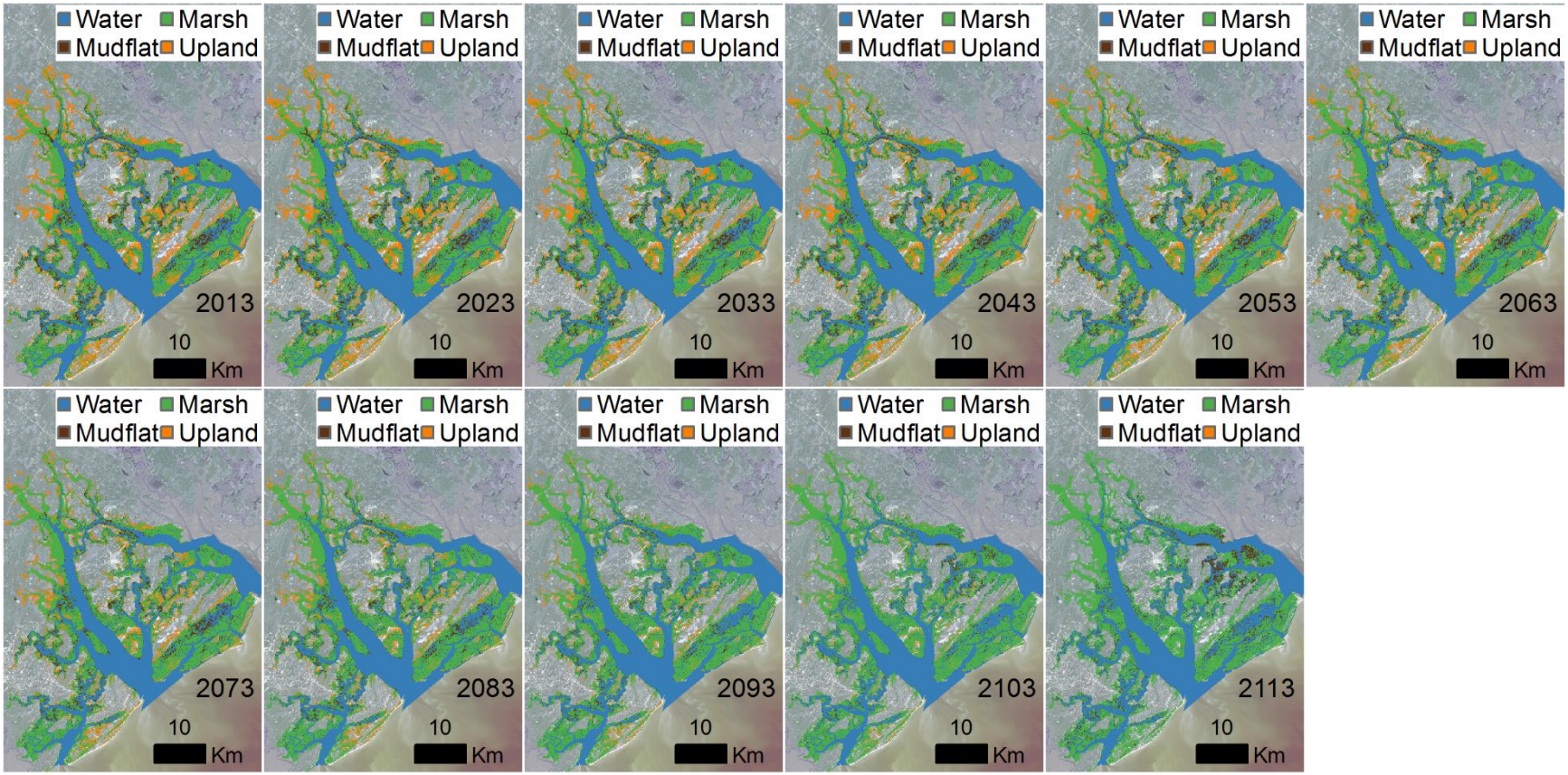

Figure 2.4. Land classification within the Port Royal Sound watershed starting in year 2013 and modeled results every 10 years ending in year 2113. Basemap: Sentinel data 2017, processed by European Space Administration

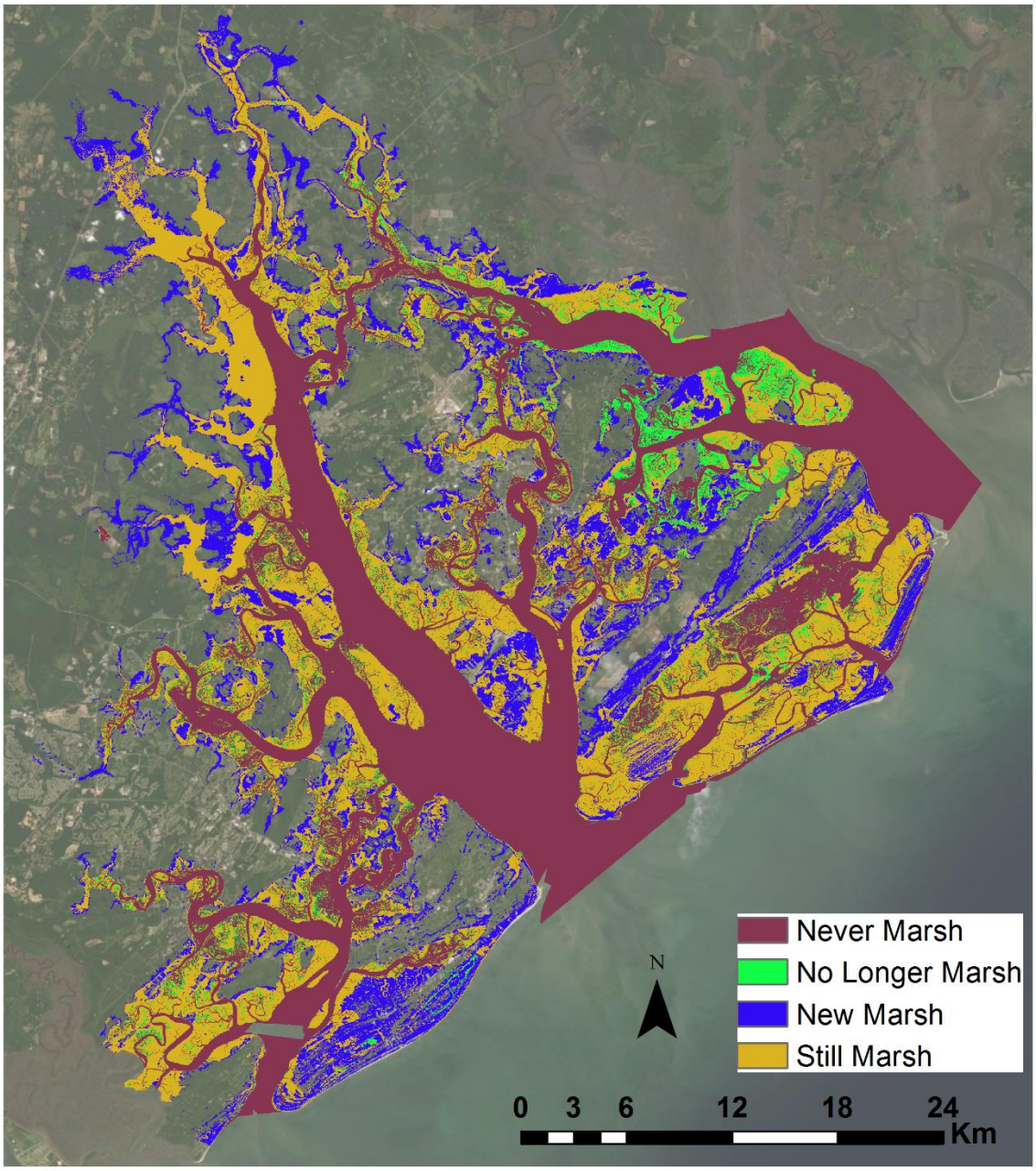

Figure 2.5 Classification of change in land type based on initial year (2013) versus final year of marsh migration model (2113). Basemap: Sentinel data 2017, processed by European Space Administration

CHAPTER 3

ESTIMATING ABOVEGROUND BIOMASS AND ITS SPATIAL DISTRIBUTION IN COASTAL WETLANDS UTILIZING PLANET MULTISPECTRAL IMAGERY[1]

[1] Miller, G. J., Morris, J. T., and Wang, C. (2019). Estimating Aboveground Biomass and Its Spatial Distribution in Coastal Wetlands Utilizing Planet Multispectral Imagery. Remote Sens. 11, 2020. doi:10.3390/rs11172020.
Reprinted here under publisher's open access policy.

Introduction

Coastal salt marshes are biologically diverse ecosystems that improve water quality, provide protection from hurricanes and storm surges, and are important habitat for wildlife (Fisher and Acreman, 2004; Möller et al., 2014; Narayan et al., 2017). Furthermore, as carbon is released from long-term storage through burning of fossil fuels to the atmosphere, understanding how carbon is stored within coastal or marine environment is becoming more important. This form of carbon storage is referred to as "blue carbon" and salt marshes are a large blue carbon reservoir with carbon stored both in above and belowground biomass (Mcleod et al., 2011; Nellemann et al., 2009). Biomass data are also used in models predicting elevation change within marshes. One such model is the marsh equilibrium model (MEM), which estimates elevation changes within salt marshes in relation to sea-level rise (Morris et al., 2002). A fundamental feature of this model is the dependence of biomass production as a function of relative elevation.

Biomass density in a salt marsh is spatially variable and difficult to quantify at the landscape scale. Elevation above sea level is one of the major determinants of primary production and plant health within salt marshes, but other variables such as grazing activity, nutrient availability, and tidal flushing are important as well (DeLaune et al., 1983; Mendelssohn, 1979; Mendelssohn and Seneca, 1980; Miller et al., 2017; Morris et al., 2002, 2013; Silliman and Bertness, 2002). Landscape-scale field analysis of biomass is impractical due to labor-intensive methods and difficulty accessing the entire marsh area. However, remote sensing

technologies are well-suited for studies at the landscape scale. Spectral data extracted from satellites allow researchers to estimate aboveground biomass (Gross et al., 1990; Lumbierres et al., 2017) over large areas at a variety of spatial resolutions. Many of the satellite platforms continuously collect images, making remote sensing data useful for time-series analysis and retrieval of past events.

Many earlier studies about multispectral analyses of salt marsh biomass utilize data from NASA's Landsat satellite series (Gross et al., 1987, 1990; Lopes et al., 2019; Mo et al., 2017). These satellites only have a 30-m resolution and 16-day revisit cycle. The 30-m pixel size limits its capacity to resolve fine-scale variations in a marsh. Landsat imagery is often unusable or only partly usable on cloudy days, which further reduces the image availability. Lastly, satellite images need to be captured during low tide when the salt marsh vegetation is not submerged. Therefore, satellites with higher spatial resolution and shorter repeat times are more desirable.

A company in the United States, Planet, has launched its PlanetScope satellites since 2009. Currently, it has over 100 PlanetScope nanosatellites in orbit, collecting multispectral imagery in blue, green, red, and near-infrared bands. It established a data-sharing program for students and researchers providing them with near-daily, 3-m PlanetScope data (Planet Team, 2018), allowing for high spatial and temporal analysis of landscapes. The goal of this study was to test the efficacy of Planet data to accurately predict aboveground biomass within salt marshes in North Inlet-Winyah Bay (North Inlet) National Estuarine Research

Reserve and Plum Island Ecosystems (PIE) Long-Term Ecological Research site and its ability to resolve spatial pattern across the marsh landscape. Results from this study will give a better understanding of aboveground biomass within salt marshes, which is useful for a variety of purposes including modeling studies, trends analysis, assessment of marsh health, and potential carbon sequestration.

Materials and Methods

Study Area

The main study area was North Inlet, in Georgetown, South Carolina (Figure 3.1 a). North Inlet has been the site of multidisciplinary ecological research for about 50 years. The intertidal marshes here consist of 29 km^2 of monospecific stands of *Spartina alterniflora* punctuated by about 121 km of creeks. *S. alterniflora* possesses long-lived, perennial rhizomes that produce a new crop of stems annually. The mild winters allow for year-round growth, though growth of the newly emergent crop of stems is greatly reduced until milder, brighter conditions prevail in springtime and summer.

Studies of primary production that begun in 1984 at North Inlet documented that interannual anomalies in mean sea level (MSL) on the order of 5 to 10 cm positively affected the productivity of *S. alterniflora* (Morris, 2000; Morris and Haskin, 1990). The effect on plant growth is thought to be due to variations in the duration (hydroperiod) and frequency of tidal flooding, which are determined largely by the marsh elevation relative to mean high water level (MHW). Primary production in the upper quadrant of the tidal frame (roughly the highest 25% of

the intertidal zone) is greater in years of high sea level. This is key to the survival of marshes, because the vegetation traps more sediment and generates greater biovolume when greater flood frequency and duration enhance vegetative growth (Morris et al., 2002).

A smaller study was conducted at the PIE, located in northeastern Massachusetts (Figure 3.1. b). PIE consists of a linked watershed–marsh–estuarine system located within the Boston metropolitan area of northeastern Massachusetts. The brackish and saline tidal wetlands of the PIE site form the major portion of the "Great Marsh", the largest intact marsh left on the northeast coast of the United States. The coastal ecosystems of PIE are in an area that is changing rapidly. Over the last 30 years, surface sea water temperatures in the Gulf of Maine have risen at 3 times the global average; over the last decade warming has increased 7-fold to 0.23 °C per year, making the Gulf of Maine one of the fastest warming regions in the global ocean (Pershing et al., 2015). The warming is also associated with a shift in the Gulf Stream that affects local sea level. This area is experiencing high rates of sea-level rise that appear to have accelerated over the last 15 years to nearly 4 mm/year compared to the long-term average of 2.8 mm/year over the last century (NOAA). PIE is dominated by *Spartina patens* at high elevations within the tidal frame and *S. alterniflora* growing at the lower elevations, especially along the creek banks. The cold winters lead to a short growing season, roughly May–August. For this study, only *S. alterniflora* areas were examined at both North Inlet and PIE.

In addition to climate, major differences between the two sites include tide range and soils. PIE marshes are built on a low-grade peat, while North Inlet marshes rest on mineral sediment. Tide range averages 2.7 m at PIE and 1.4 m at North Inlet (Morris et al., 2013; Schwing et al., 1980). The relative elevation of the marsh within the tidal frame, meaning the vertical position between the low- and high-tide levels, is critically important to the resilience of these ecosystems, because it determines their ability to maintain elevation relative to sea level within a favorable vertical range. Spartina marshes exist approximately between mean high water (MHW) and MSL (McKee and Patrick, 1988), and the biomass of the vegetation is dependent on relative elevation (Morris et al., 2002). Thus, theory predicts that biomass should vary across a marsh landscape as a function of elevation. Our analysis of high-resolution data from Planet provided a test of this theory.

Field Data Collection

For North Inlet, biomass samples were collected at seven sites in each of two years, September 2017 and September 2018. At each site, four sample locations were randomly selected; in total, 54 biomass samples were collected (Figure 3.1.a). These sites were selected because they are accessible and have nearby established sediment elevation tables (SET). A SET is a portable, mechanical leveling device designed to attach to a stable benchmark pipe for the purpose of measuring change in marsh surface elevation (Boumans and Day, 1993; Cahoon et al., 2002). Established site names are: DDC—Debidue Creek, OL—Oyster Landing, GI—

Goat Island, BASS—Sixty Bass Creek, OMC—Old Man Creek, BCR—Bly Creek, and STC—South Town Creek. For PIE, biomass samples were collected at nine sites during July 2018. Similarly, three to four sample locations were randomly selected and a total of 36 biomass samples were collected. Only areas with monocultures of *S. alterniflora* were sampled (Figure 3.1.b). At both North Inlet and PIE, a 25 cm × 25 cm quadrat was placed over the plants and plant matter was clipped to the soil surface, excluding fallen litter. The plants were bagged and returned to the laboratory where samples were washed and dried in an oven at 60 °C for 72 h, or until a constant weight was reached. GPS measurements were taken over mudflat locations in North Inlet (12 locations) and PIE (7 locations) to better establish the zero biomass records.

For validation, biomass data collected at North Inlet during monthly surveys at established survey locations were used. This independent dataset is part of a long-term study of biomass production within North Inlet, and is described by Morris and Haskin (Morris and Haskin, 1990). Standing biomass was estimated nondestructively by measuring stem heights, and calculating stem weights based on an established empirical relationship (Davis et al., 2017; Morris and Haskin, 1990). Only biomass data from locations that were far enough from the creek edge were used, to avoid interference from water with the spectral data. Biomass values were averaged if multiple sample locations fell within the same pixel, which resulted in a collection of 26 pixel-wise points for model validation in this study.

Satellite Data

The downloaded PlanetScope images data were acquired on dates close to field sample dates subject to cloud-free and low-tide conditions. For North Inlet, those were 30 October 2017 and 20 September 2018. For PIE, data were collected on 20 July 2018. Planet provided atmospherically corrected multispectral data using the second simulation of a satellite signal in the solar spectrum (6S) radiative transfer model, as has been used successfully in other wetland studies (Byrd et al., 2014; Li and Gong, 2016; O'Donnell et al., 2016). The atmospheric correction process uses information from moderate-resolution imaging spectroradiometer (MODIS) for ozone, water vapor, and aerosol inputs (Planet Team, 2019). Greater detail about Planet's sensor specifications is given in Table 3. 1.

Vegetation Indices

For each Planet image, the vegetation indices (VI) shown in Table 2 were calculated. The normalized difference vegetation index (NDVI) is a commonly used index measuring plant greenness, with larger values closer to 1.0 indicating the maximum amount of vegetation (Rouse et al., 1973). Its first salt marsh application was possibly by Hardisky et al. (Hardisky et al., 1983) who used a handheld sensor in a Delaware marsh. Background absorption (and reflectance) from soil can have a significant effect on the reflected light, and to account for soil influencing the VI, an adjustment factor (L) is sometimes incorporated into the NDVI calculation resulting the soil adjusted vegetation index (SAVI). Factor L can range from 0 to 1 where 0 indicates complete vegetation coverage and no

background effects from soil (Huete, 1988). An L value of 0.5 minimizes soil brightness variations and is commonly used, but L is based on the amount of vegetation coverage within the study area. Building upon SAVI, the modified soil adjusted vegetation index 2 ($MSAVI_2$) uses a functional L factor that eliminates the need to estimate vegetation density (Qi et al., 1994). The renormalized difference vegetation index (RDVI) is an index that reduces oversaturation issues that can be associated with densely vegetated areas (Roujean and Breon, 1995). Next, the visible difference vegetation index (VDVI) was originally developed for unmanned aerial systems to highlight plant greenness and uses only values in the visible spectrum (Wang et al., 2015), and the green normalized vegetation index (GNDVI) can be more sensitive to chlorophyll than NDVI (Gitelson and Merzlyak, 1998). At each of the field sample locations, we extracted the VI values and surface reflectance from each of the four individual bands and fitted each of these models to square-root normalized biomass.

Statistical Analysis

The R statistical program was used to run a stepwise method of multiple regression models and determine the best-fit model (R Core Team, 2017). The model was initially built using the following formula or a subset of it:

$$\text{Biomass} = \beta_0 + \beta_1 NDVI + \beta_2 SAVI + \beta_3 MSAVI2 + \beta_4 RDVI + \beta_5 VDVI + \beta_6 GNDVI + \beta_7 blue + \beta_8 green + \beta_9 red + \beta_{10} NIR \quad (1)$$

where β_0 is the intercept and each subsequent β of 1–10 is the fitted coefficient related to the input variables. Symbols *blue*, *green*, *red*, and *NIR* represent surface

reflectance in each corresponding spectral band. Within R, only models that passed the assumption of non-collinearity were considered.

To normalize the data, the biomass in Equation (1) was input as the square root of field-measured biomass (g/m^2). Furthermore, biomass was regressed against the original VIs as well as the logged VIs; the indices can saturate at higher biomass values following a logged shaped curve. We created and compared models with all combinations of vegetation indices and individual spectral bands against each other and selected the best-fit regressions.

This study adopted the Akaike information criterion (AIC) analysis for model comparison. AIC estimates the quality of a model relative to the other models within an analysis, with the smallest AIC model being the best. This allowed us to compare each model against each other by assessing their AIC values and AIC weights (AIC_w). The AIC_w calculates the weight of evidence for one model over another model and is calculated based on the entire series of linear regressions in the analysis. The summation of AIC_w values is 1, which makes for easier model comparison (Burnham and Anderson, 2002). The AIC values and AIC weights (AIC_w) can be calculated as (Akaike, 1974; Burnham and Anderson, 2002):

$$\mathrm{AIC} = -2\log(L) + 2K \tag{2}$$

$$\mathrm{AICw} = \frac{\exp\left\{-\frac{1}{2}\,\Delta_i(\mathrm{AIC})\right\}}{\sum_{k=1}^{K}\exp\left\{-\frac{1}{2}\Delta_k(\mathrm{AIC})\right\}} \tag{3}$$

where *K* is the number of parameters in the model, *L* is the maximum likelihood function of the model, and $\Delta_i(\mathrm{AIC})$ is the AIC value for the model minus the AIC value of the smallest model. The model with the lowest AIC and highest AIC_w is the best model at predicting aboveground biomass.

Three evaluation metrics were examined for performance assessment of the regression model, which was computed using back-transformed output values (biomass g/m^2). Its accuracy was quantified using Willmott's index of agreement (d) (Willmott, 1982), which was calculated using the hydroGOF package in R (Zambrano-Bigiarini, 2017). The index of agreement ranges from 0 to 1, with 1 indicating a perfect fit, and has been used in several remote sensing studies for accuracy assessment (Almeida et al., 2016; García et al., 2010; Hardisky et al., 1984; Yebra and Chuvieco, 2009). Squared Willmott's index of agreement (d^2) was also included since its values are more similar to the frequently used coefficient of determination (R^2) values (Valbuena et al., 2019). Lastly, root mean square error (RMSE) was calculated as:

$$\mathrm{RMSE} = \sqrt{\frac{1}{\mathrm{n}} \times \sum (\mathrm{B_{obs}} - \mathrm{B_{mod}})^2} \qquad 4)$$

where n is the number of validation samples, B_{obs} is the observed biomass (g/m^2), and B_{mod} is the modeled biomass (g/m^2).

Results

North Inlet

The regression model that best predicted aboveground biomass (AIC_w = 0.3848, d = 0.74) was:

$$\sqrt{\text{Biomass}} = 76.99 + 39.10 \times log_{10}(\text{MSAVI2}) + 28.55 \times log_{10}(\text{VDVI}) \quad 5)$$

In AIC analysis, more dependent variables are counted against the model fit, as shown in Equation (2), and some of the variables such as $MSAVI_2$ and SAVI were autocorrelated, violating the assumption of non-multicollinearity. Therefore, within our analysis, only models with one or two variables were the best-supported models. In Table 3. 3, we include models that showed the most support from our analysis as indicated by an AIC_w greater than 0.

The model accuracy was tested using the independent biomass dataset and there was a good model fit; d = 0.74, d^2 = 0.55, n = 26, RMSE = 223.38 g/m^2 (Figure 3.2). The modeled (predicted) values versus the actual values from the validation dataset followed a linear trend that did not significantly deviate from the 1:1 line. Furthermore, the index of agreement was not far from 1 (d = 0.74), indicating a good model fit. The root mean square error (RMSE) of the validation dataset was 223.38 g/m^2.

Using the best-fitting model and Planet spectral 3-m data, North Inlet biomass maps were created for 2017 (Figure 3.2.a) and 2018 (Figure 3.2.b). Total aboveground, *S. alterniflora* biomass across the entire marsh landscape in North Inlet was estimated to be 3423 Mg in 2017 and 2655 Mg in 2018. The maximum area-specific aboveground biomass was 2483 g/m^2 and 1823 g/m^2 in 2017 and

2018, respectively (Figure 3.4). The locations of biomass maxima differed between 2017 and 2018. Thus, in addition to interannual temporal variability in the standing crop, there was interannual spatial variability as well, most likely due to varying environmental conditions. To further investigate how biomass differed between the seven locations, modeled biomass values were extracted from 100-m buffers around the sample locations. Most locations had a wide range of biomass, with DDC having a relatively small range. In 2017, BASS had the largest mean biomass and BCR had the lowest (Figure 3.4). In 2018, DDC had the largest mean biomass and GI had the lowest (Figure 3.4).

The dependence of biomass on elevation was examined using the model-derived aboveground biomass data (Figure 3.4) and a 2007 bare-earth lidar-derived digital elevation model. Across the entire marsh landscape, 3000 points were randomly sampled from both the 2017 and 2018 datasets. Using the geolocation of each point, the georeferenced elevation and modeled biomass data were matched. Modeled biomass demonstrated a highly significant parabolic relationship to elevation, with peak biomass near 36 cm above NAVD88 (Figure 5a; $p < 0.001$). This relationship to elevation was very close to that observed earlier (Figure 3.5.a) in a bioassay experiment in North Inlet (Morris et al., 2013).

Plum Island

Harvested aboveground biomass at PIE, like North Inlet, was dependent on elevation (Figure 3.5.b). However, the relationship was linear, which was the case both with the harvest data from this study and a bioassay conducted earlier

(Morris et al., 2013). The decline in biomass with elevation suggests that the *S. alterniflora* marshes at PIE occupy the upper half of their possible growth range, at least among the sites we sampled. Unlike PIE, at North Inlet we found *S. alterniflora* across its entire growth range.

The application of multispectral data in this study for biomass predictions at PIE was less than satisfactory. For example, model Equation (5) fitted to the PIE data showed low model performance d = 0.22 and d^2 = 0.05, indicating that Equation (5) might be site-specific and cannot be applied across dissimilar sites. None of the other models were satisfactory either. Additionally, the two vegetation indices $MSAVI_2$ and VDVI, which were used in Equation (5), did not show a relationship with normalized biomass (Figure 3.6).

Discussion

Planet data were applied successfully to estimate aboveground biomass at North Inlet. A good model fit (d = 0.74, d^2 = 0.55, RMSE = 223.38 g/m^2) was obtained using the model developed within this study to estimate biomass at the validation sites. The extracted biomass map provided interesting insights about this marsh's growth dynamics that correlated well with data from marsh organ studies, including correspondence with the vertical growth ranges.

Within North Inlet we found that mean biomass varied by sample location. As indicated in Figure 3.4, differences in biomass density were significant due to variable growth conditions within the estuary. STC had the largest biomass concentration and is also the location closest to Winyah Bay. Winyah Bay is an

estuary adjacent to North Inlet (Figure 3.3) with a large freshwater discharge, and its adjacent marshes are less saline than the majority of North Inlet estuary. The water from Winyah Bay only influences the southern region of North Inlet, due to a tidal node that limits the intrusion of brackish water further into North Inlet (Schwing et al., 1980). STC was the only site we sampled that was influenced by Winyah Bay, and the freshwater influence presumably provided for more favorable growth conditions, allowing for larger biomass growth.

There are other sources of variation that have not been fully explained. For instance, total biomass in 2017 was greater than in 2018, however it is unclear what led to this change. The images used in 2017 and 2018 both were taken at low tide (−0.5 m and −0.42 m relative to NAVD, respectively) and in the same season, so influences of tide and time-of-year were minimal. However, it is possible that atmospheric conditions differed between images and were not perfectly or uniformly corrected using atmospheric correction. Alternatively, rainfall may have been a factor (Morris and Haskin, 1990; O'Donnell et al., 2016). Based on the Palmer drought severity index for the northeast region in South Carolina, 2017 experienced more "incipient wet spells during the growing season than in 2018, which should have been more favorable for growth. Then in February/March of 2018 there was a period of "mild drought" (Figure 3.7) (NOAA; Palmer, 1965), which likely depressed growth. Although there was no notable prolonged drought in 2018, the average summer temperature was slightly cooler in 2017 and springtime wetter than 2018, both of which may have resulted in somewhat more

favorable 2017 growing conditions (Figure 3.8). Other factors that influence aboveground biomass include herbivory, interannual variation in sea level, and storms (Dame and Kenny; Li and Pennings, 2017; Morris and Haskin, 1990; O'Donnell et al., 2016; Tyler and Zieman). Thus, the remote imagery has opened up future work on the possible drivers of these inter-annual differences in marsh primary production.

Elevation also played a role in biomass growth, and similar to other studies, biomass followed a parabolic relationship with elevation (Morris et al., 2002, 2013; Walters and Kirwan, 2016). Furthermore, the biomass curve closely follows the curve found in a marsh organ experiment conducted at North Inlet and PIE (Morris et al., 2013). The comparison of results from this study and that of the marsh organ study (shown in Figure 3.5.a,b) demonstrates that PlanetScope data are useful in deriving biomass growth curves, and can be an alternative to labor-intensive, in situ bioassay experiments. Though the overall harvested biomass at PIE was lower than what was found in a PIE marsh organ experiment, perhaps due to time of harvest, the slope of the two growth curves were similar. For North Inlet, the peak biomass is at mid elevations within its vertical range. As noted earlier, the optimal elevation for *S. alterniflora* growth is approximately midway between mean sea level and the level of mean higher high water (Morris et al., 2013), which is presumably the least stressful elevation (Morris et al., 2002). This is consistent with our biomass model and supports that Planet data or alternative remote imagery can be utilized to derive a relationship between elevation and

biomass production based on vegetation indices and a DEM. This would expand the utility of predictive models such as MEM and allow for better predictions of marsh survival and migration in the face of rising sea level.

There is a north-south elevation gradient within North Inlet (Figure 3.9a,b) that may also influence the biomass. As noted above, there are differences in biomass among sample sites, and the mosaic of biomass (Figure 3.3) clearly shows a preponderance of high biomass at the south end of North Inlet. The elevation at that end of the estuary (Figure 3.9) is close to the optimum (Figure 3.5), while elevations at the north end are suboptimal. Consequently, marsh areas at the north end are at greater risk of drowning due to sea-level rise.

The sample size for PIE was possibly too small to realize a significant correlation between the spectral data and aboveground biomass. Another factor may have been the dark organic-rich soils that are characteristic of PIE marshes. Further, based on field observations, biomass, plant form, and stem density at PIE are extremely variable. For instance, biomass was over 160 cm tall at one site and under 20 cm at another. The issues of large biomass variance and possible spectral saturation with tall dense vegetation at PIE could potentially have been overcome using a larger sample size. In addition, a better correlation between satellite data and biomass may have been established if *S. patens* samples had been included, but the architecture of the two species is radically different. To maintain consistency across sites, only *S. alterniflora* was included. Future work should be

conducted at PIE to include more plant species, larger sample size, and a wider growth range.

The biomass density observed at PIE in this study was lower than what was found in a marsh organ study (Figure 3.5.b), although the trends with elevation were the same, confirming that growth of *S. alterniflora* varies with elevation. However, the growth curves for North Inlet and PIE were different (Figure 3.5). Within PIE, *S. alterniflora* growth is largely confined to the higher end of its growth range. Moreover, as noted earlier, the tide range at PIE is greater than at North Inlet. Consequently, the potential or fundamental vertical growth range of *S. alterniflora* is greater at PIE than at North Inlet. However, *S. alterniflora's* realized growth range in North Inlet spans the entirety of its fundamental range, which our data fully captured, which is possibly another reason for the model's success at North Inlet and failure at PIE.

Biomass and satellite data from PIE were collected earlier in the annual growth cycle than at North Inlet, which also may have affected the fidelity of the models because the spectral signature of *S. alterniflora* varies throughout the year (Jialin et al., 2011; Ouyang et al., 2013). Satellite and field data for PIE were collected in July while samples were collected in North Inlet during early autumn. The growing season also differs between the two sites, as discussed above. Therefore, the spectral signatures of PIE and North Inlet plants were likely very different, which would lead to differences in vegetation indices values. To better determine if a universal biomass model using Planet or other spectral data could

be used, future work should match field and satellite data during peak VI values at each sample site.

This study supports the use of small satellites as a reliable platform to provide data that may be used to compute and map marsh biomass. The commonly applied medium-resolution data such as Landsat is less helpful since the fine-scale spatial variability of marsh biomass is smoothed in those images. As one example of the rapidly developing small satellite technologies, PlanetScope have data originating in 2009. However, their target for near-daily data was reached in 2017. Planet continues to launch their PlanetScope satellites several times a year ridesharing with other missions. These low-cost small satellites have a lifespan of about three years, which allows the company to update the satellite's hardware. The low cost and frequent launch of new satellites also reduces the cost risk of a failed mission. An added benefit of PlanetScope data is that the satellites are always in operation, while other high-resolution satellites are often task-based. This feature provides PlanetScope users with high spatial and temporal coverage of data. Data accessibility is an issue. Since Planet is a commercial company, its data are not as easily accessible as NASA's frequently used Landsat data. In addition, taken with frame cameras, the radiometric accuracy of Planet data may not be as high as that of Landsat. However, this has not yet been widely studied. Despite these drawbacks, the high spatial resolution and temporal frequency of PlanetScope makes it especially useful within heterogeneous wetland systems that are influenced by tides and summer cloud covers.

Conclusions

This study successfully utilized Planet multispectral data to create 3-m spatial scale resolution maps within the North Inlet Winyah Bay National Estuarine Research Reserve. The derived model cannot universally be applied to all wetlands, such as the Plum Island Ecosystems Long-Term Ecological Research site, however this may have been due to differences in season and small sample size, among other possibilities. The advantage of using Planet's data is its high spatial resolution and repeat time, which allows for analysis of biomass distribution and temporal change on a finer scale. The finer scale analysis is particularly useful for land and coastal managers interested in assessing marsh health. Furthermore, the frequent repeat time of Planet's satellite series provides more usable coastal data; analysis within a salt marsh requires imagery collected during low tide, and clouds often cover the coast during the summer making it difficult to find suitable data.

Pairing the model-derived landscape scale map with elevation data, a robust biomass curve with elevation was established. This is important for establishing a better understanding of factors that control biomass growth and is an important input to biogeomorphic models of marsh response to rising sea level. This study not only highlights the usefulness of a newer satellite sensor, but also shows how high-resolution satellite-derived products help answer questions about spatial variability within a marsh and overall marsh condition.

Table 3. 1. Summary of PlanetScope sensor characteristics.

Characteristic	Value
Blue wavelength (nm)	455–415
Green wavelength (nm)	500–590
Red wavelength (nm)	590–670
NIR wavelength (nm)	780–860
Spatial Resolution (m)	3 × 3
Temporal Resolution	Near daily
Image size (km)	24 × 7

Table 3. 2. Vegetation indices and the associated formulas used in the analysis.

Vegetation Index	Equation	Reference
NDVI	$\frac{NIR\ -\ red}{NIR + red}$	(Rouse et al., 1973)
SAVI [1]	$(1 + L)\ \times \frac{(NIR - red)}{NIR + red + L}$	(Huete, 1988)
$MSAVI_2$	$\frac{2NIR + 1 - \sqrt{(2\,NIR + 1)^2 - 8(NIR - red)}}{2}$	(Qi et al., 1994)
RDVI	$\frac{NIR\ -\ red}{\sqrt{NIR + red}}$	(Roujean and Breon, 1995)
VDVI	$\frac{2\ \times green\ - red\ - blue}{2\ \times green\ + red\ + blue}$	(Wang et al., 2015)
GNDVI	$\frac{NIR\ -\ green}{NIR + green}$	(Gitelson and Merzlyak, 1998)

[1] L is a soil adjustment factor ranging from 0 to 1, with 0 indicating no background effect from soil. A frequently used value is 0.5, which was adopted in this study.

Table 3. 3. All models were fitted to square-root normalized aboveground biomass. The model with the highest Akaike information criterion (AIC) weight (AIC_w) is the best model. The table only included models that had an AIC_w larger than 0.

Model	**AIC**	**AIC_w**
log_{10}(MSAVI2) + log_{10}(VDVI)	364.4	0.3848
MSAVI2 + VDVI	365.2	0.2636
SAVI + VDVI	365.6	0.2122
VDVI + GNDVI	367.3	0.0856
VDVI	370.4	0.0231
log_{10}(B3) + log_{10}(VDVI)	371.8	0.0096
B3 + log_{10}(VDVI)	372.3	0.0073
MSAVI2 + B3	372.6	0.0064
log_{10}(MSAVI2) + log_{10}(B3)	373.3	0.0045
SAVI + NDVI	374.5	0.0025
MSAVI2	382.4	0.0001

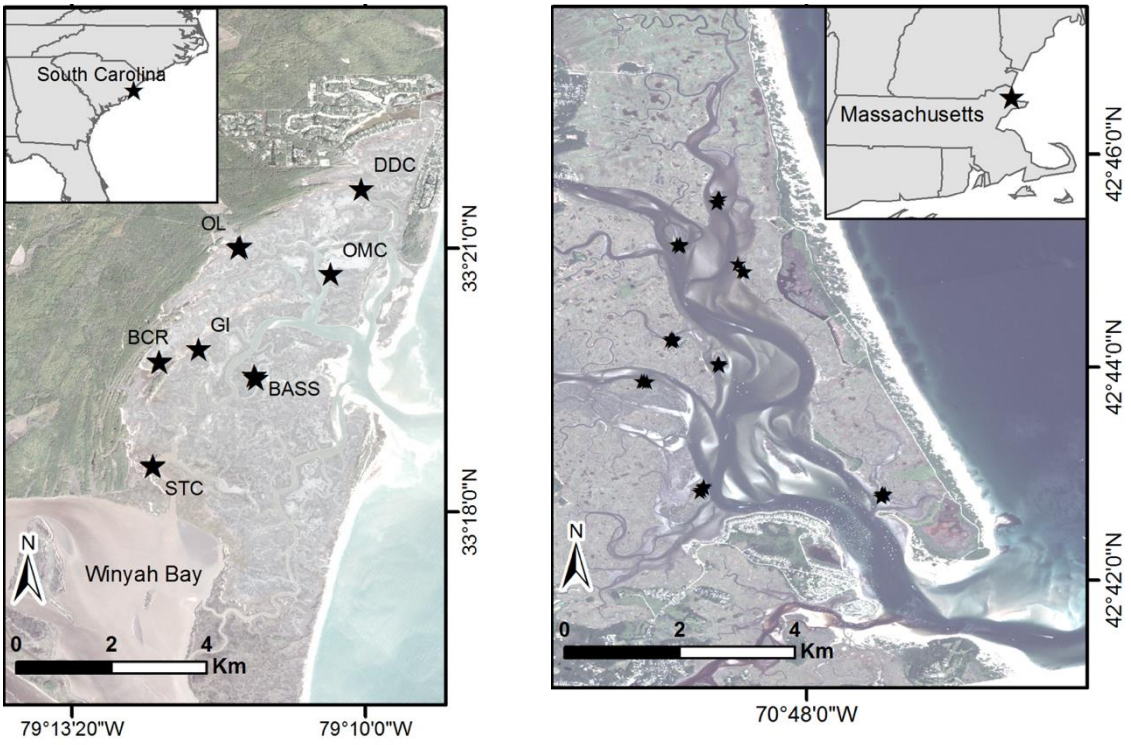

(a) (b)

Figure 3.1. Study areas and sample sites, with stars indicating sample locations. (**a**) North Inlet-Winyah Bay National Estuarine Research Reserve within South Carolina. Established sample locations names are: DDC—Debidue Creek, OL—Oyster Landing, GI—Goat Island, BASS—Sixty Bass Creek, OMC—Old Man Creek, BCR—Bly Creek, STC—South Town Creek. (**b**) Study site at the Plum Island Ecosystems Long-Term Ecological Research site within Massachusetts. Basemap images courtesy of Planet Labs, Inc. (San Francisco, CA, USA).

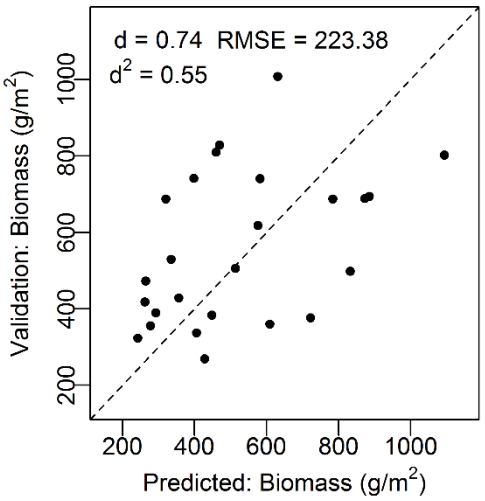

Figure 3.2. Modeled biomass (g/m^2) from the combined modified soil vegetation index 2 ($MSAVI_2$) and visible difference vegetation index (VDVI) versus the validation biomass (g/m^2) data. Dashed line corresponds to the 1:1 line indicating a perfect match between the measured and predicted values. Root mean square error (RMSE) = 223.38 g/m^2, Willmott's index of agreement (d) = 0.74, and squared Willmott's index of agreement (d^2) = 0.55.

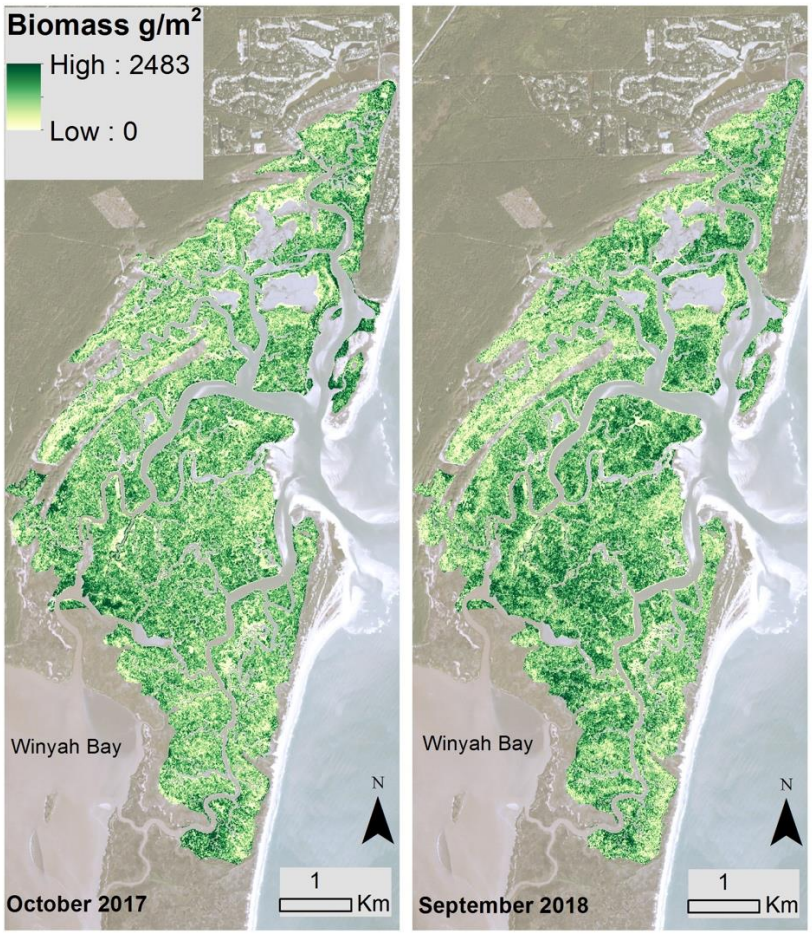

(a) (b)

Figure 3.3. Modeled biomass from the back-transformation of Equation (2) across the marsh landscape at North Inlet from Planet satellite data acquired in (a) October 2017 and (b) September 2018. Basemap images courtesy of Planet Labs, Inc.

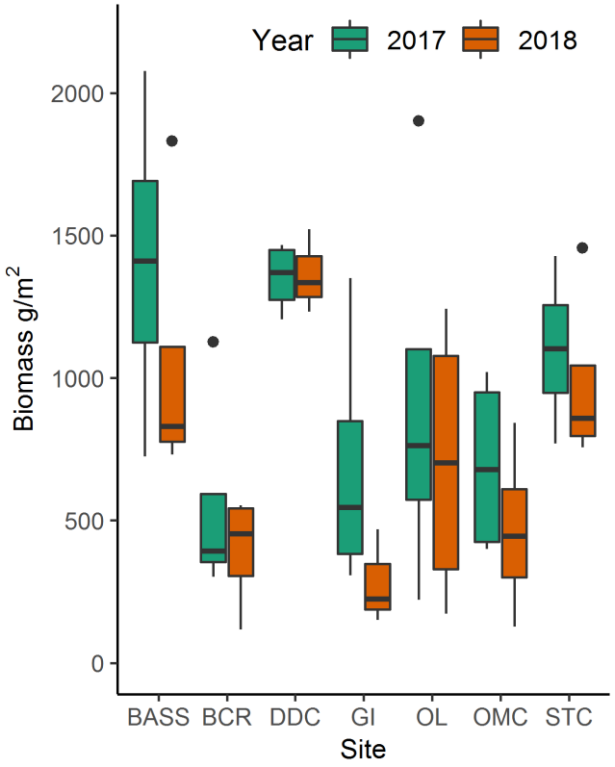

Figure 3.4. Whisker and box plot of field-collected biomass samples within North Inlet. Top and bottom of the boxes indicate the third and first quartile, respectively. Horizontal line within the box indicates the median value and the whiskers indicate the maximum and minimum.

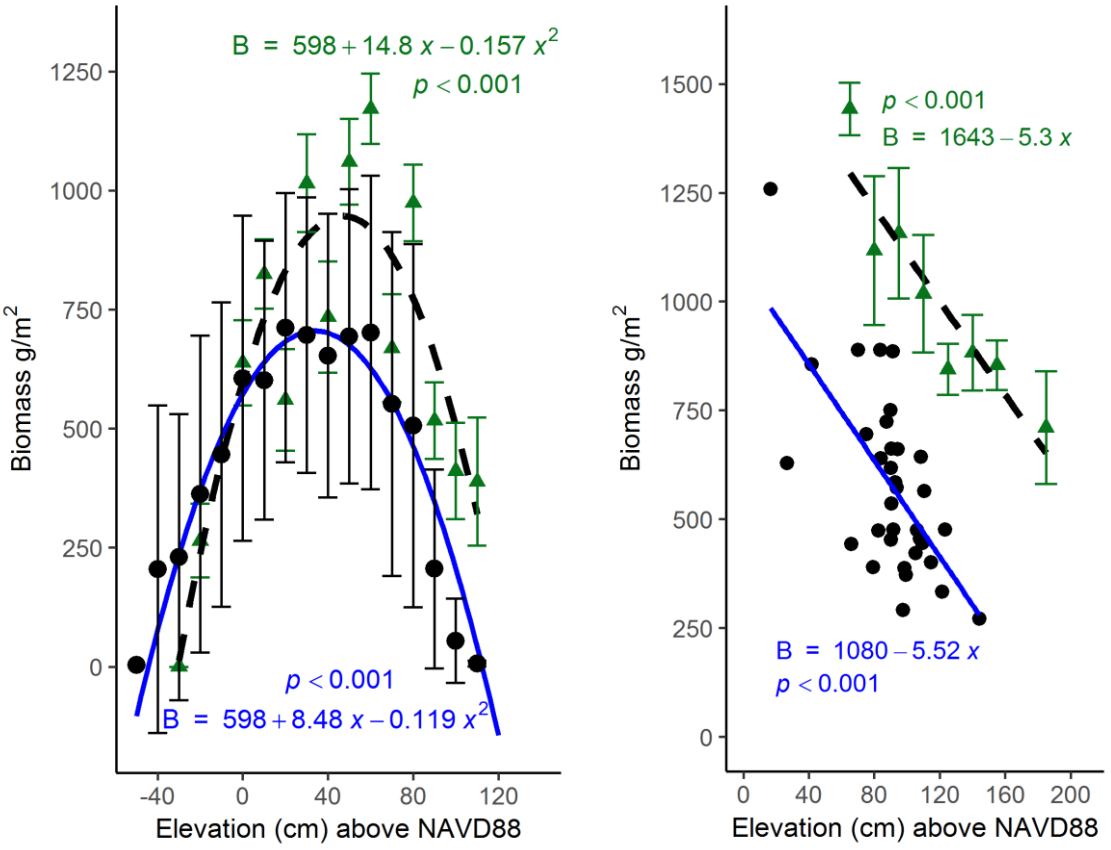

Figure 3.5. Aboveground biomass (g/m²) versus plot elevation (cm) above NAVD88 within North Inlet and PIE. (**a**) North Inlet—shown in black are the means (±1 SD) of calculated biomass found at North Inlet across a range of elevations modeled using Equation (2). Biomass predictions shown here were back-transformed by squaring the model calculation. The blue line is a least-squares fit of a parabola ($p < 0.001$) to these data. Shown in green are the means (±1 SE) from a North Inlet marsh-organ experiment (Morris et al., 2013) and the least-squares best fit of a parabola. (**b**) PIE—black circles are (June) harvested biomass samples from this study collected in salt marshes dominated by *Spartina alterniflora*. The blue regression line indicates dependence of field collected biomass (g/m²) on elevation (cm). Green triangles are means (±1 SE) of end-of-season biomass from in PIE marsh organ experiment (Morris et al., 2013) with dashed linear regression line.

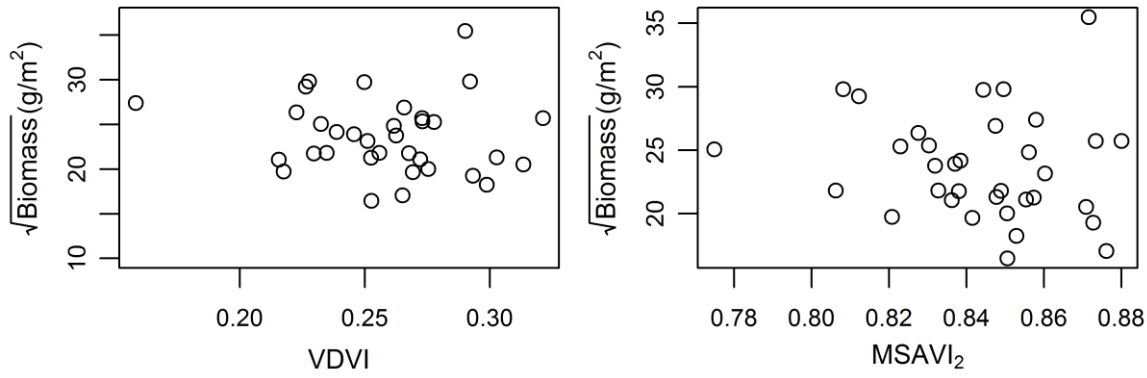

(**a**) (**b**)

Figure 3.6. Square-root biomass g/m² plotted against vegetation indexes within PIE. (**a**) Visible differences vegetation index (VDVI); (**b**) modified soil vegetation index 2 ($MSAVI_2$).

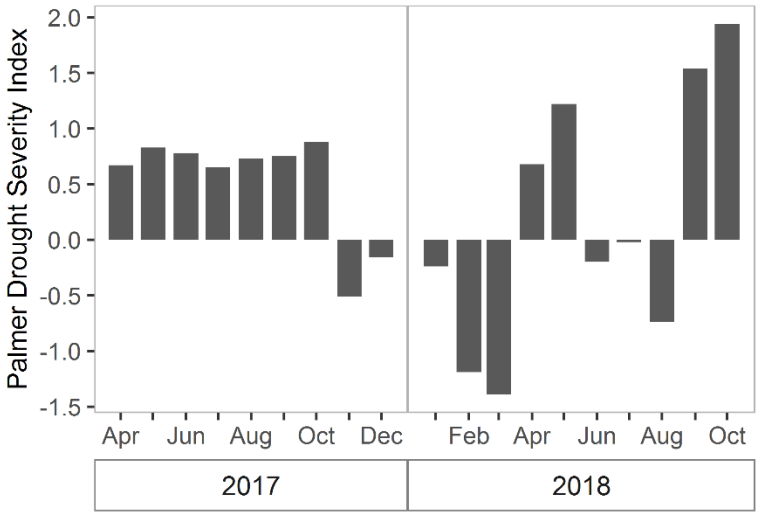

Figure 3.7. Palmer drought severity index for the Northeast South Carolina region. This region encompasses North Inlet. Negative values indicate drought and positive values indicate wet periods. Values between 0.5 and 1 indicate "inceptive wet periods," values between 1 and 2 indicate slightly wet, values between −0.5 and −1 indicate incipit dry spells, and values between −1 and −2 indicate mild drought.

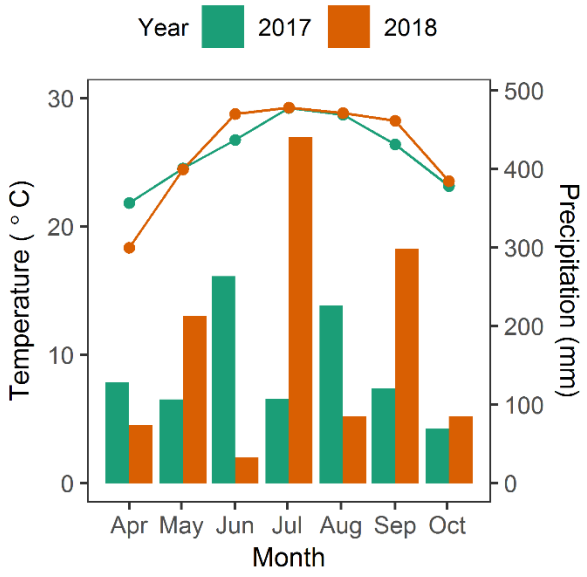

Figure 3.8. Average monthly temperature (°C) and cumulative monthly precipitation during the growing season within North Inlet for 2017 and 2018. The bar graph indicates precipitation and line graph indicates temperature. Data are from a weather station at North Inlet.

(**a**)

(**b**)

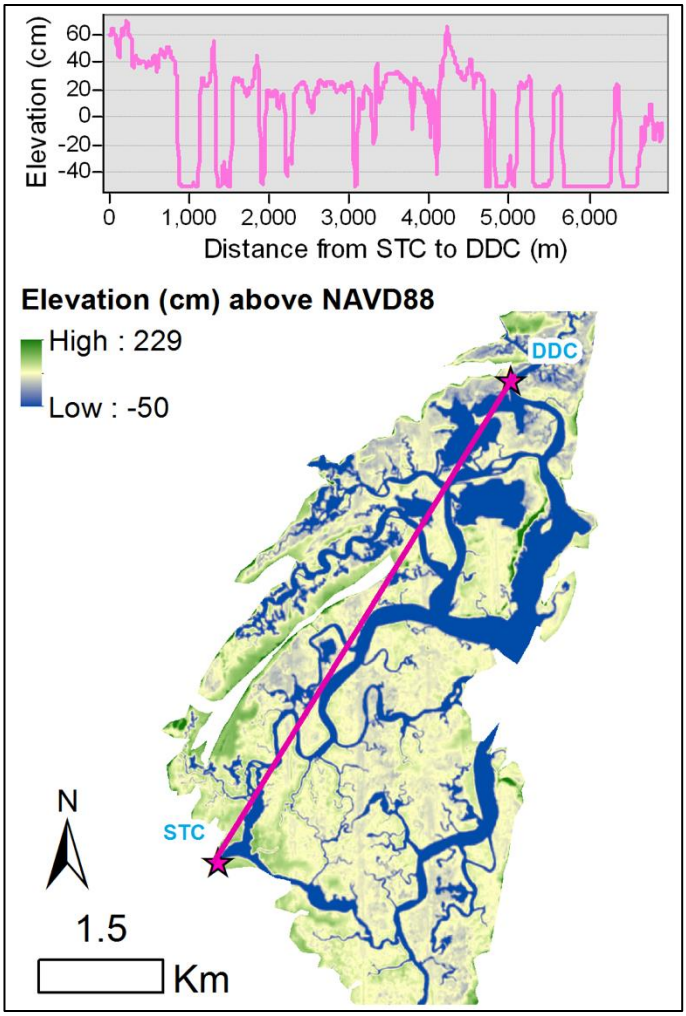

Figure 3.9. Elevation within North Inlet: (**a**) Elevation profile across the estuary from the southernmost sample site (STC) to the northernmost site (DDC) and (**b**) elevation (cm) above NAVD88 with a pink line representing the transect shown in (a).

CHAPTER 4

USE OF COMPUTED TOMOGRAPHY TO INVESTIGATE THE INFLUENCE OF ELEVATION ON BELOWGROUND BIOMASS WITHIN A SALT MARSH

Introduction

Salt marshes provide an array of ecosystem services including improving water quality, sequestering carbon, providing essential habitat for wildlife, acting as a nursery ground for fish, and protecting the coast from storm surges and hurricanes (Fisher and Acreman, 2004; Möller et al., 2014; Mulholland et al., 2009; Whiting and Chanton, 2001). Furthermore, South Carolina is home to the largest extent of salt marshes along the United States East coast and coastal tourism within South Carolina accounts for a large portion of the state's revenue (Salvino and Wachsman, 2013; Willis and Straka, 2017). Sea-level rise threatens salt marsh survival, and salt marsh elevation must increase over time to ensure survival.

Low decomposition rates due to anoxic or hypoxic conditions within salt marshes allow for belowground biomass accumulation (in the form of roots and rhizomes) and peat formation. This accumulation of carbon helps salt marshes build elevation. Within a marsh, areas exhibit varying degrees of aboveground biomass and marsh health, which maybe similar for belowground biomass (Miller et al., 2017; Wang et al., 2017). In the Southeast *Spartina alterniflora* is a dominant salt marsh plant and is often found in large monocrops, making it an ideal study organism. Some factors that control *S. alterniflora* belowground biomass include physical variations, nutrient availability, and the presence of other organisms. There are numerous modelling efforts that predict how a marsh may respond to sea-level rise, and belowground biomass is a key component of these models (Clough et al., 2016; Morris et al., 2002; Mudd et al., 2009). The main aim of this

study is to better understand belowground biomass within *S. alterniflora* dominated salt marshes and observe how elevation and nutrient additions influence biomass production.

Challenges in understanding what is happening belowground

Although belowground biomass has received increased attention due to its high ability to sequester carbon and its importance in marsh survival, analysing this biomass is particularly challenging (Coleman et al., 2004; Morris et al., 2016; Turner et al., 2009; White and Howes, 1994; Wigand et al., 2015). The most common way to quantify belowground biomass reduces important data as it involves collecting soil cores and manually sorting the roots/rhizomes from the soil. This is a labor intensive and time-consuming task and can be impractical when sampling a large volume of data. When washing soil from the root mass, some of the sample is lost and the spatial complexity of the rhizosphere is completely lost. It is also challenging to separate live biomass from dead biomass since the samples are typically sorted by eye, and there are often only minor differences between the dead and live fractions (Darby and Turner, 2008; White and Howes, 1994). Furthermore, when separating roots/rhizomes from the sediment, particles adhere to the biomass skewing the measured weights since it is impossible to completely remove all the sediment (Figure 4.1).

Influences on biomass – Physical variations

S. alterniflora growing close to the creek banks is often called tall form since the height of the grass is taller than *S. alterniflora* growing in the inner portion of

the marsh (which is referred to as short form). Gross et al. (1991) found no seasonal difference in belowground biomass for the short form biomass, while belowground biomass declined during the winter months for tall form *S. alterniflora.* Additionally, when observing belowground biomass versus elevation, past research indicates belowground biomass follows a parabolic dependence on elevation, with the smallest amount of belowground biomass at the lowest and highest elevations (Kirwan and Guntenspergen, 2012; Morris et al., 2013). However, this study looked at plants growing in marsh organs (Figure 4.2), which may not realistically represent what is found within the natural marsh system (Dibbell Burns, 2015). A marsh organ easily facilities studying the effects of elevation on plant growth, but the containers likely have an impact on plant growth since there is limited horizontal water flow, thermal insulation likely is different.

Influences on biomass – Nutrient availability

Nutrients likely have an impact on belowground biomass production, but past studies have conflicting results, indicating that there are possibly additional cofactors that influence root and rhizome growth (Deegan et al., 2012; Wigand et al., 2015). A study in Louisiana found decreased live belowground biomass when applying fertilizers containing phosphorous, iron, or the combination of phosphorous, iron and nitrogen while nitrogen alone had no influence on belowground biomass production (Darby and Turner, 2008). They attributed the decrease in roots and rhizome biomass to reduced nutrient foraging since for

phosphorous was relaxed. Several other studies similarly indicate that nutrient amendments decreased belowground biomass for *S. alterniflora* (Alldred et al., 2017; Deegan et al., 2012; Hines et al., 2006; Valiela et al., 1976; Watson et al., 2014). These reports are countered by many other studies finding nutrient enrichments lead to increased belowground biomass production (Gallagher, 1975; Haines, 1979; Ravit et al., 2007; Wigand et al., 2015).

Computed tomography

Previous marsh studies often made simplifications, such as growing plants in the laboratory or in marsh organs and inaccurately sorting roots/rhizomes and sediment, in order to get needed data. In this study I will overcome these challenges by adopting an underutilized approach by running field collected soil cores through a Computed Tomography (CT) scanner. CT scanners are typically used in the medical field to take images within the body, but can provide a 3 dimensional view of below ground biomass that can distinguish between roots, rhizomes, peat, water, soil and gas (Davey et al., 2011; Sander et al., 2008; Wigand et al., 2015). Most existing studies use General Electric (GE) medical systems instruments or other Fan beam CT instruments in a hospital setting to analyse belowground biomass (Davey et al., 2011; Flavel et al., 2012; Grose et al., 1996; Paya et al., 2015), while no study has use an Epica Pegaso veterinary CT scanner, which is a newer instrument and uses a cone beam .

The use of CT gives a picture of how roots and rhizomes are distributed within the soil and can separate live versus dead organic matter based on their

differences in density (Davey et al., 2011). Past work within *S. alterniflora* marshes investigated the differences between belowground biomass in fertilized versus unfertilized plots (Wigand et al., 2015), but this work did not apply CT technology to assess how belowground biomass changes spatially at different elevations within a marsh. Within this research project I will investigate if belowground biomass production follows a similar parabolic function with elevation above mean sea level, and how fertilizer application influences live and dead belowground biomass abundance. Results from this study will provide valuable information on how belowground biomass changes throughout a marsh. It may also introduce an important new tool for investigating marsh ecology.

Methods

I collected soil cores from the North Inlet- Winyah Bay National Estuarine Research Reserve (North Inlet) at both the Oyster Landing and Goat Island sites (Figure 4.3). At Oyster Landing, I collected two cores from four elevations totalling eight cores per sampling date. I collected cores in October 2018 and May 2019, totalling 16 cores collected at Oyster Landing. Using a Sokkia Series 30R total station, I measured the elevation at each coring location. There are two USGS benchmark locations at Oyster Landing that I used to help establish the elevations along the transect.

I used Goat Island to assess how fertilizer application influences belowground biomass. Goat Island is part of a long-term experiment analysing monthly change in surface elevation. Previously, plots at Goat Island were

fertilized six times a year from June 1996 to August 2004 and May 2006 to August 2016 with 30 and 15 mol/$m^2 \cdot yr$ of NH_4NO_3 and P_2O_5 respectively. Starting in 2014, the nitrogen fertilizer was switched from NH_4NO_3 to NH4/SO4/urea (8.5% Ammoniacal Nitrogen; 25.5% Urea Nitrogen; 10% Combined Sulfur; 1% Chlorine). Fertilizer applications commenced again in June 2017 and are expected to continue monthly for five years. Fertilizer application includes 30 and 15 mol/$m^2 \cdot yr$ N and P, respectively as NH_4/SO_4/urea and P_2O_5 . In all cases the nutrients were buried in small aliquots throughout the plot.

At Goat Island I collected four samples in May 2017, October 2018 and May 2019 totalling 12 cores. The first set of cores taken May 2017 occurred before fertilizer treatments were started in June 2017. During each sampling event, two control and two fertilized cores were extracted. A larger sample size was not possible due to the limited plot size receiving fertilizer. Since USGS benchmark locations were not available for establishing elevation with a total station, I did not measure elevation at Goat Island. However, elevation was previously measured using RTK-GPS and elevations ranged from 0.42 - 0.44 (m) above mean sea level.

Sample Collection and preparation

For sample collection, I used PVC tubes in October 2018 and polycarbonate tubes in May 2017 and May 2019. The PVC tubes were 30 cm long by 10 cm diameter and the polycarbonate tubes were 40 cm long with a 10 cm diameter all tubes were 6.35 mm thick. I placed the tubes over the sample locations and clipped

the aboveground biomass to the soil surface. Cores were pounded into the ground, extracted and placed in a cooler for later analysis.

In order to separate root/rhizomes, peat, sand, air, and water within each scan, I placed calibration rods of known densities into half of the soil cores. A previous study demonstrated calibration rods of sea water, 34% colloidal silica, air and glass allowed for the separation of the materials in question (Davey et al., 2011). The attenuation of X-rays depends strongly on the specimen density. Hence, using calibration rods of known density allows for determination of the densities for the remaining features in the acquired CT scans, based on the image contrast recorded. This in turn allowed me to classify organic matter as root, peat, sand, air etc. Each of the selected cores contained four different rods; glass, 34% colloidal silica, water or air. The colloidal silica, water and air calibration rods were fabricated by filling 8 mm plastic pipets with the respective material and sealing the ends with silicone sealant. The glass calibration rod was an 8 mm diameter stirring rod. These calibration rods were selected based on previous studies (Davey et al., 2011). The density of the material scanned influences the Hounsfield unit (HU) value, which is a normalized unit of measurement for image contrast in the CT scanner.

I transported the cores to the Charleston Aquarium for analysis on their Epica Pegaso veterinary CT scanner. The CT scanner operator set the instrument to run with an X-ray tube current of 100 mA, a voltage of 100 kV and slice thickness of 300 µm; using several tests runs with various X-ray tube currents and voltages,

the CT scanner operator determined the ideal settings for this analysis. The cores were laid down latterly and scanned horizontally (Figure 4.4).

To process the data, I used Horos Project software, which allows the user to visualize the CT data and manipulate the Images, including removal of images of the PVC or Polycarbonate tubes and calibration rods from the data. The software also allows the user to highlight features based on their HU readings, which allows for the classification into features such as roots and rhizomes.

After the cores were scanned through the CT scanner, they were brought back to the laboratory and the roots and rhizomes were separated from the soil. Live and dead belowground biomass was further separated and dried at 60°C for 72 h, or until a constant weight was reached. Aboveground biomass was also dried at 60 °C for 72 h, or until a constant weight was reached.

Statistical Analysis

The R coreCT package was used to quantify the different materials in each core (Hill and Davey, 2017). CoreCT uses the HU ranges to distinguish and automatically categorize the target materials and integrate each material over depth. This allows the user to visualize the total area and mass of each variable in the soil core, as well as how the total area of each variable changes with depth in the core. The HU ranges are derived from the calibration rods as discussed earlier. Based on the HU units and densities of the materials in the calibration rods, CoreCT automatically estimates the mass (g) of each target material. The package

does this by multiplying the voxel (volumetric pixel) bulk density by volume (cm^3).

Linear regression analysis was used to examine the relationship between elevation and either live or dead biomass. A nested ANOVA analysis was performed to test for differences in biomass by sample date and site. For Goat Island, I used ANOVA analysis to compare average live and dead biomass versus May 2017, October 2018 and May 2019 date categories. I also ran a nested ANOVA for average live and dead biomass versus May 2017, October 2018 and May 2019 date categories group by treatment (fertilized or control). To examine how live and dead biomass changed with depth, I calculated the cumulative sum or live roots/rhizomes and the cumulative sum of dead roots and rhizomes and graphed them versus depth. I then calculated the depth where a 50% and 90% of the biomass lies above. For easier visualization, only 13 random cores where graphed.

Results/Discussion

The Epica Pegaso CT scanner successfully imaged soil cores for belowground biomass analysis (Figure 4.5 and Figure 4.6). Throughout this study, I used the wet weight CT derived values however, CT derived wet weight can be multiplied by 35% to convert the weight to its estimated dry weight equivalent. This correction factor is based on previous work done by the Environmental Protection Agency (Kibby et al., 1980). For higher hand sorted and dried weights, there appears to be more error between the CT values and the hand sorted values (Figure 4.5). However, the error might be attributed to increased small rocks in the

hand sorted weights (Figure 4.1). It was progressively more difficult to remove the small rocks from the larger samples, which likely skewed the hand sorted weights.

At Oyster Landing, both live and dead belowground biomass increased with elevation, and this effect was more pronounced in the dead biomass fraction (Figure 4.7). Since the slope of the regression line relating elevation to biomass was larger for the dead biomass fraction over the live biomass fraction, the turnover rate is likely higher for the plants in higher elevations. If the turnover rates were equivalent then the slopes of the two regressions should be similar. There was no significant difference between fall (October) and spring (May) belowground biomass, though the average biomass value in spring appeared to be higher than in fall ($p > 0.05$; Figure 4.8). These results indicate that belowground biomass does not substantially change between fall and spring and belowground biomass abundance is influenced by elevation. Since belowground biomass increases with elevation above MSL, one may predict that as sea-level rises plants will begin to reduce their belowground biomass production. This is because the plants at the higher elevations above mean sea level produce more belowground biomass within the elevations sampled, as sea level rises the relative elevation above mean sea level will decrease. This subsequently may cause the plants to produce less belowground biomass However due to the nature of the sampling location, I could not sample belowground biomass at the higher end of *S. alterniflora*'s growth curve. Future work can be conducted to extend the range of elevations to incorporate the upper end of the growth curve. This will help determine if

belowground biomass follows a parabolic relationship similar to aboveground with elevation above mean sea level as suggested by previous work (Kirwan and Guntenspergen, 2012; Miller et al., 2019; Morris et al., 2013).

The average total volume of the larger roots/rhizomes collected from Oyster Landing did increase from October 2018 to May 2019 (Figure 4.9). In May 2019, the 0.2 mm to 10 mm diameter roots/rhizomes volume was greater than in October 2018 ($p < 0.04$), while there was no difference between the smaller size fractions ($p > 0.1$). The rhizomes likely decreased in volume over the winter and started to increase in volume again in spring at the beginning of the growing season. However, more work should be conducted to investigate this since this study did not collect data throughout the entire year.

The final parameter I analysed at Oyster Landing was belowground biomass abundance as a function of depth. Greater than 50% of live roots/rhizome mass occur within the top 7.9 cm of the soil surface while greater than 50% of the dead root/rhizome mass occurs within the top 10.7 cm of the soil surface (Figure 4.10). As roots and rhizomes die, they either decompose or they resist decay and remain buried. Therefore, depth of the dead biomass is deeper than that of the live fraction. For both the live fraction and dead fraction of biomass, 90% of the mass occurs within the roughly the first 22 cm of the soil surface (Figure 4.10). Based on visual inspection, occasionally a rhizome would extend down the length of the core. Which is likely the reason why 90% of the live and dead fraction fall within similar depths. This depth analysis validates our selection of using 30 cm cores for

analysis since the majority of the live and dead biomass mass falls within this depth.

Belowground biomass between Oyster Landing and Goat Island shows that live spring belowground biomass is higher at Goat Island than Oyster landing ($p < 0.01$), and there was no difference observed between live fall biomass abundance ($p > 0.05$). Observed dead belowground biomass in the fall and spring was higher at Goat Island than at Oyster Landing ($p < 0.01$). It should also be noted that despite no elevation measurements taken at Goat Island within this study, past work indicates that the sampled locations are roughly 0.4♣m above MSL. This puts the elevations of the Goat Island samples within the median elevation range of oyster landing. Given this, the difference in biomass is not due to elevational differences between Goat Island and Oyster Landing.

Comparing sample date results amongst the Goat Island treatments (Fertilized and Control), date sampled may influence live belowground biomass (Figure 4.8). May 2019 had higher average live belowground biomass than in October 2018 ($p < 0.01$). However, when looking at pre-fertilizer treatments (May 2017), I observe May 2017 had significantly less live biomass than May 2019 ($p < 0.01$; Figure 4.11). This may indicate there being a strong inter-annual difference in belowground biomass.

When separating the treatments, it is not apparent that the fertilizer treatment increased live belowground biomass within Goat Island ($p > 0.1$) nor the ratio of live belowground biomass to aboveground biomass (Figure 4.13 and

Figure 4.12). The average belowground to aboveground ratio for all samples combined was 1.56 (Figure 4.12). The average belowground to aboveground ratio for May samples at oyster landing was 1.80, and 0.85 for October. For Goat Island, the belowground biomass to aboveground biomass ratio was 1.86 for fertilized and 2.04 for control samples. The belowground biomass to aboveground biomass ratio seemed to decline with the fertilized treatment, which is supported with past research (Good et al., 1982). However, there was no significant difference between the ratios for each of the four categories (Oyster Landing - October, Oyster Landing -May, Goat Island - Fertilized, Goat Island - Control; $p = 0.29$). There was no significant difference observed between control and fertilized belowground biomass samples within each sample date. However, it is evident that live belowground biomass in both treatments were higher in May 2019 than in May 2017, indicating that at Goat Island there possibly was inter-annual variability contributing to differences in belowground biomass production. The total volume (cm^3/L) also did not differ between the control and fertilized samples for any of the root diameter size classes. The root volume for both treatments was greatest for larger root/rhizome diameter class (2.5-10 mm), but there was no difference between the control and fertilized samples ($p > 0.05$).

For dead belowground biomass at Goat Island, May 2017 had higher overall average dead belowground biomass than October 2018 ($p < 0.01$) and May 2019 ($p < 0.01$) while there was no significant difference between October 2018 and May 2019 ($p > 0.90$; Figure 4.11). When separating the different treatments (fertilized

and control), there was no difference between any of the categories (date or treatment $p > 0.19$; Figure 4.15). This indicates that fertilizer application had no effect on dead belowground biomass, however the sample size was small (n = 2 for each date and treatment) which may have been why no significant difference was detected for either the live or dead fraction. The previous study looking at fertilizer application and belowground biomass within Goat Island occurred in August 2008, when the nitrogen fertilizer type was different (NH_4NO_3 in Wigand's study versus NH4/SO4/urea in this study) and the plots started to receive fertilizer treatment in June 1996 (Wigand et al., 2015). Fertilizer treatment may have a delayed response in belowground biomass growth which may not have been captured in this study but was in Wigand et al.'s work (2015). Furthermore, though their samples were also collected at Goat Island, their sample location was different than this study. *S. alterniflora* phenotypic traits can vary even if they have the same genotypes, thus the plants may respond differently to fertilizer application (Hughes, 2014). These factors may be partially why Wigand et al.'s results were different from this study (2015).

Conclusion

The use of Computed Tomography is a helpful tool for better understanding belowground biomass production. Using CT to classify belowground biomass reduces classification error between live and dead biomass. Hand sorting the samples also often contained small rocks that were adhered to many of the roots, CT classification further reduces this error since the need for

manual sorting was eliminated. Results from this study can help improve modelling efforts by filling a current knowledge gap of how belowground biomass changes over elevation within the landscape. A majority of similar work is conducted within constructed microcosms may laterally constrained root/rhizome growth and limit horizontal water flow. These constructed systems therefore may skew what is observed in a more natural setting. Though there are limited studies analysing how marsh organs or other constructed microcosms differ from the natural marsh, one study indicates that growth patterns differ between the two (Dibbell Burns, 2015).

Through this study I found that both live and dead belowground biomass follow a positive trend with elevation, with the highest elevations sampled having the highest belowground biomass. Though this study did not find a significant difference between fertilized and control samples, there was a significant difference between biomass abundance at different sites within North Inlet. This indicates that elevation alone does not completely dictate belowground biomass abundance within North Inlet (and likely other marshes as well), and more work should be conducted to analyse other factors that may be causing this difference such as suspended sediment concentration, biotic life, soil type and pore water nutrient concentrations. Furthermore, though there might be a fall/spring change in belowground biomass, this is trumped by the apparent larger inter-annual variation in belowground biomass as observed at the Goat Island location.

Figure 4.1. Image highlighting how particles adhere to the roots and rhizomes, making it difficult to completely separate the sediment from the biomass

Figure 4.2. Image showing the profile view of a marsh organ, representing the highest elevation. The plants are all contained within the PVC tubes, which are open at the bottom.

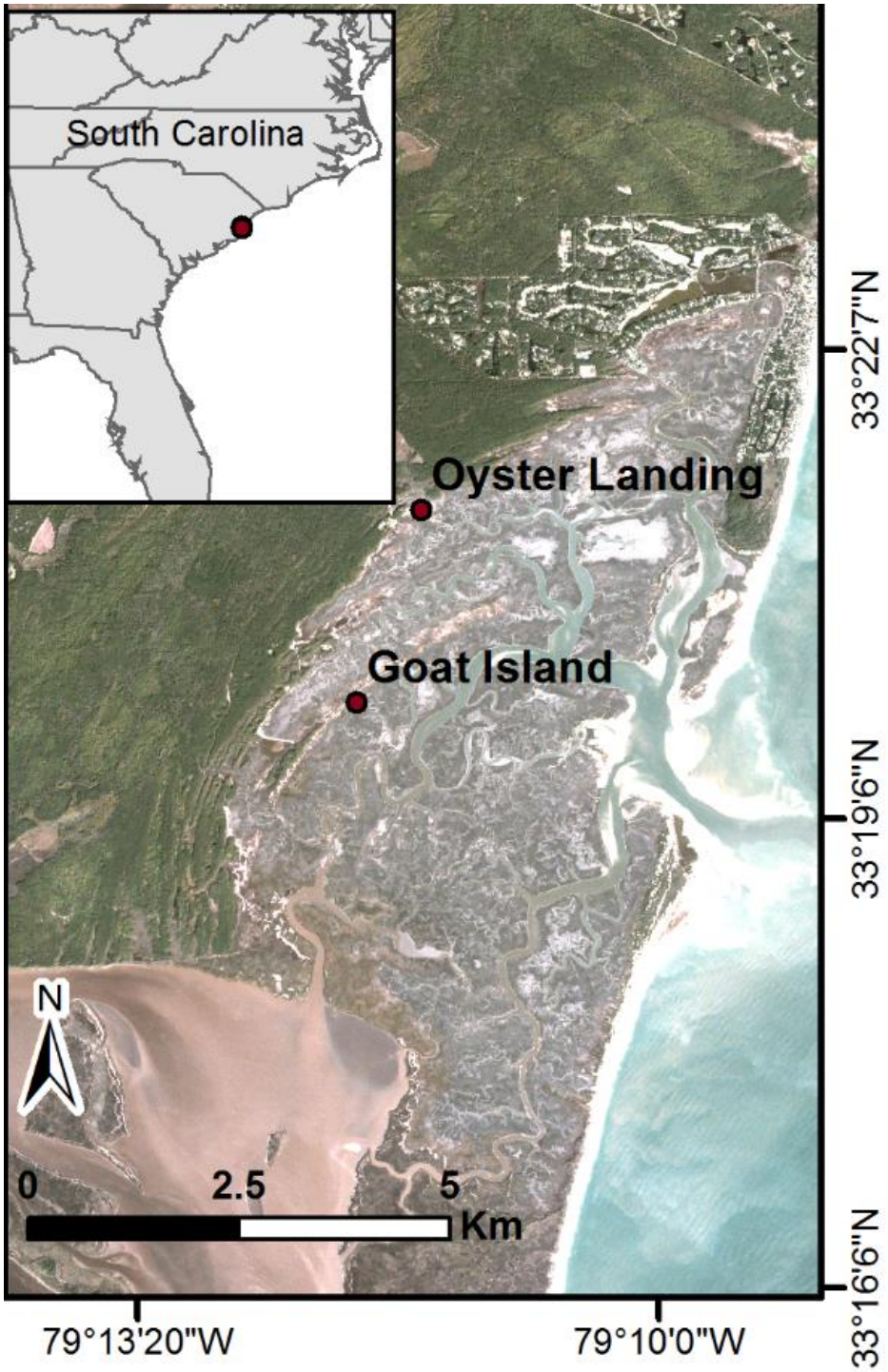

Figure 4.3. The study location is at the North Inlet Winyah Bay National Esturine Research Reserve In South Carolina. The two sampling sites, Oyster Landing and Goat Island, and shown by red dots.

Figure 4.4. Soil core being scanned through an Epica Pegaso CT scanner at the Charleston Aquarium

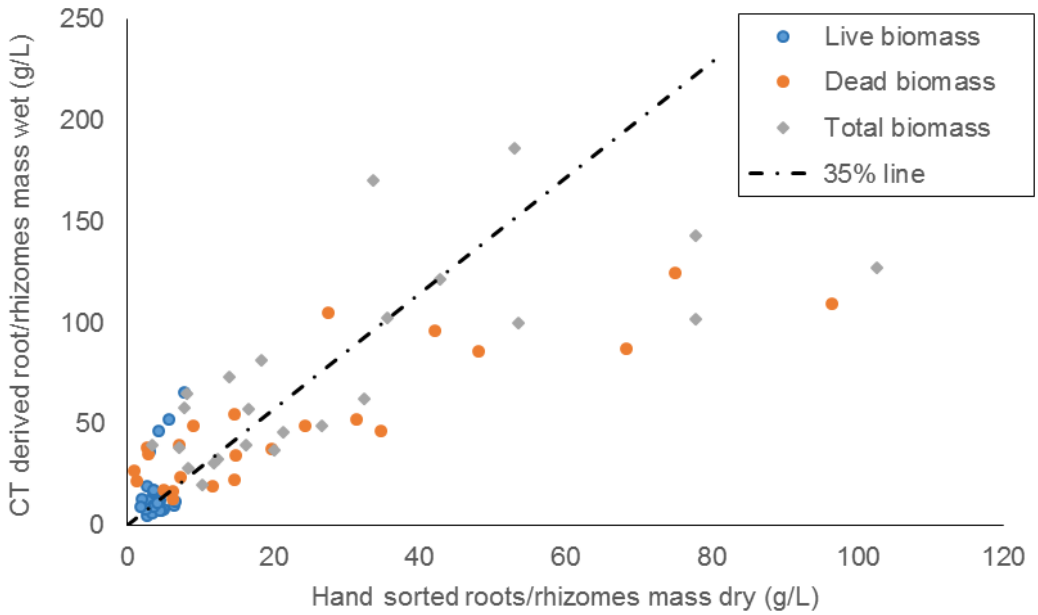

Figure 4.5. Relationship between CT derived wet belowground biomass mass (g/L) and hand sorted dry belowground biomass mass (g/L). Blue circles indicate only the live fraction, orange circles only the dead fraction and grey diamonds represent the summed live and dead belowground biomass. The dry weight of *S. alterniflora* is estimated to be 35% of its wet weight. The 35% line thus is where a 1:1 CT dry weight equivalent to the hand dry weight lies.

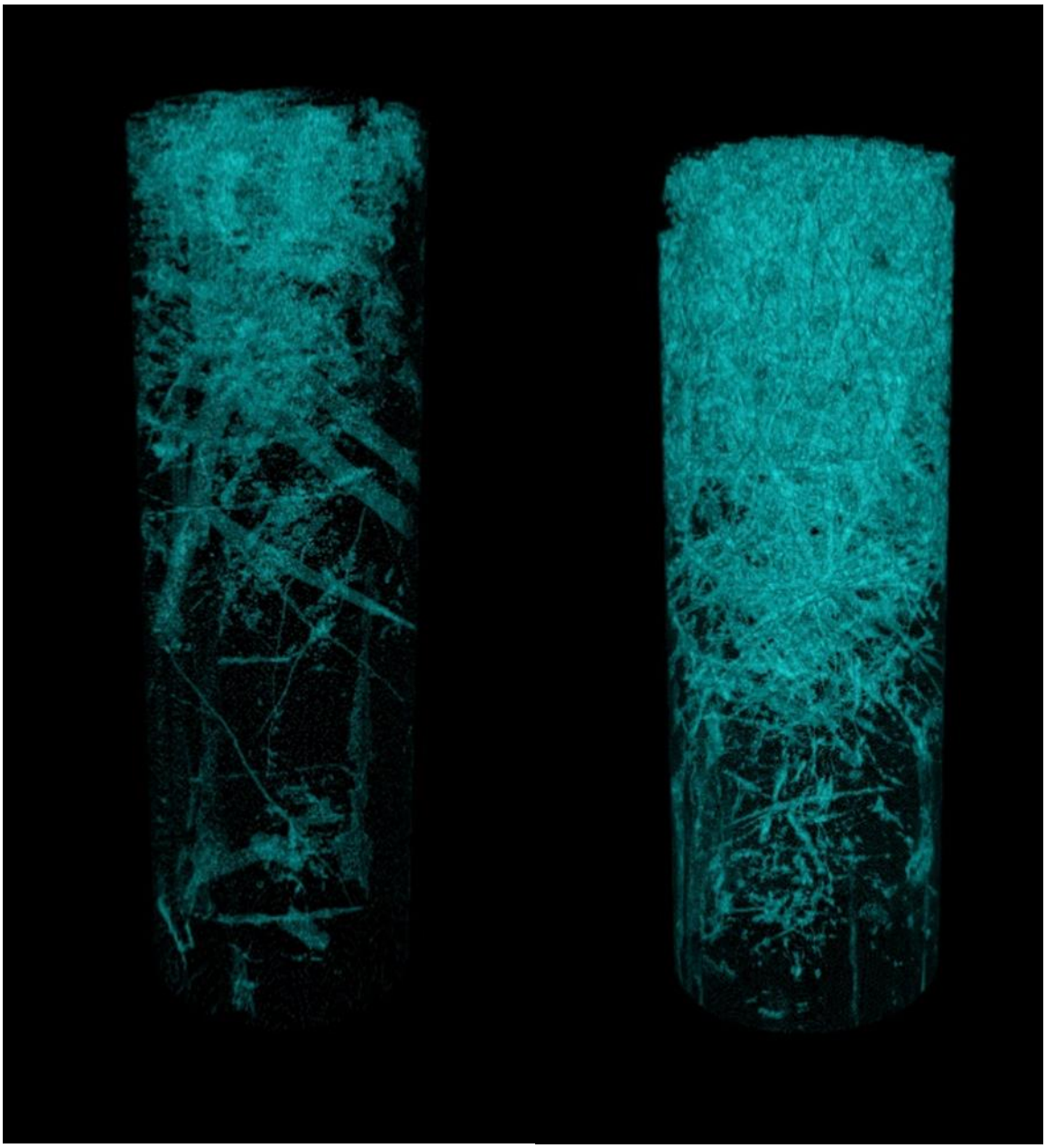

(A) (B)

Figure 4.6. Example of dead biomass detected from CT scan analysis. Figure A is a core from a control treatment at Goat Island and Figure B is a core from Oyster landing. Both cores were collected in May 2019.

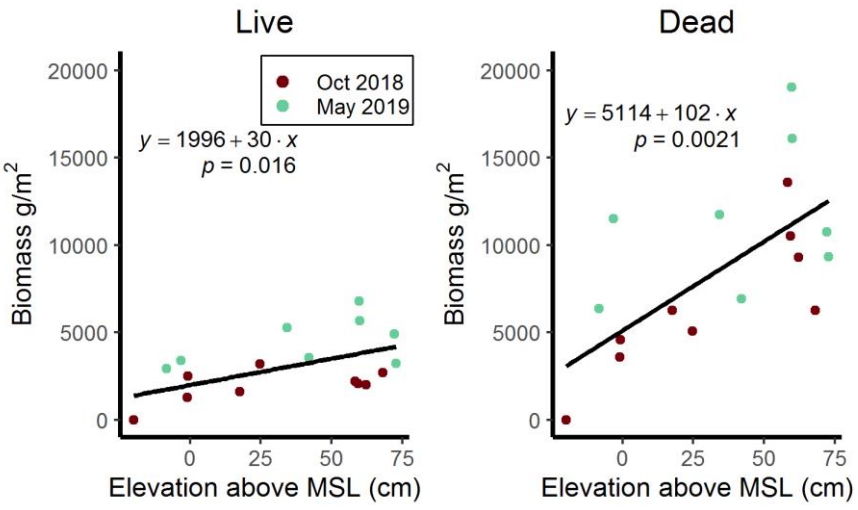

(A) (B)

Figure 4.7. Belowground biomass (wet g/L) versus elevation detected by CT analysis for both the (A) live fraction and (B) dead fraction within Oyster Landing.

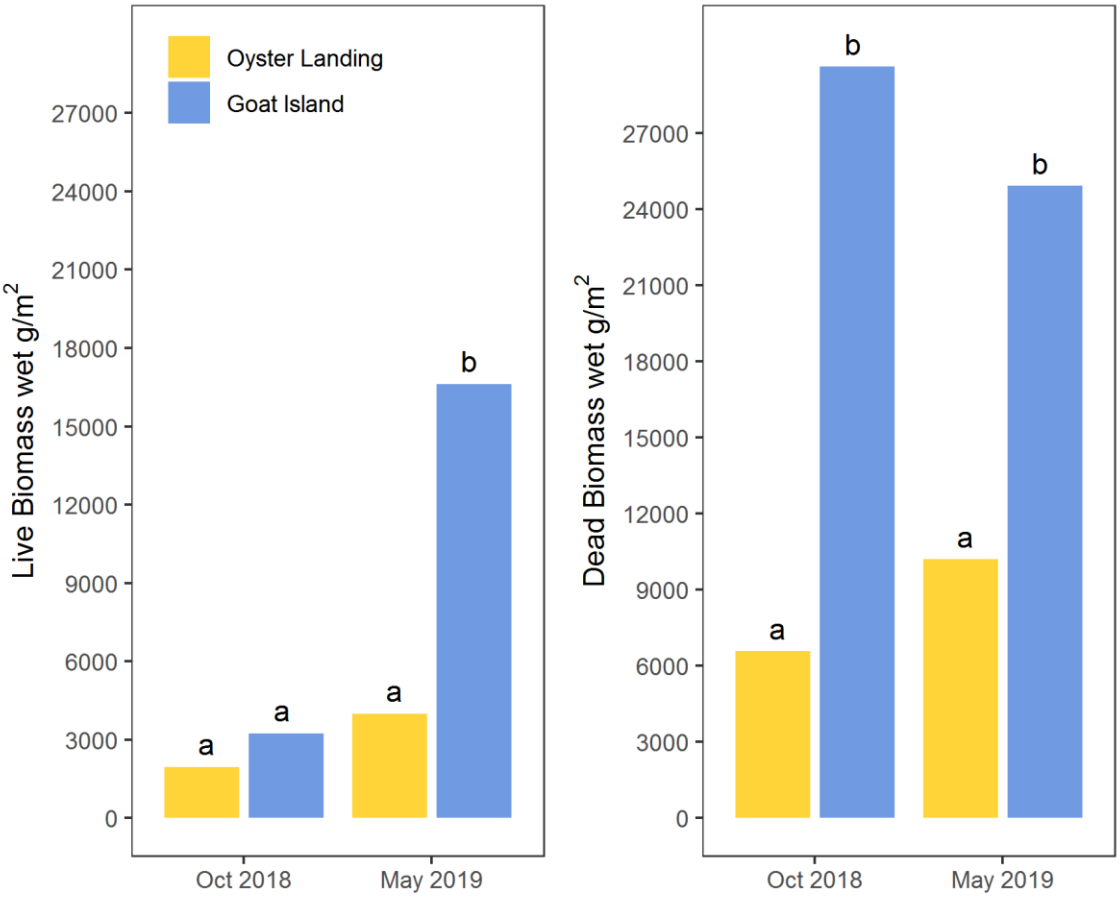

Figure 4.8. Belowground biomass detected by CT analysis sorted by sampling date for (A) the average live fraction (wet g/m^2) and (B) dead fraction (wet g/m^2). Yellow represents samples collected at Oyster Landing and blue represents samples collected at Goat Island. Bars with different letters indicate significant differences ($p < 0.05$).

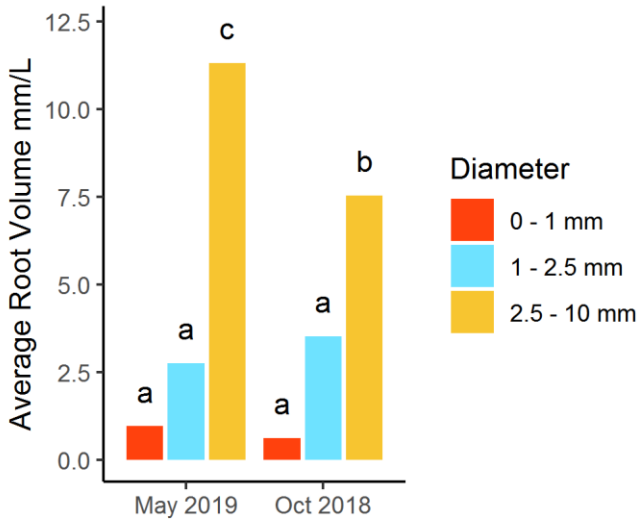

Figure 4.9. Averaged total root/rhizome volume (cm^3/L) detected by CT analysis in cores collected from Oyster Landing broken up by root/rhizome diameter size class. Different letters indicate significant differences ($p < 0.05$).

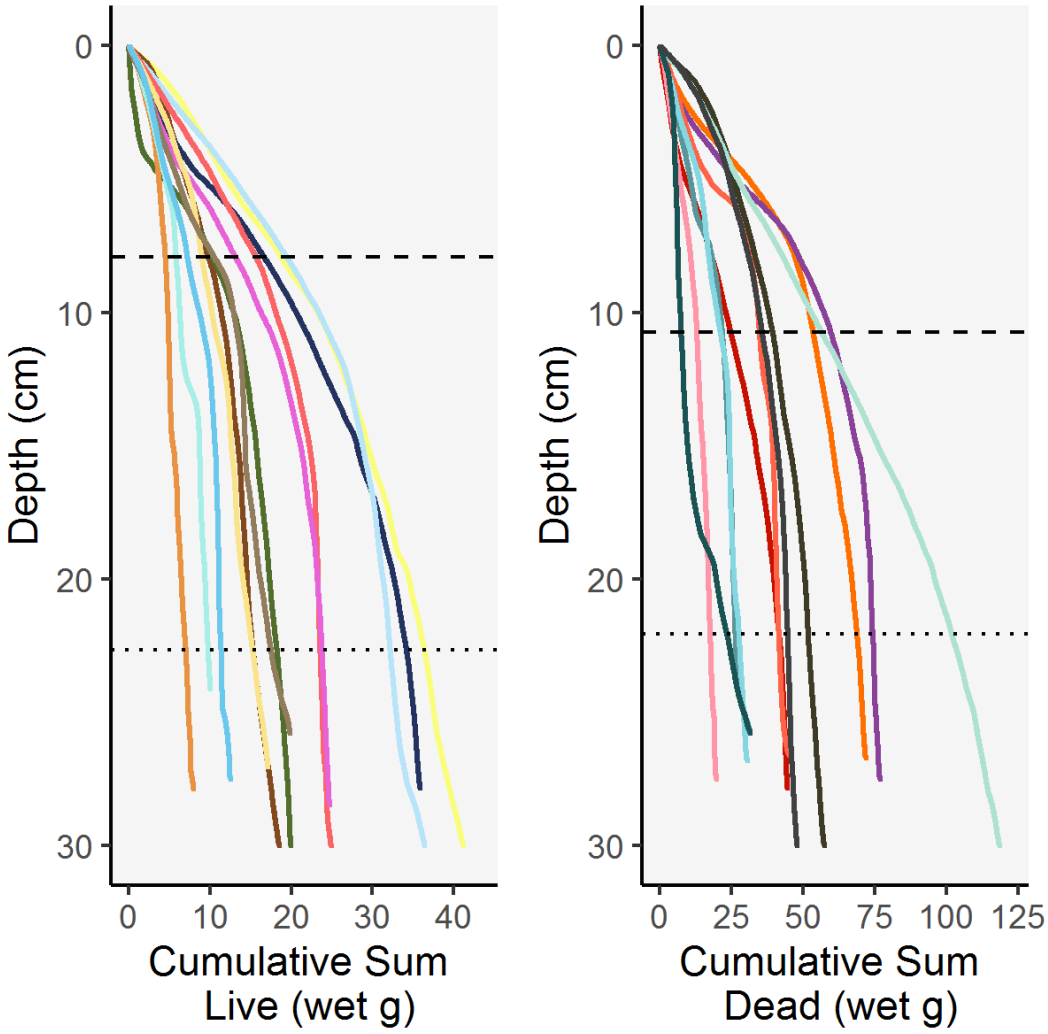

(A) (B)

Figure 4.10. Cumulative Sum of the (A) live belowground biomass and (B) dead belowground biomass as a function of depth within Oyster Landing. Greater than 50% of the cumulative summed biomass weight falls above the black dashed line and 90% of the cumulative summed biomass falls above the black dotted line. Solid colored lines each represent a different core sampled at Oyster Landing. For easier visual representation only a portion of the samples are displayed.

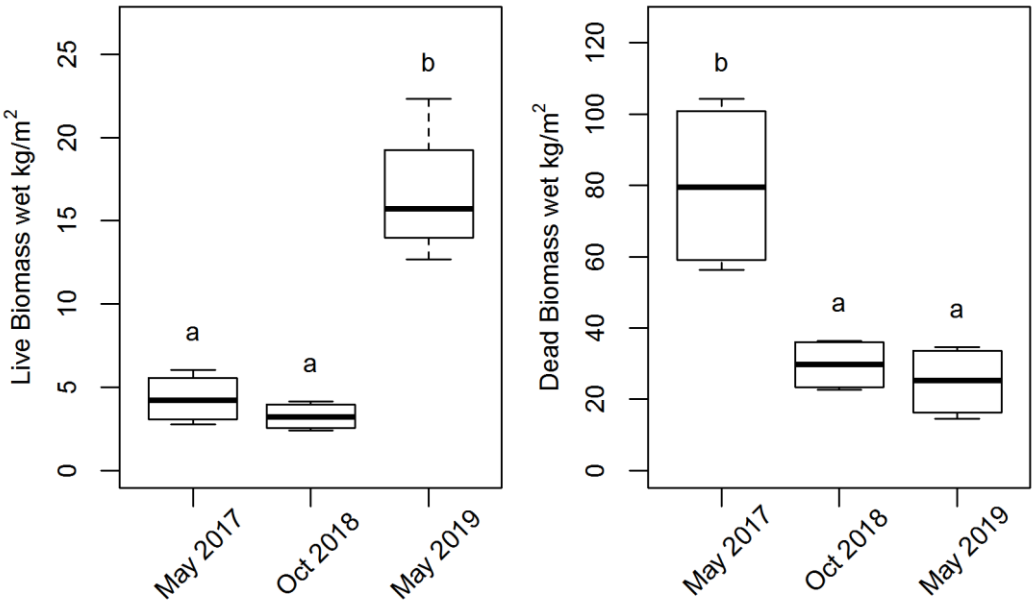

(A) (B)

Figure 4.11. (A) Average live belowground biomass (wet kg/m^2) and (B) average dead belowground biomass (wet kg/m^2) detected by CT analysis within Goat Island plots. Data represent pooled fertilized and control data. Different letters indicate significant difference ($p < 0.05$) between each of the sample dates.

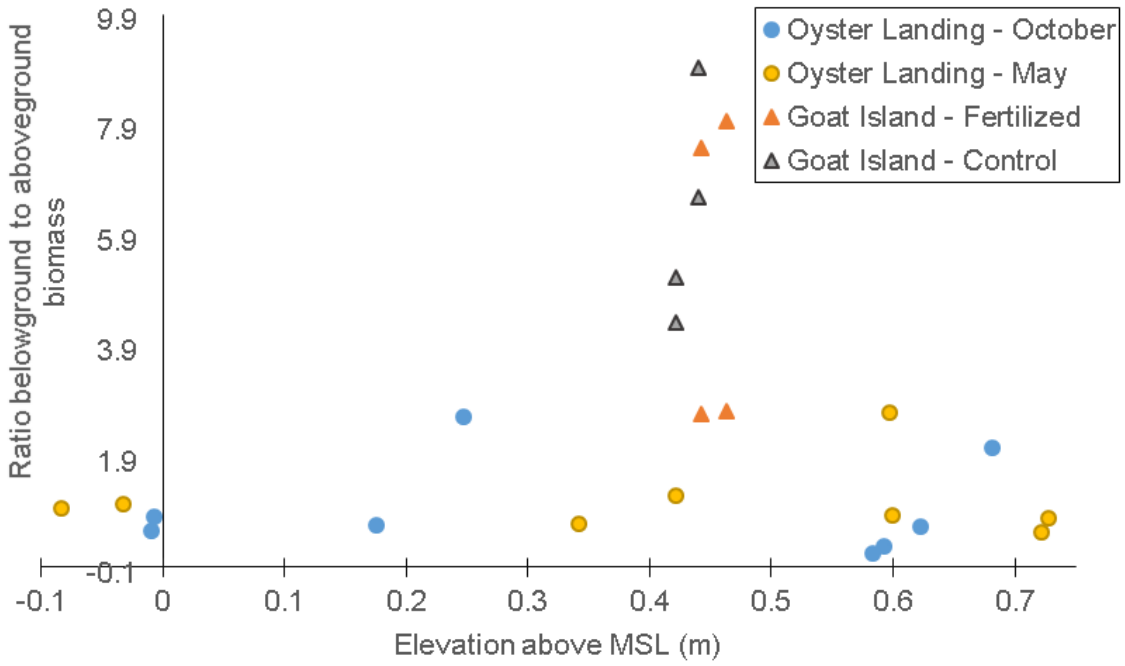

Figure 4.12. Ratio of belowground biomass to aboveground biomass. Aboveground biomass is dry weight (g), and belowground biomass is the CT derived wet weight (g) with a correction factor to convert the wet weight to dry weight

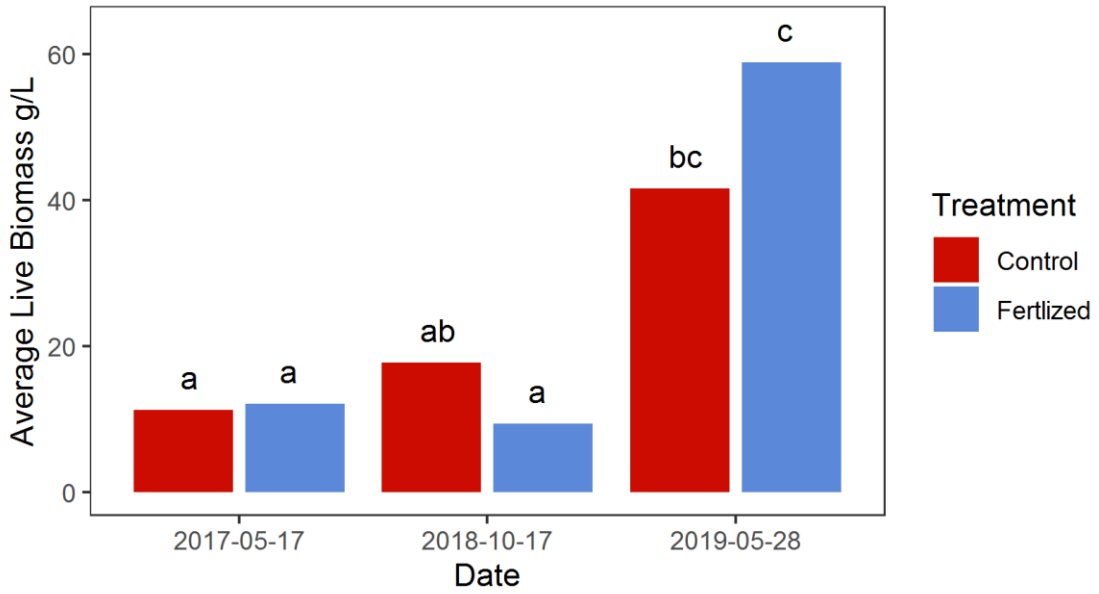

Figure 4.13. Average live belowground biomass (wet g/L) detected by CT analysis within Goat Island. Red bars indicate control plots while blue bars indicate fertilized plots. Different letters indicate significant difference ($p < 0.05$) between fertilized and control plots for each of the sample dates.

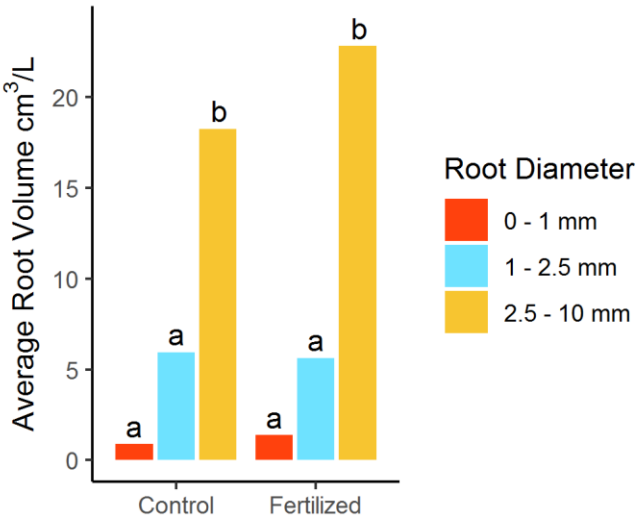

Figure 4. 14. Averaged total root/rhizome volume (cm^3/L) detected by CT analysis in cores collected from Goat Island broken up by root/rhizome diameter size class and treatment (control versus fertilized). Different letters indicate significant differences ($p<0.05$).

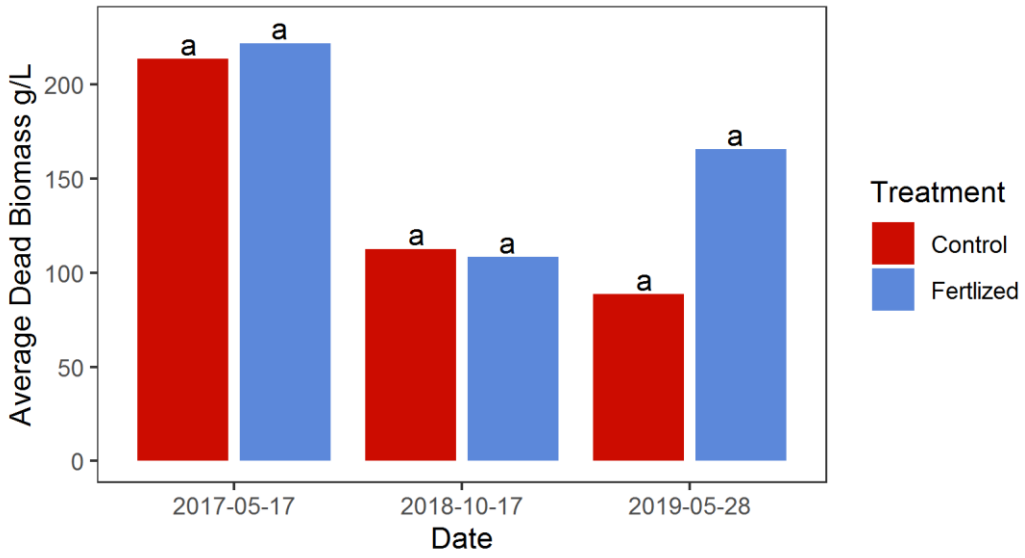

Figure 4.15. Average dead belowground biomass (wet g/L) detected by CT analysis in Goat Island plots. Red bars indicate control plots while blue bars indicate fertilized plots. There was no significant difference ($p < 0.05$) between fertilized and control plots for each of the sample dates.

CHAPTER 5

MAPPING SALT MARSH DIEBACK AND CONDITION IN SOUTH CAROLINA'S NORTH INLET-WINYAH BAY NATIONAL ESTUARINE RESEARCH RESERVE USING REMOTE SENSING[2]

[2] Miller, G. J., Morris, J. T., and Wang, C. (2017). Mapping salt marsh dieback and condition in South Carolina's North Inlet-Winyah Bay National Estuarine Research Reserve using remote sensing. *AIMS Environ. Sci.* 4, 677–689. doi:10.3934/environsci.2017.5.677
Reprinted with permission of publisher

Introduction

Salt marshes are ecologically important and provide an array of ecosystem services such as storm-surge protection, carbon storage, improvement of water quality, and habitat for wildlife (Möller et al., 2014; Webster et al., 2005). Within the east and gulf coasts of the United States, hurricanes and sea-level rise are two large threats to human populations and infrastructure. The salt marshes in these regions are particularly valuable in protecting communities against these environmental events. With climate change projections, sea-level rise will continue and hurricane intensity is predicted to increase (Michener et al., 1997; Webster et al., 2005). Threats to salt marsh health arise with development, pollution, and environmental changes. One such phenomenon that occurs on a global scale is marsh dieback (also known as brown marsh), where periodically large areas of smooth cordgrass, *Spartina alterniflora*, suddenly thin in coverage or die, resulting in a sparsely vegetated area or transformation into a mudflat (Elmer et al., 2012; Ogburn and Alber, 2006; Ramsey and Rangoonwala, 2005). Though typically marsh dieback impacts *S. alterniflora*, other salt marsh plants such as *Juncus roemerianus, J. geradii, Distichlis spicata*, *S. patens*, *and S. phenomena* are also affected (Alber et al., 2008; Ogburn and Alber, 2006; Smith and Carullo, 2007). Dieback events can be quite large, such as an event in Louisiana which impacted more than 100,000 ha of salt marsh habitat (McKee et al., 2004). Regions impacted by marsh dieback often grow back, usually over a period of years and ecosystem services are degraded during this period (Elmer et al., 2012). The exact cause of marsh

dieback is unclear, but herbivory, sulphide toxicity, elevated salinity and drought are believed to contribute to the dieback in some regions (Alber et al., 2008; Elmer et al., 2012; McKee et al., 2004).

Researchers have conducted both field campaigns and remote sensing analysis to better understand the causes and extent of marsh dieback. In Louisiana, several researchers conducted remote sensing analysis to detect biophysical changes within dieback regions. One such study analysed the changes in leaf reflectance in blue, green, red, near infrared (NIR) wavelengths using multispectral sensors in various dieback and healthy regions. They found the band ratio NIR/green was most effective for monitoring impacts (Ramsey and Rangoonwala, 2005). Another study used satellite data from Landsat Thematic Mapper (ETM+), Satellite Pour l'Observation de la Terre (SPOT), and NASA Uninhabited Aerial Vehicle synthetic aperture radar (UAVSAR) to map marsh dieback during the 2008 event (Ramsey et al., 2014). They took a slightly different approach from Ramsey and Rangoonwala (2005) and estimated biomass changes within dieback regions using before and after imagery from the same region. They determined that UAVSAR'S horizontally sent and vertically received (HV) backscatter was the best polarization for detecting changes within marsh biomass. They also determined that, for SPOT and ETM+, the band ratio of NIR/red was an effective vegetation index to use for change detection mapping of marsh extent. This vegetation index was also used for assessing *S. alterniflora* health (Couvillion and Beck, 2013). Within Georgia, a study using geographic object-based image

analysis with multispectral very high resolution (0.3 m) data to classify marsh coverage within a dieback affected region (Kim et al., 2011). The study determined that using both multi-scales and texture data when segmenting an image for land type classification improved the accuracy of image classification.

South Carolina has roughly 344,500 acres of salt marsh habitat, and is home to the largest expanse of salt marsh of any state on the U.S. East Coast (South Carolina Department of Natural Resources, 2015). Field studies of marsh dieback events in South Carolina have focused on the causes. With herbivory experiments, Kiehn and Morris (2009) found that periwinkle snail densities, which primarily forage on the epiphytes on leaves of *S. alterniflora*, causing leaf damage (Silliman and Bertness, 2002), had no significant relationship with marsh primary production on permanent plots at North Inlet, SC. Researchers also used the Palmer drought severity index to assess the importance of drought. Though it is not a definite link to dieback events, several locations that experienced drought subsequently experienced a dieback event (Alber et al., 2008; Hughes et al., 2012). Agrelius (2015) examined methylation of *S. alterniflora* DNA, an epigenetic process affecting fitness, but did not find evidence for a change in global methylation as the cause of brown marsh at North Inlet estuary, SC. DNA is methylated when a methyl group is added to DNA; this helps control gene expression, but may also reduce stress tolerance (Agrelius, 2015).

Despite these studies, there is no spatial analysis of marsh dieback within South Carolina, which might help determine causes of dieback events. This study

aims to map the extent of marsh dieback during a 2001-2003 event at North Inlet estuary, South Carolina. This event also was coincident with widespread dieback within an adjacent state (Georgia) that started in 2001/2002 and was the largest dieback on record in that state, impacting the whole coast (Elmer et al., 2012; Ogburn and Alber, 2006). The dieback region was still evident between 2003 and 2005, after which a slow recovery was observed (Mcfarlin, 2012; Ogburn and Alber, 2006). Using satellite-extracted vegetation indices, the present study maps the continuous distribution of marsh stress in North Inlet estuary. The work was undertaken to assess the spatial extent of stress to marsh vegetation within the estuary during this period, which we believe can add new information about the causes of marsh dieback and stress in general. This spatial information is beneficial for understanding the extent of marsh dieback within South Carolina and regionally, and should be useful for marsh management and conservation efforts.

Materials and Methods

Study Area

The study area is North Inlet located near Georgetown, South Carolina (Figure 5.1). North inlet is bordered by the Atlantic Ocean on the east and Winyah Bay to the west and south. Within this estuary, researchers have observed that at least two locations were effected by marsh dieback during the 2001–2003 event (Alber et al., 2008; Hughes et al., 2012).

North Inlet experiences a semi-diurnal tidal regime meaning there are two high and two low tides each lunar day (24.8 hours). North Inlet is dominated by a

monoculture of native *S. alterniflora* living between approximately mean sea level and mean higher high water, or the mean of the higher of the two daily high tides. The species has a wide range of salinity tolerances and usually is found in low lying regions with salinities between 2 and 35 psu. The high marsh is irregularly flooded and *S. alterniflora* is typically shorter than the stands found in the low marsh (South Carolina Department of Natural Resources, 2015). Precipitation averages between 127 cm to 132 cm per year, with maxima in August and minima in November to April. Average coastal temperatures vary from 9–11 ℃ in the winter to 25–27 ℃ during the summer, though average minimum January temperatures are 1.89 ℃ and average maximum summer temperatures are 32.7 ℃ (South Carolina Department of Natural Resources, 2016).

The study area is North Inlet located near Georgetown, South Carolina (Figure 5.1). North inlet is bordered by the Atlantic Ocean on the east and Winyah Bay to the west and south. Within this estuary, researchers have observed that at least two locations were effected by marsh dieback during the 2001–2003 event (Alber et al., 2008; Hughes et al., 2012).

North Inlet experiences a semi-diurnal tidal regime meaning there are two high and two low tides each lunar day (24.8 hours). North Inlet is dominated by a monoculture of native *S. alterniflora* living between approximately mean sea level and mean higher high water, or the mean of the higher of the two daily high tides. The species has a wide range of salinity tolerances and usually is found in low lying regions with salinities between 2 and 35 psu. The high marsh is irregularly

flooded and *S. alterniflora* is typically shorter than the stands found in the low marsh (South Carolina Department of Natural Resources, 2015). Precipitation averages between 127 cm to 132 cm per year, with maxima in August and minima in November to April. Average coastal temperatures vary from 9–11 ℃ in the winter to 25–27 ℃ during the summer, though average minimum January temperatures are 1.89 ℃ and average maximum summer temperatures are 32.7 ℃ (South Carolina Department of Natural Resources, 2016).

The NOAA national estuarine research reserve system (NERRS) provides land use land cover data created from high resolution orthoimagery and field verification (NOAA National Estuarine Research Reserve System (NERRS), 2012). For the study region we only included areas classified by the research reserve as wetlands with emergent vegetation dominated by *S. alterniflora* and non-vegetated mudflats around the tidal creeks.

Datasets and Pre-processing

Five Landsat images were utilized in this study: one Landsat7 ETM+ scene acquired on September 4, 1999 and four Landsat5 Thematic Mapper (TM) scene acquired on September 13, 1996, September 24, 2003, September 19, 2004, and September 16, 2006. All images were atmospherically corrected surface reflectance products downloaded from USGS data clearinghouse. USGS uses the Landsat ecosystem disturbance adaptive processing system (LEDAPS) to create on demand surface reflectance products created using the second simulation of a satellite signal in the solar spectrum (6S) radiative transfer model. Several other researchers

successfully used LEDAPS for surface reflectance within coastal marshes (Byrd et al., 2014; Li and Gong, 2016; O'Donnell et al., 2016). Images were either cloud free or had small cloud patches masked out. We also utilized the National Oceanic and Atmospheric Administration's tides and currents website (https://tidesandcurrents.noaa.gov) to select images collected during lower tides which reduces influence of tidal submergence of plants on vegetation indices (Table 5.1). We used the 1999 Landsat scene as the pre dieback image and the 2003 Landsat scene as the post dieback image. The 1996, 2004, and 2006 Landsat scenes provided additional imagery to further assess spectral indices before and after the dieback period, and insure the spectral change is not just happenstance.

Axillary datasets include high spatial resolution (0.25 m) digital orthographic photos from 2003 and 0.7 m multispectral airborne data acquisition and registration (ADAR) imagery from 2000 available from South Carolina's Department of Natural resources (refer to reference (Morris et al., 2005) for a detailed description of ADAR imagery). The 2000 image covers the entire marsh while the 2003 photo covers a majority of the marsh. Resolutions of these aerial images are high enough to visually detect the change of salt marshes between 2000 and 2003, and therefore, they serve as validation sources to the satellite-extracted marsh change in this study. Visual interpretation of high resolution photos has proven effective in past studies (Lunetta et al., 2006). We randomly generated 100 points within the marsh and removed points that were difficult to classify due to clouds or cloud shadows, leaving 84 points as ground truthing samples.

Furthermore, we obtained a 2007 light detecting and ranging (LiDAR) digital elevation model of North Inlet, through a nondisclosure agreement with Georgetown County, which gave us a high resolution (5 m) dataset of elevation relative to North American Vertical Datum of 1988.

Change Detection and Accuracy Assessment

Histogram match was performed with the histMatch function within the open source R statistical program to reduce the radiometric noises between the two Landsat images in 1999 and 2003 (R Core Team, 2017). Histogram matching forces the histogram shape of one data set to match another, but the range of values remains the same. To determine plant greenness and extent we used the normalized difference vegetation index (NDVI), this vegetation index is widely used and is successful in measuring change within vegetation (Al-doski et al., 2013; Lunetta et al., 2006; Mancino et al., 2014). The NDVI for 1999 and 2003 along with the NDVI difference (NDVId) were calculated using the following equations:

$$\mathrm{NDVI} = \frac{(\mathrm{NIR}-\mathrm{RED})}{(\mathrm{NIR}+\mathrm{RED})} \qquad \text{(Eq 1)}$$

$$\mathrm{NDVId} = \mathrm{NDVI}_{2003} - \mathrm{NDVI}_{1999} \qquad \text{(Eq 2)}$$

where NIR is the spectral reflectance of the near infrared band (wavelength 0.77–0.90 μm) and, RED is that of red band (wavelength 0.63–0.69 μm).

NDVI values range from −1 to 1. Water usually has NDVI less than 0 and healthy vegetation has high values close to 1. Since marsh dieback causes vegetation to thin or completely dieoff, NDVI values should reflect this decreased

vegetation change. The resulting NDVId values follow a normal distribution with a mean close to zero (Figure 5.2).

Thresholding approaches have been commonly applied in change detection analysis (Al-doski et al., 2013; Wang et al., 2007), where the histogram of the change image was used to identify levels of changes in vegetation. Here we adopt the same method to statistically determine marsh changes. Specifically, the following thresholds were used:

- Marsh decrease: NDVId < $-\sigma$
- No change: $-\sigma$ < NDVId < σ
- Marsh increase: NDVId > σ

where σ is standard deviation from the mean NDVId values. Following the method in Wang et al. (2007), we use the same threshold of one standard deviation to represent vegetation change (in either direction). At a given pixel, when the absolute change of NDVId is less than one standard deviation, we assume that the change is not statistically significant and assign it as no change. In Figure 5.3, areas with negative NDVId values are considered marsh dieback, while those with positive values are increased vegetated regions.

The error matrix approach was then applied for accuracy assessment of the NDVId-based change map. Since each Landsat pixel is 30 meters, we created a 90 meter buffer around each of the 84 ground truthing points and visually observed if the NDVId within the majority of the buffered region increased, decreased or stayed no change. We then assessed the accuracies of the three categories.

Lastly, we created 110 random points within the areas classified as dieback (NDVI decrease) and increase. A total of 50 points were within the increase area and 60 were within the dieback area. We then extracted the NDVI values for each year (1996, 1999, 2003, 2004 and 2006) for each point. We further separated the points by dieback experienced within the northern portion of the marsh and dieback within the southern portion of the marsh. NDVI values for each of the three categories were then plotted for each year, so we can observe the changes in NDVI values over time. We used this method to further validate the inferences made within the study.

Results/Discussion

In the error matrix (Table 5.2), we classified 27 points categorized by the NDVId assessment as dieback, 26 as increase, and 31 as no change (Table 5.2). This yielded an overall accuracy of 76.2% while the no change category had the highest user's accuracy and the dieback category had the highest producer's accuracy. The conditional kappa values were 0.69, 0.51 and 0.74 for the dieback, increase, and no change categories, respectively. The conditional kappa value ranges between −1 and 1 and gives an indication of individual category agreement (Congalton and Green, 2009). As revealed in the table, the low conditional kappa of the increase category was related to its high confusion with the no change category. For marsh dieback, a conditional kappa of about 0.7 indicated that our NDVId-based change detection method fairly identified the dieback marshes in the study area. The detection of regions with marsh increase had lower accuracy, and was occasionally

classified as no change. The NDVI derived classification for marsh increase had a higher misclassification category of no change. This could be due to variations in plant growth within the two Landsat images. The satellite image from 2003 was taken 20 days later in the growing season than the 1999 image, both in September, but at a time of year when the plants should be at peak greenness, followed soon after by senescence (Morris and Haskin, 1990). The timing of plant senescence can vary from year to year which may influence the NDVI values, and without field verification it is difficult to know if the degree of senescence is equal in each satellite image.

The zones within the marsh that were classified as no change, vegetation increase, and decline in vegetation are spatially represented in Figure 5.3. The region with the largest amount of marsh increase was across the southwest of North Inlet adjacent to Winyah Bay. The northern and southern ends of North Inlet experienced the largest decrease in vegetation (Figure 5.3). Though the elevation range within the marsh is small (Figure 5.4), it is apparent the southern end of the marsh has the highest elevation while the northern end has the lowest. Visually, the areas with both the highest and lowest elevations experienced the most pronounced decline in vegetation. Plotting the NDVId versus elevation further shows that areas within the highest and lowest elevation had a decline in NDVI between 1999 and 2003 (Figure 5.5). The width of each of the bars in the plot are scaled based on the number of data points within each category, this shows that the majority of study area falls within elevations between −0.25 m and 1.5 m. At

elevations greater than 1.5 meters the NDVId did increase from 1999 to 2003 but there is markedly less area of interest within that elevation range. The mid elevations had the greatest amount of NDVId increase occurrences, which indicates that the plants living within the mid elevations are the healthiest and less impacted by environmental stressors.

The mean elevation within North Inlet is 37 cm above sea level and the southern end of the marsh is at a slightly higher elevation than the north end (Morris et al., 2005; Figure 5.4). The small changes in elevation most likely influence the health of the marsh; a past study at North Inlet indicated that the marsh is not keeping up with sea-level rise which would result in vegetation decline at the lower elevation areas. *S. alterniflora* grown at low elevations have the lowest above ground biomass production which traps less sediment and does not facilitate vertical sediment accretion as well as higher biomass areas (Morris et al., 2002, 2013). However, climate anomalies can produce interannual changes in mean summer sea level of 15 cm (Morris et al., 2002); during 2003 the mean sea level was −3.5 cm while the mean sea level for 1999 was 2.6 cm (https://tidesandcurrents.noaa.gov). Another explanation for the decline in marsh health within lower elevations is due to increased toxin accumulation or hypoxia. Hydrogen sulphide is a by-product of microbial activity within anoxic conditions such as those within salt marshes. At high concentrations, hydrogen sulphide becomes toxic to plants and limits biomass production (Koch and Mendelssohn, 1989). Tidal flushing and drainage may mitigate the negative effects

of hydrogen sulphide and varies with relative elevation. At lower elevations the marsh experiences more tidal flushing but less drainage, leading to higher and growth-limiting accumulations of this toxin. It is likely that the plants suffering from the dieback event suffered from increased hypoxia reducing their overall fitness, which is highlighted by the overall decline in NDVId and increased frequency of marsh decline areas at lower elevations (Figures 5.5 and 5.6).

In contrast, regions that are at higher elevation may experience hypersalinity and osmotic stress during years of drought and lower sea level which could lead to plant death. Hypersalinity results from the minimal flow of fresh water into North Inlet, evapotranspiration concentrating the salt in sediments, and tidal flushing being less pronounced in higher elevations than lower elevations. Within South Carolina much of the state was in a drought during both 2001 and 2002 (Figure 5.7). Osmotic stress from hypersalinity likely impacted the vegetation within North Inlet within the higher elevation areas. This hypothesis is supported by the increased frequency of vegetation loss in higher elevations (Figure 5.6). Figure 5.6 also illustrates that plants within mid elevations experienced the least amount of vegetation decline. The plants within the mid elevations are exposed hypoxia and hypersalinity at reduced rates and are overall less stressed than plants at higher and lower elevations.

The trend in NDVI over time further highlights the results from this study (Figure 5.8). The NDVI values prior to the marsh dieback event were all similar. NDVI declined in both northern and southern areas during the drought, and was

within the northern section of the marsh, which also is located within the lower marsh elevations (Figure 5.8b). Furthermore, there was a significant ($p < 0.0001$) declining trend in NDVI values after the brown marsh event within the northern area. This indicates that the marsh situated at the lowest elevation is most prone to declining health. The area classified with increased NDVI in 2003 had higher NDVI values than both the years before and after the marsh dieback event. This indicates that the factors contributing to the dieback event likely had a positive influence in vegetation growth within other areas of the marsh (Figure 5.8c).

It is important to note a few limitations within this study. Landsat imagery only has a 30 meter spatial resolution, making it difficult to analyse landscape changes at a smaller scale. But a significant decrease in NDVI between the two dates is detectable within a Landsat pixel. In addition, all areas within this study that show a decrease in vegetation were classified as marsh dieback. Though the area classified as marsh dieback may not have a total loss in vegetation, there was still a marked decline in vegetation health or coverage which resulted in that area being classified as marsh dieback. Furthermore, thinning of vegetation is also a symptom of marsh dieback. Given these limitations, the study still highlights the locations of decreased and increased vegetation and improves our knowledge about the spatial distribution of vegetation change. Using the spatial data the potential causes of the event are further understood. Results from this study also highlight the importance of elevation on controlling the health of a marsh. When assessing the extent of future brown marsh events researchers or land managers

should focus on the locations that are at the minimum and maximum elevations within the marsh.

Conclusion

The Landsat-extracted NDVI change between 1999 and 2003 highlights regions of growth and decline within the North Inlet estuary. The overall accuracy of marsh change reached 76% and the conditional kappa value of marsh dieback was 0.7. The northern portion of the marsh experienced the largest thinning or dieback while the southern end of marsh region near the northern part of Winyah Bay experienced the largest increase in greenness. Slight elevation change was a key controller of health within the marsh. The dieback area occurred less frequently within the mid elevations of the marsh, while high elevations experienced increased dieback likely linked to hypersalinity and the low elevations within the marsh experienced increased dieback area likely caused by hypoxia.

Table 5. 1. Date and time of Landsat data acquisition and associated tidal height (m) above mean sea level.

Date	Time (GMT)	Tidal height above mean sea level (m)
Sept. 13, 1996	15:05:53	0.229
Sept. 05, 1999	15:47:09	-0.464
Sept. 24, 2003	15:31:51	-0.471
Sept. 19, 2004	15:31:58	0.587
Sept. 16, 2006	15:48:01	-0.229

Table 5. 2. Error matrix for the NDVI derived and visually derived change of marsh growth between 1999 and 2003 for North Inlet.

	Visual Classification				
NDVI Classification	Dieback	Increase	No Change	Count	User's Accuracy
Dieback	21	0	6	27	77.8%
Increase	0	16	10	26	61.5%
No Change	2	2	27	31	87.1%
Count	23	18	43	84	
Producer's Accuracy	91.3%	88.9%	62.8%		Total Accuracy 76.2%

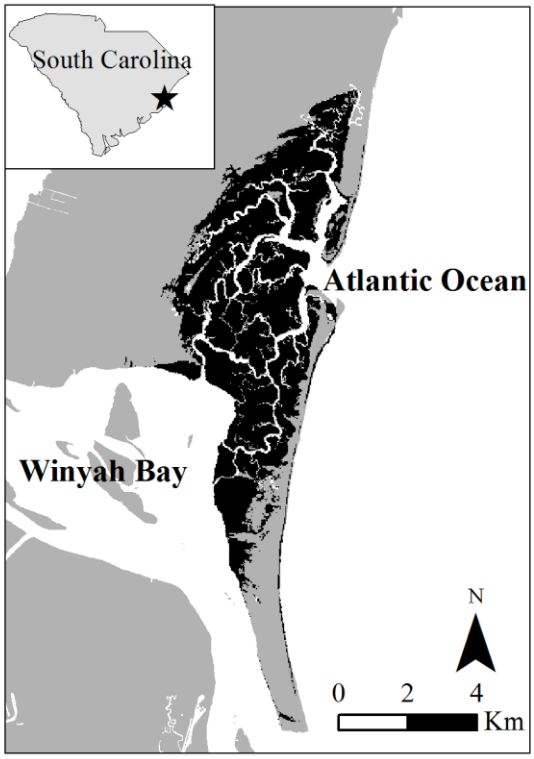

Figure 5.1. The Study Area within the North Inlet. Marshes are shown in black.

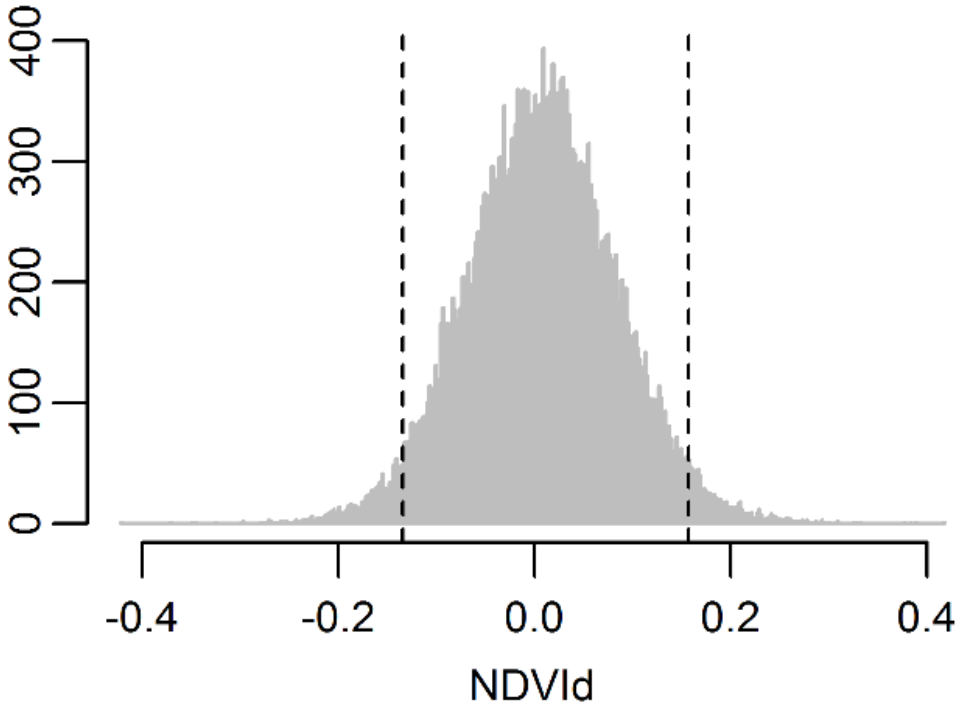

Figure 5.2. Histogram of NDVId between 2003 and 1999. Vertical dashed lines indicate where the sigma 0.05 (z = 1.96) values falls.

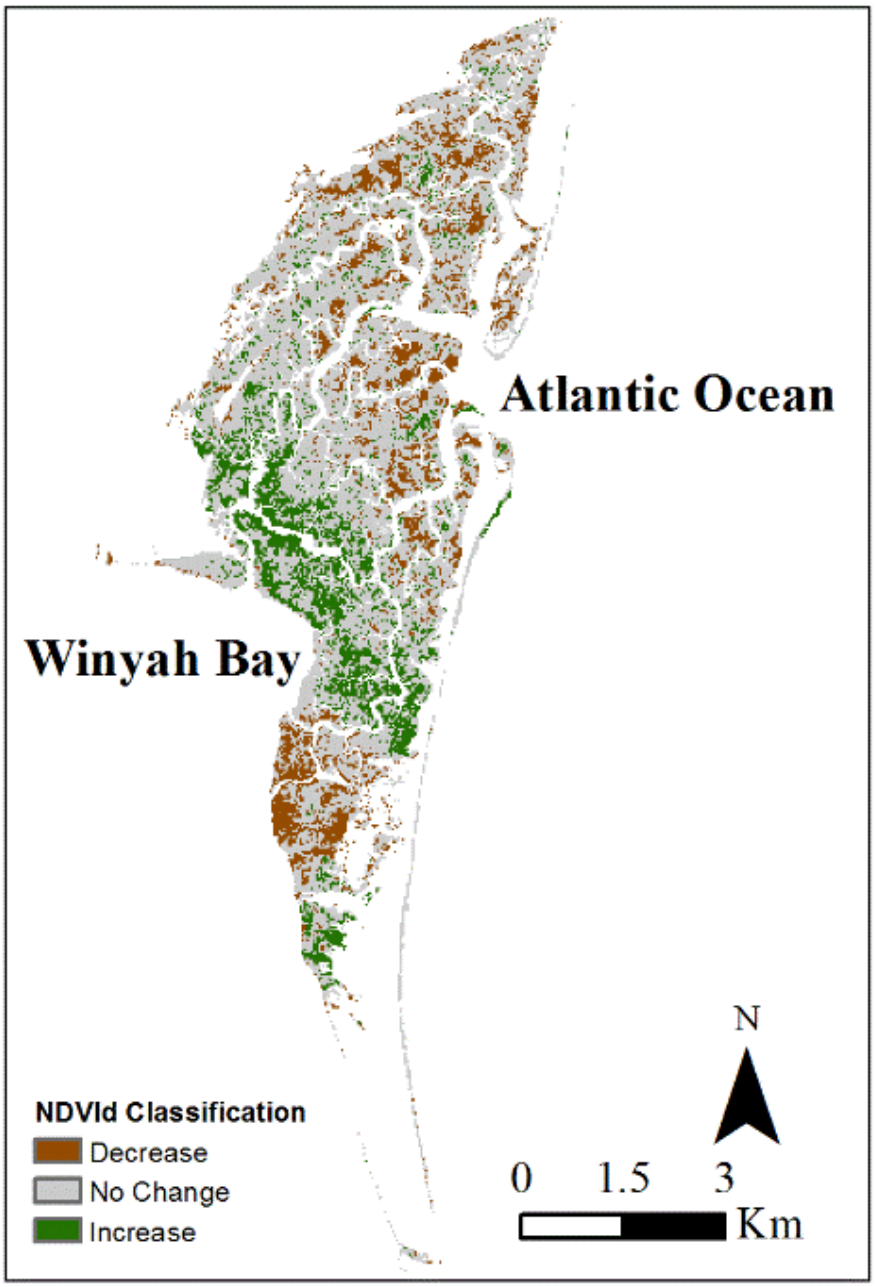

Figure 5.3. Regions in green indicate vegetation growth and regions in brown indicate regions of decreased vegetation between 1999 and 2003 for North Inlet.

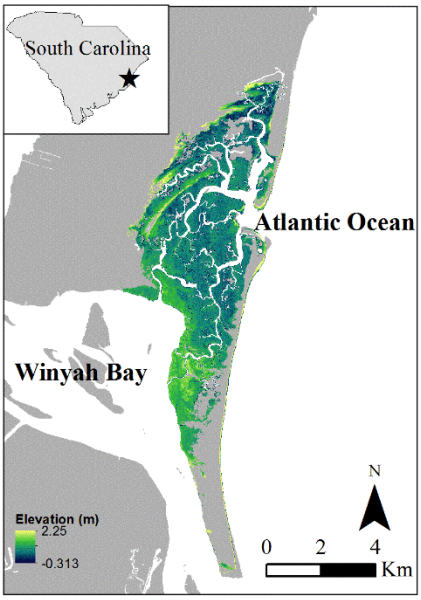

Figure 5.4. Elevation (m) in reference to North American Vertical Datum 1988 within the study area of North Inlet

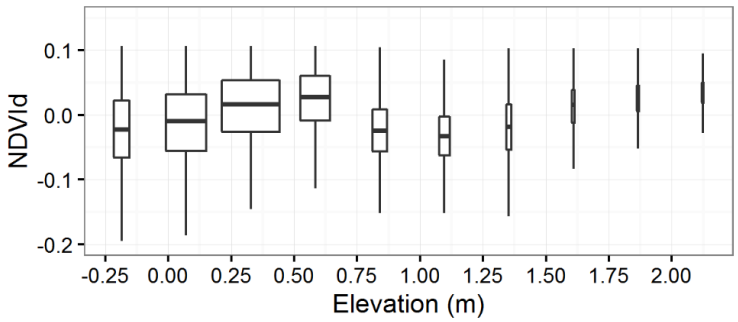

Figure 5.5. Boxplot of NDVId versus elevation (referenced to North American Vertical Datum 1988) within North Inlet. Elevation was binned into 10 equally spaced categories. The width of the boxes are scaled to the number of samples in each bin.

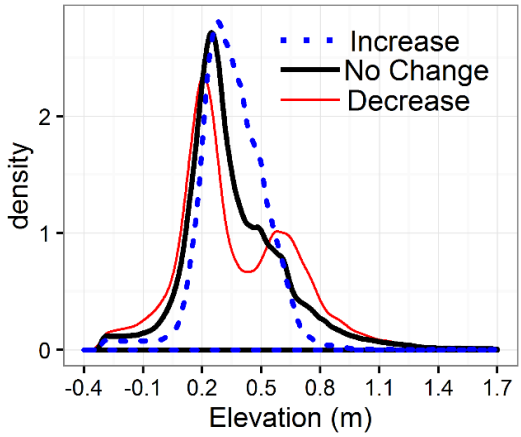

Figure 5.6. Histogram of elevation (m) at each area classified with decreased vegetation. Density = count/N where N is the values of elevation points found at an elevation and count is the total number of points within each elevation for each category.

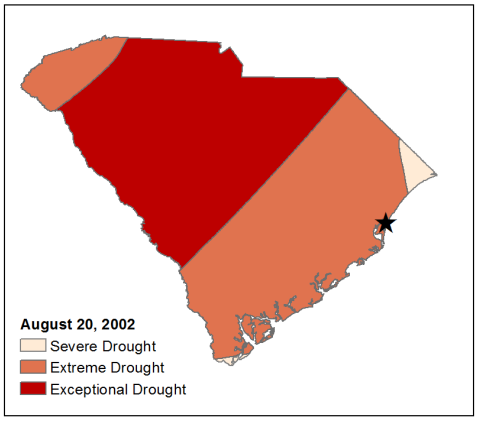

Figure 5.7. Palmer drought index during August 2002 showing most of the coast is in "Extreme Drought." Most South Carolina remained in a drought until early 2003. The started area is where North Inlet is located. Data provided by the National Drought Mitigation Center, the USDA, and NOAA.

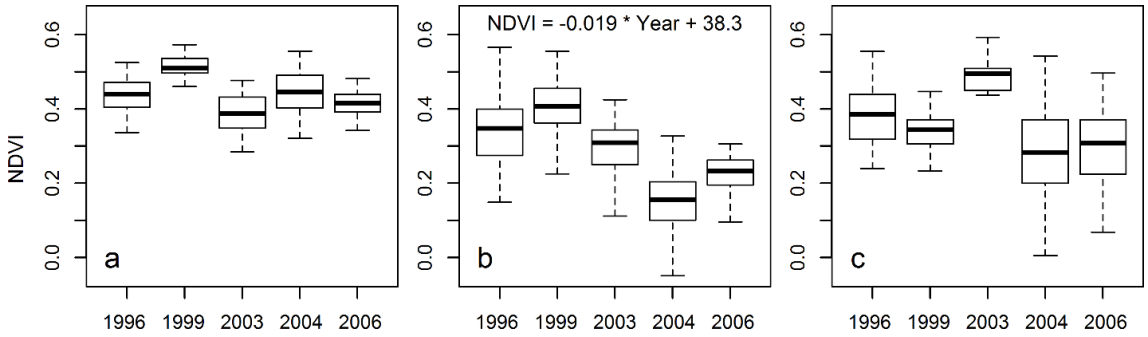

Figure 5.8. NDVI trends for 5 years within the southern area classified as marsh dieback (a), northern area classified as marsh dieback (b), and area marked as increase (c). The NDVI graphs were separated due to the elevation within the northern area being lower than the elevation of the southern portion of the marsh

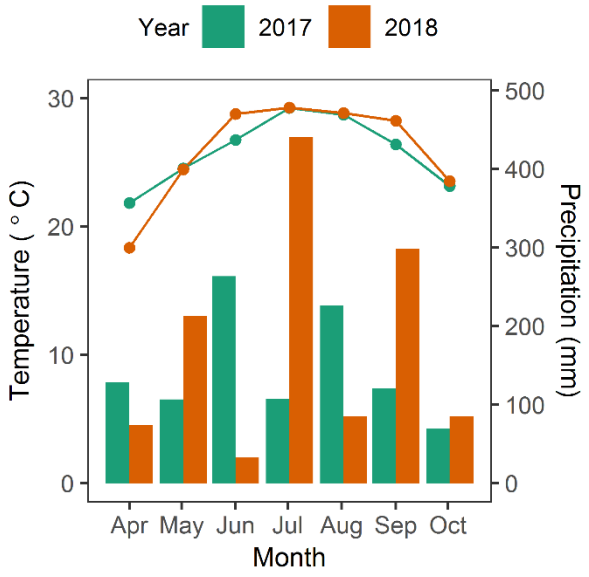

Figure 5.9. Average monthly temperature (°C) and cumulative monthly precipitation during the growing season within North Inlet for 2017 and 2018. Bar graph indicates precipitation and line graph indicates temperature. Data is from a weather station at North Inlet.

CHAPTER 6

CONCLUSION

This research measures how marshes responds to the environment and makes projections of change into the future. Climate change will bring higher occurrences of drought, warmer temperatures and sea-level rise. Grasping an understanding of how these variables impact marsh health is essential not only on a biotic scale but also human-centered one. Coastal marshes are well known to be a biologically productive ecosystem frequented by migrated birds, improving water quality, acting as a home to wildlife and breeding ground for fauna (Fisher and Acreman, 2004; Mulholland et al., 2009; Whiting and Chanton, 2001). On the human side marshes provide flood protection during storm surge events, are essential to the fishing industry, and draw crows for touristic economic revenue (Faulkenberry et al., 2000; Möller et al., 2014; Osland et al., 2016).

In Chapter 2, I applied the Marsh Equilibrium Model (MEM) to Beaufort and Jasper Counties to better inform state holders on marsh migration with sea-level rise. In order to accomplish this, MEM was written in Python which allowed for large spatial-scale analysis. This study highlighted areas that are likely to remain marsh and likely to drown after 100 years of sea-level rise. The results were

delivered to the South Carolina Nature Conservancy, who can use the data to help determine which plots of land are more desirable for acquisition.

In Chapter 3 I explore using Planet's PlanetScope data to estimate landscape scale aboveground biomass within a marsh. I found the PlanetScope can be used to produce 3-meter resolution spatial maps of aboveground biomass if sufficient model training data is collected. These high-resolution maps not only help pinpoint where the marsh is the most and least productive but can also be used to establish a biomass growth curve with elevation. Many cities/counties/states have publicly available elevation data, pairing this elevation data with the landscape scale biomass map, one can determine how biomass changes as a function of elevation. This relationship then can be used as an input into models predicting how marshes may migrate with sea-level rise.

The 4th Chapter continues analyses of biomass, but moves belowground to look at roots, rhizomes, and dead biomass. I also found that biomass was correlated with elevation. I found the highest belowground biomass at the highest elevations sampled, and the smallest belowground biomass at the lowest elevations. I also found that there was also significant inter-annual variability in belowground biomass production, and biomass differed significantly between two sites (which was not accounted for in elevational differences). Furthermore, counter to a previous study, I did not find a significant different in biomass between control and treatment samples with fertilizer application, but this could

be due to the small sample sized and potentially not allowing enough time to pass for the effects of fertilizer application to be visualized.

Chapter 5 moves to assessing past events, which will better inform us about the future. In this Chapter, I utilized NASA's Landsat data to map a marsh dieback event. Through this study I found that plant health decreased at both the lower and higher elevations within the marsh. The marsh dieback event also coincided with a period of drought which likely impacted both the lower and higher elevations of the marsh. With summer drought conditions, there is high evapotranspiration leading to high salt content. Rain helps to reduce this salt accumulation, however in periods of extended drought, plants can become stressed and their health will decline. In the lower elevations of the marsh, plants experience a longer hydroperiod, when paired with higher sea-level the prolonged flooding can lead to higher concentrations of growth limiting toxins. Throughout this Chapter, I obtain a better grasp on how climate variability can impact marsh health. Pairing all the Chapters together, there is increased knowledge of drivers of marsh health and insight on how to improve modelling efforts

REFERENCES

Agrelius, T. (2015). Global Methylation of DNA Among Spartina Alterniflora Clones Differing in Age at North Inlet, SC. Available at: http://scholarcommons.sc.edu/etd/3282/.

Akaike, H. (1974). A new look at the statistical model identification. *IEEE Trans. Automat. Contr.* 19, 716–723. doi:10.1109/TAC.1974.1100705.

Al-doski, J., Mansor, S. B., Zulhaidi, H., and Shafri, M. (2013). NDVI differencing and post-classification to detect vegetation changes in Halabja City, Iraq. *J. Appl. Geol. Geophys.* 1, 1–10.

Alber, M., Swenson, E. M., Adamowicz, S. C., and Mendelssohn, I. A. (2008). Salt Marsh Dieback: An overview of recent events in the US. *Estuar. Coast. Shelf Sci.* 80, 1–11. doi:10.1016/j.ecss.2008.08.009.

Alldred, M., Liberti, A., and Baines, S. B. (2017). Impact of salinity and nutrients on salt marsh stability. *Ecosphere* 8. doi:10.1002/ecs2.2010.

Almeida, D. R. A. de, Nelson, B. W., Schietti, J., Gorgens, E. B., Resende, A. F., Stark, S. C., et al. (2016). Contrasting fire damage and fire susceptibility between seasonally flooded forest and upland forest in the Central Amazon using portable profiling LiDAR. *Remote Sens. Environ.* 184, 153–160. doi:10.1016/J.RSE.2016.06.017.

Boumans, R. M. J., and Day, J. W. (1993). High Precision Measurements of Sediment Elevation in Shallow Coastal Areas Using a Sedimentation-Erosion Table. *Estuaries* 16, 375. doi:10.2307/1352509.

Burnham, K. P., and Anderson, D. R. (2002). *Model Selection and Multimodel Inference: A Practical Information-Theoretic Approach*. Springer Science & Business Media.

Byrd, K. B., O'Connell, J. L., Di Tommaso, S., and Kelly, M. (2014). Evaluation of sensor types and environmental controls on mapping biomass of coastal marsh emergent vegetation. *Remote Sens. Environ.* 149, 166–180. doi:10.1016/j.rse.2014.04.003.

Cahoon, D. R., Lynch, J. C., Hensel, P., Boumans, R., Perez, B. C., Segura, B., et al. (2002). High-Precision Measurements of Wetland Sediment Elevation: I. Recent Improvements to the Sedimentation-Erosion Table. *J. Sediment. Res.* 72, 730–733. doi:10.1306/020702720730.

Clough, J., Park, Ri., Propato, M., Polaczyk, A., Brennan, M., Behrens, D., et al. (2016). SLAMM 6.2 Technical Documentation. Available at: http://warrenpinnacle.com/prof/SLAMM6/SLAMM_6.7_Technical_Documentation.pdf.

Coleman, D. C., Crossley, D. A., and Hendrix, P. F. (2004). *Fundamentals of soil ecology*. Elsevier Academic Press.

Congalton, R. G., and Green, K. (2009). *Assessing the Accuracy of Remotely Sensed Data: Principles and Practices*. 2nd Editio. Taylor & Francis Group

doi:10.1111/j.1477-9730.2010.00574_2.x.

Conlon, K. J., and Journey, C. A. (2008). *Evaluation of Four Structural Best Management Practices for Highway Runoff in Beaufort and Colleton Counties, South Carolina, 2005–2006*. U.S. Geological Survey Scientific Investigations Report 2008–5150.

Couvillion, B. R., and Beck, H. (2013). Marsh Collapse Thresholds for Coastal Louisiana Estimated Using Elevation and Vegetation Index Data. *J. Coast. Res.* 63, 58–67. doi:10.2112/SI63-006.1.

Dame, R. F., and Kenny, P. D. Variability of Spartina alterniflora primary production in the euhaline North Inlet estuary. *Mar. Ecol. Prog. Ser.* 32, 71–80. doi:10.2307/24825479.

Darby, F. A., and Turner, R. E. (2008). Below- and Aboveground Spartina alterniflora Production in a Louisiana Salt Marsh. *Estuaries and Coasts* 31, 223–231. doi:10.1007/s12237-007-9014-7.

Davey, E., Wigand, C., Johnson, R., Sundberg, K., Morris, J., and Roman, C. T. (2011). Use of computed tomography imaging for quantifying coarse roots, rhizomes, peat, and particle densities in marsh soils. *Ecol. Appl.* 21, 2156–2171. doi:10.1890/10-2037.1.

Davis, J., Currin, C., and Morris, J. T. (2017). Impacts of Fertilization and Tidal Inundation on Elevation Change in Microtidal, Low Relief Salt Marshes. *Estuaries and Coasts* 40, 1677–1687. doi:10.1007/s12237-017-0251-0.

Deegan, L. A., Johnson, D. S., Warren, R. S., Peterson, B. J., Fleeger, J. W.,

Fagherazzi, S., et al. (2012). Coastal eutrophication as a driver of salt marsh loss. *Nature* 490, 388–392. doi:10.1038/nature11533.

DeLaune, R. D., Smith, C. J., and Patrick, W. H. (1983). Relationship of Marsh Elevation, Redox Potential, and Sulfide to Spartina alterniflora Productivity1. *Soil Sci. Soc. Am. J.* 47, 930. doi:10.2136/sssaj1983.03615995004700050018x.

Dibbell Burns, T. N. (2015). Spartina alterniflora Responses to Flooding in Two Salt Marshes on the Eastern Shore of Virginia.

Edwards, J. D. (2016). Applicability of LiDAR Technology in Saltmarshes: Landscape-Scale Predictive Models to Local-Scale Biomass Estimation. *Theses Diss.* Available at: https://scholarcommons.sc.edu/etd/3550 [Accessed September 20, 2019].

Elmer, W. H., LaMondia, J. A., and Caruso, F. L. (2012). Association Between Fusarium spp. on Spartina alterniflora and Dieback Sites in Connecticut and Massachusetts. *Estuaries and Coasts* 35, 436–444. doi:10.1007/s12237-011-9448-9.

Faulkenberry, L. V, John M Coggeshall, K. B., and Backman, S. (2000). A culture of servitude: The impact of tourism and development on South Carolina's coast. *Hum. Organ.* doi:10.17730/humo.59.1.353730461t724j02.

Fisher, J., and Acreman, M. (2004). Wetland nutrient removal: a review of the evidence. *Hydrol. Earth Syst. Sci.* 8, 673–685.

Flavel, R. J., Guppy, C. N., Tighe, M., Watt, M., McNeill, A., and Young, I. M.

(2012). Non-destructive quantification of cereal roots in soil using high-resolution X-ray tomography. *J. Exp. Bot.* 63, 2503–2511. doi:10.1093/jxb/err421.

Gallagher, J. L. (1975). Effect of an Ammonium Nitrate Pulse on the Growth and Elemental Composition of Natural Stands of Spartina alterniflora and Juncus roemerianus. *Am. J. Bot.* 62, 644. doi:10.2307/2441945.

García, M., Riaño, D., Chuvieco, E., and Danson, F. M. (2010). Estimating biomass carbon stocks for a Mediterranean forest in central Spain using LiDAR height and intensity data. *Remote Sens. Environ.* 114, 816–830. doi:10.1016/J.RSE.2009.11.021.

Gitelson, A. A., and Merzlyak, M. N. (1998). Remote sensing of chlorophyll concentration in higher plant leaves. *Adv. Sp. Res.* 22, 689–692. doi:10.1016/S0273-1177(97)01133-2.

Good, R. E., Good, N. F., and Frasco, B. R. (1982). "A REVIEW OF PRIMARY PRODUCTION AND DECOMPOSITION DYNAMICS OF THE BELOWGROUND MARSH COMPONENT," in *Estuarine Comparisons* (Elsevier), 139–157. doi:10.1016/b978-0-12-404070-0.50015-6.

Grose, M. J., Gilligan, C. A., Spencer, D., and Goddard, B. V.D. (1996). Spatial heterogeneity of soil water around single roots: Use of CT-scanning to predict fungal growth in the rhizosphere. *New Phytol.* 133, 261–272. doi:10.1111/j.1469-8137.1996.tb01893.x.

Gross, M. F., Hardisky, M. A., Klemas, V., and Wolf, P. L. (1987). Quantification

of Biomass of the Marsh Grass Spartina altfernifara Loisel Using Landsat Thematic Mapper Imagery. *Photogramm. Eng. Remote Sensing* 53, 1577–1583. Available at: https://www.asprs.org/wp-content/uploads/pers/1987journal/nov/1987_nov_1577-1583.pdf [Accessed February 6, 2018].

Gross, M. F., Hardisky, M. A., Wolf, P. L., and Klemas, V. (1991). Relationship between Aboveground and Belowground Biomass of Spartina alterniflora (Smooth Cordgrass). *Estuaries* 14, 180. doi:10.2307/1351692.

Gross, M. F., Klemas, V., and Hardisky, M. A. (1990). Long-term remote monitoring of salt marsh biomass. in, 1300–1312. Available at: http://dx.doi.org/10.1117/12.21390.

Haines, E. B. (1979). Growth dynamics of cordgrass, Spartina alterniflora loisel., on control and sewage sludge fertilized plots in a Georgia salt marsh. doi:10.2307/1352040.

Hardisky, M. A., Daiber, F. C., Roman, C. T., and Klemas, V. (1984). Remote sensing of biomass and annual net aerial primary productivity of a salt marsh. *Remote Sens. Environ.* 16, 91–106. doi:10.1016/0034-4257(84)90055-5.

Hardisky, M. A., Smart, R. M., and Klemas, V. (1983). Seasonal Spectral Characteristics and aboveground Biomass of the Tidal Marsh Plant, Spartina alterniflora. Available at: https://www.asprs.org/wp-content/uploads/pers/1983journal/jan/1983_jan_85-92.pdf [Accessed August 1, 2019].

Hill, T. D., and Davey, E. (2017). Programmatic analysis of sediment cores using computed tomography imaging. Available at: https://github.com/troyhill/coreCT.

Hines, J., Megonigal, J. P., and Denno, R. F. (2006). Nutrient subsidies to belowground microbes impact aboveground food web interactions. *Ecology* 87, 1542–1555. doi:10.1890/0012-9658(2006)87[1542:NSTBMI]2.0.CO;2.

Hinkel, J., Lincke, D., Vafeidis, A. T., Perrette, M., Nicholls, R. J., Tol, R. S. J., et al. (2014). Coastal flood damage and adaptation costs under 21st century sea-level rise. *Proc. Natl. Acad. Sci. U. S. A.* 111, 3292–7. doi:10.1073/pnas.1222469111.

Huete, A. . (1988). A soil-adjusted vegetation index (SAVI). *Remote Sens. Environ.* 25, 295–309. doi:10.1016/0034-4257(88)90106-X.

Hughes, A. L. H., Wilson, A. M., and Morris, J. T. (2012). Hydrologic variability in a salt marsh: Assessing the links between drought and acute marsh dieback. *Estuar. Coast. Shelf Sci.* 111, 95–106. doi:10.1016/j.ecss.2012.06.016.

Hughes, A. R. (2014). Genotypic diversity and trait variance interact to affect marsh plant performance. *J. Ecol.* 102, 651–658. doi:10.1111/1365-2745.12244.

Jensen, J. R., Schill, S. R., Porter, D. E., and Morris, J. T. (2002). Remote Sensing of Biomass , Leaf-Area-Index , and Chlorophyll a and b Content in the ACE Basin National Estuarine Research Reserve Using Sub-meter Digital Camera Imagery. *Geocarto Int.* 17, 27–36. doi:10.1080/10106040208542241.

Jialin, L., Hanbing, Z., and Xiaoping, Y. (2011). Study on the seasonal dynamics

of zonal vegetation of NDVI/EVI of costal zonal vegetation based on MODIS data: A case study of Spartina alterniflora salt marsh on Jiangsu Coast, China. *African J. Agric. Res.* 6, 4019–4024. doi:10.5897/AJAR11.769.

Karl, T. R., Melillo, J. M., and Peterson, T. C. (2009). *Global Climate Change Impacts in the United States*.

Kibby, H. V., Gallagher, J. L., and Sanville, W. D. (1980). Field Guide To Evaluate Net Primary Production Of Wetlands. Corvallis, OR: Environmental Protection Agency Available at: https://nepis.epa.gov/Exe/ZyPURL.cgi?Dockey=20007QNE.txt.

Kiehn, W. M., and Morris, J. T. (2009). Relationships betweenSpartina alterniflora andLittoraria irrorata in a South Carolina salt marsh. *Wetlands* 29, 818–825. doi:10.1672/08-178.1.

Kim, M., Warner, T. A., Madden, M., and Atkinson, D. S. (2011). Multi-scale GEOBIA with very high spatial resolution digital aerial imagery: scale, texture and image objects. *Int. J. Remote Sens.* 32, 2825–2850. doi:10.1080/01431161003745608.

Kirwan, M. L., Christian, R. R., Blum, L. K., and Brinson, M. M. (2012). On the Relationship Between Sea Level and Spartina alterniflora Production. *Ecosystems* 15, 140–147. doi:10.1007/s10021-011-9498-7.

Kirwan, M. L., and Guntenspergen, G. R. (2012). Feedbacks between inundation, root production, and shoot growth in a rapidly submerging brackish marsh. *J. Ecol.* 100, 764–770. doi:10.1111/j.1365-2745.2012.01957.x.

Koch, M. S., and Mendelssohn, I. A. (1989). Sulphide as a Soil Phytotoxin: Differential Responses in Two Marsh Species. *J. Ecol.* 77, 565. doi:10.2307/2260770.

Li, S., and Pennings, S. C. (2017). Timing of disturbance affects biomass and flowering of a saltmarsh plant and attack by stem-boring herbivores. *Ecosphere* 8, e01675. doi:10.1002/ecs2.1675.

Li, W., and Gong, P. (2016). Continuous monitoring of coastline dynamics in western Florida with a 30-year time series of Landsat imagery. *Remote Sens. Environ.* 179, 196–209. doi:10.1016/J.RSE.2016.03.031.

Lopes, C. L., Mendes, R., Caçador, I., and Dias, J. M. (2019). Evaluation of long-term estuarine vegetation changes through Landsat imagery. *Sci. Total Environ.* 653, 512–522. doi:10.1016/J.SCITOTENV.2018.10.381.

Lumbierres, M., Méndez, P., Bustamante, J., Soriguer, R., and Santamaría, L. (2017). Modeling Biomass Production in Seasonal Wetlands Using MODIS NDVI Land Surface Phenology. *Remote Sens.* 9, 392. doi:10.3390/rs9040392.

Lunetta, R. S., Knight, J. F., Ediriwickrema, J., Lyon, J. G., and Worthy, L. D. (2006). Land-cover change detection using multi-temporal MODIS NDVI data. *Remote Sens. Environ.* 105, 142–154. doi:10.1016/j.rse.2006.06.018.

Mancino, G., Nolè, A., Ripullone, F., and Ferrara, A. (2014). Landsat TM imagery and NDVI differencing to detect vegetation change: Assessing natural forest expansion in Basilicata, southern Italy. *IForest* 7, 75–84. doi:10.3832/ifor0909-007.

Mcfarlin, C. R. (2012). Salt marsh dieback: the response of Spartina alterniflora to disturbances and the consequences for marsh invertebrates.

McKee, K. L., Mendelssohn, I. A., and Materne, M. D. (2004). Acute salt marsh dieback in the Mississippi River deltaic plain: A drought-induced phenomenon? *Glob. Ecol. Biogeogr.* 13, 65–73. doi:10.1111/j.1466-882X.2004.00075.x.

McKee, K. L., and Patrick, W. H. (1988). The Relationship of Smooth Cordgrass (Spartina alterniflora) to Tidal Datums: A Review. *Estuaries* 11, 143. doi:10.2307/1351966.

Mcleod, E., Chmura, G. L., Bouillon, S., Salm, R., Björk, M., Duarte, C. M., et al. (2011). A blueprint for blue carbon: toward an improved understanding of the role of vegetated coastal habitats in sequestering CO 2. *Front. Ecol. Environ.* 9, 552–560. doi:10.1890/110004.

Mendelssohn, I. A. (1979). Nitrogen Metabolism in the Height Forms of Spartina Alterniflora in North Carolina. *Ecology* 60, 574–584. doi:10.2307/1936078.

Mendelssohn, I. A., and Seneca, E. D. (1980). The influence of soil drainage on the growth of salt marsh cordgrass Spartina alterniflora in North Carolina. *Estuar. Coast. Mar. Sci.* doi:10.1016/S0302-3524(80)80027-2.

Michener, W. K., Blood, E. R., Bildstein, K. L., Brinson, M. M., and Gardner, L. R. (1997). Climate Change, Hurricanes and Tropical Storms, and Rising Sea Level in Coastal Wetlands. *Ecol. Appl.* 7, 770. doi:10.2307/2269434.

Miller, G. J., Morris, J. T., and Wang, C. (2017). Mapping salt marsh dieback and

condition in South Carolina's North Inlet-Winyah Bay National Estuarine Research Reserve using remote sensing. *AIMS Environ. Sci.* 4, 677–689. doi:10.3934/environsci.2017.5.677.

Miller, G. J., Morris, J. T., and Wang, C. (2019). Estimating Aboveground Biomass and Its Spatial Distribution in Coastal Wetlands Utilizing Planet Multispectral Imagery. *Remote Sens.* 11, 2020. doi:10.3390/rs11172020.

Mo, Y., Kearney, M. S., and Riter, J. C. A. (2017). Post-deepwater horizon oil spill monitoring of Louisiana salt marshes using landsat imagery. *Remote Sens.* 9, 547. doi:10.3390/rs9060547.

Möller, I., Kudella, M., Rupprecht, F., Spencer, T., Paul, M., van Wesenbeeck, B. K., et al. (2014). Wave attenuation over coastal salt marshes under storm surge conditions. *Nat. Geosci.* 7, 727–731. doi:10.1038/ngeo2251.

Morris, J. T. (2000). "Effects of sea-level anomalies on estuarine processes," in *Estuarine science: A synthetic approach to research and practice*, ed. J. E. Hobbie, 107–127.

Morris, J. T., Barber, D. C., Callaway, J. C., Chambers, R., Hagen, S. C., Hopkinson, C. S., et al. (2016). Contributions of organic and inorganic matter to sediment volume and accretion in tidal wetlands at steady state. *Earth's Futur.* 4, 110–121. doi:10.1002/2015EF000334.

Morris, J. T., and Haskin, B. (1990). A 5-yr record of aerial primary production and stand characteristics of Spartina alterniflora. *Ecology* 71, 2209–2217. doi:10.2307/1938633.

Morris, J. T., Porter, D., Neet, M., Noble, P. a., Schmidt, L., Lapine, L. a., et al. (2005). Integrating LIDAR elevation data, multi- spectral imagery and neural network modelling for marsh characterization. *Int. J. Remote Sens.* 26, 5221–5234. doi:10.1080/01431160500219018.

Morris, J. T., Sundareshwar, P. V, Nietch, C. T., and Kjerfve, B. (2002). Responses of Coastal Wetlands to Rising Sea Level. *Ecol. Soc. Am.* 83, 2869–2877.

Morris, J. T., Sundberg, K., and Hopkinson, C. S. (2013). Salt Marsh Primary Production and Its Response to Relative Sea Level and Nutrients in Estuaries at Plum Island, Massachusets, and North Inlet, South Carolina, USA. *Oceanography* 26, 78–84. doi:https://doi.org/10.5670/oceanog.2013.48.

Mudd, S. M., Howell, S. M., and Morris, J. T. (2009). Impact of dynamic feedbacks between sedimentation, sea-level rise, and biomass production on near-surface marsh stratigraphy and carbon accumulation. *Estuar. Coast. Shelf Sci.* 82, 377–389. doi:10.1016/j.ecss.2009.01.028.

Mulholland, P. J., Hall, R. O., Sobota, D. J., Dodds, W. K., Findlay, S. E., Grimm, N. B., et al. (2009). Nitrate removal in stream ecosystems measured by 15N addition experiments: Denitrification. *Limnol. Oceanogr.* 54, 666–680.

Narayan, S., Beck, M. W., Wilson, P., Thomas, C. J., Guerrero, A., Shepard, C. C., et al. (2017). The Value of Coastal Wetlands for Flood Damage Reduction in the Northeastern USA. *Sci. Rep.* 7, 9463. doi:10.1038/s41598-017-09269-z.

National Oceanic and Atmospheric Administration (2012). NOAA Tides and Currents. *NOAA Tides Curr.*

National Water Quality Monitoring Council (2017). Water Quality Portal. Available at: https://www.waterqualitydata.us/ [Accessed September 1, 2017].

Nellemann, C., Corcoran, E., Duarte, C. M., Valdés, L., De Young, C., Fonseca, L., et al. (2009). *Blue Carbon - The Role of Healthy Oceans in Binding Carbon*. United Nations Environment Programme, GRID-Arendal Available at: http://books.google.com/books?id=onCVCHQl4RoC [Accessed June 19, 2017].

NOAA Boston Tide Gage, Tides & Currents. *Tides Curr.* Available at: https://tidesandcurrents.noaa.gov/stationhome.html?id=8443970 [Accessed July 30, 2019a].

NOAA National Climatic Data Center. Available at: https://www7.ncdc.noaa.gov/CDO/CDODivisionalSelect.jsp# [Accessed May 26, 2019b].

NOAA National Estuarine Research Reserve System (NERRS) (2012). System-wide Monitoring Program.

Nyman, J. A., Walters, R. J., Delaune, R. D., and Patrick, W. H. (2006). Marsh vertical accretion via vegetative growth. *Estuar. Coast. Shelf Sci.* doi:10.1016/j.ecss.2006.05.041.

O'Donnell, J., Schalles, J., O'Donnell, J. P. R., and Schalles, J. F. (2016). Examination of Abiotic Drivers and Their Influence on Spartina alterniflora Biomass over a Twenty-Eight Year Period Using Landsat 5 TM Satellite

Imagery of the Central Georgia Coast. *Remote Sens.* 8, 477. doi:10.3390/rs8060477.

Ogburn, M. B., and Alber, M. (2006). An investigation of salt marsh dieback in Georgia using field transplants. *Estuaries and Coasts* 29, 54–62. doi:10.1007/BF02784698.

Osland, M. J., Enwright, N. M., Day, R. H., Gabler, C. A., Stagg, C. L., and Grace, J. B. (2016). Beyond just sea-level rise: considering macroclimatic drivers within coastal wetland vulnerability assessments to climate change. *Glob. Chang. Biol.* 22, 1–11. doi:10.1111/gcb.13084.

Ouyang, Z.-T., Gao, Y., Xie, X., Guo, H.-Q., Zhang, T.-T., and Zhao, B. (2013). Spectral Discrimination of the Invasive Plant Spartina alterniflora at Multiple Phenological Stages in a Saltmarsh Wetland. *PLoS One* 8, e67315. doi:10.1371/journal.pone.0067315.

Palmer, W. C. (1965). *Meteorological drought*. doi:10.1111/j.1467-9523.2006.00307.x.

Paya, A. M., Silverberg, J. L., Padgett, J., and Bauerle, T. L. (2015). X-ray computed tomography uncovers root–root interactions: Quantifying spatial relationships between interacting root systems in three dimensions. *Front. Plant Sci.* 6. doi:10.3389/fpls.2015.00274.

Pershing, A. J., Alexander, M. A., Hernandez, C. M., Kerr, L. A., Le Bris, A., Mills, K. E., et al. (2015). Slow adaptation in the face of rapid warming leads to collapse of the Gulf of Maine cod fishery. *Science* 350, 809–12. doi:10.1126/science.aac9819.

Planet Team (2018). Planet Application Program Interface: In Space for Life on Earth. *San Fr. CA*. Available at: https://api.planet.com/ [Accessed December 2, 2018].

Planet Team (2019). Planet Imagery Product Specification. *San Fr. CA, USA*., 99. Available at: https://assets.planet.com/docs/combined-imagery-product-spec-final-may-2019.pdf [Accessed May 20, 2019].

Qi, J., Chehbouni, A., Huete, A. R., Kerr, Y. H., and Sorooshian, S. (1994). A Modified Soil Adjusted Vegetation Index. Available at: https://pubag.nal.usda.gov/download/50306/PDF [Accessed May 9, 2019].

R Core Team (2017). R: A Language and Environment for Statistical Computing. *R Found. Stat. Comput.* Available at: https://www.r-project.org/.

Ramsey, E., and Rangoonwala, A. (2005). Leaf Optical Property Changes Associated with the Occurrence of Spartina alterniflora Dieback in Coastal Louisiana Related to Remote Sensing Mapping. *Photogramm. Eng. Remote Sens.* 71, 299–311. doi:10.14358/PERS.71.3.299.

Ramsey, E., Rangoonwala, A., Chi, Z., Jones, C. E., and Bannister, T. (2014). Marsh Dieback, loss, and recovery mapped with satellite optical, airborne polarimetric radar, and field data. *Remote Sens. Environ.* 152, 364–374. doi:10.1016/j.rse.2014.07.002.

Ravit, B., Ehrenfeld, J. G., Häggblom, M. M., and Bartels, M. (2007). The effects of drainage and nitrogen enrichment on Phragmites australis, Spartina alterniflora, and their root-associated microbial communities. *Wetlands* 27,

915–927. doi:10.1672/0277-5212(2007)27[915:TEODAN]2.0.CO;2.

Redfield, A. C. (1972). Development of a New England Salt Marsh. *Ecol. Monogr.* 42, 201–237. doi:10.2307/1942263.

Roujean, J.-L., and Breon, F.-M. (1995). Estimating PAR absorbed by vegetation from bidirectional reflectance measurements. *Remote Sens. Environ.* 51, 375–384. doi:10.1016/0034-4257(94)00114-3.

Rouse, J. W., Hass, R. H., Schell, J. A., and Deering, D. W. (1973). Monitoring vegetation systems in the great plains with ERTS. in *Third Earth Resources Technology Satellite (ERTS) symposium*, 309–317. doi:citeulike-article-id:12009708.

Salvino, R., and Wachsman, Y. (2013). The Economic Impact of the 29576 Zip Code – Murrells Inlet/Garden City Beach, SC; Economic Activity and Marsh Valuation. Available at: http://murrellsinletsc.com/wp-content/uploads/2016/09/MI2020-Economic-Impact.pdf.

Sander, T., Gerke, H. H., and Rogasik, H. (2008). Assessment of Chinese paddy-soil structure using X-ray computed tomography. *Geoderma* 145, 303–314. doi:10.1016/J.GEODERMA.2008.03.024.

Schwing, F. B., Kjerfve, B., and Kjerfve, B. (1980). Longitudinal Characterization of a Tidal Marsh Creek Separating Two Hydrographically Distinct Estuaries. *Estuaries* 3, 236. doi:10.2307/1352078.

Silliman, B. R., and Bertness, M. D. (2002). A trophic cascade regulates salt marsh primary production. *Proc. Natl. Acad. Sci. U. S. A.* 99, 10500–10505.

doi:10.1073/pnas.162366599.

Smith, J. P., and Carullo, M. (2007). Survey of Potential Marsh Dieback Sites in Coastal Massachusetts. Available at: http://www.mass.gov/eea/docs/czm/habitat/marsh-dieback-report.pdf [Accessed August 11, 2016].

South Carolina Department of Natural Resources (2015). Dynamics of the Salt Marsh. Available at: https://www.dnr.sc.gov/marine/pub/seascience/pdf/2015RevisedSaltMarsh.pdf.

South Carolina Department of Natural Resources (2016). South Carolina State Climatology Office. Available at: http://www.dnr.sc.gov/climate/sco/ClimateData/cli_sc_climate.php#temperature [Accessed March 4, 2016].

Sweet, W. V., Kopp, R. E., Weaver, C. P., Obeysekera, J., Horton, R. M., Thieler, E. R., et al. (2017). Global and Regional Sea Level Rise Scenarios for the United States. NOAA Technical Report NOS CO-OPS 083.

Turner, R. E., Howes, B. L., Teal, J. M., Milan, C. S., Swenson, E. M., and Tonerb, D. D. G.- (2009). Salt marshes and eutrophication: An unsustainable outcome. *Limnol. Oceanogr.* 54, 1634–1642. doi:10.4319/lo.2009.54.5.1634.

Tyler, A. C., and Zieman, J. C. Patterns of development in the creekbank region of a barrier island Spartina alterniflora marsh. *Mar. Ecol. Prog. Ser.* 180, 161–177. doi:10.2307/24852099.

USFWS (2015). National Wetlands Inventory. *Wetl. mapper*, 1. Available at: http://www.fws.gov/wetlands/data/mapper.HTML.

Valbuena, R., Hernando, A., Manzanera, J. A., Görgens, E. B., Almeida, D. R. A., Silva, C. A., et al. (2019). Evaluating observed versus predicted forest biomass: R-squared, index of agreement or maximal information coefficient? *Eur. J. Remote Sens.* 52, 1–14. doi:10.1080/22797254.2019.1605624.

Valiela, I., Teal, J. M., and Persson, N. Y. (1976). Production and dynamics of experimentally enriched salt marsh vegetation: Belowground biomass. *Limnol. Oceanogr.* 21, 245–252. doi:10.4319/lo.1976.21.2.0245.

Walters, D. C., and Kirwan, M. L. (2016). Optimal hurricane overwash thickness for maximizing marsh resilience to sea level rise. *Ecol. Evol.* 6, 2948–56. doi:10.1002/ece3.2024.

Wang, C., Lu, Z., and Haithcoat, T. L. (2007). Using Landsat images to detect oak decline in the Mark Twain National Forest, Ozark Highlands. *For. Ecol. Manage.* 240, 70–78. doi:10.1016/j.foreco.2006.12.007.

Wang, J., Liu, Z., Yu, H., and Li, F. (2017). Mapping Spartina alterniflora biomass using LiDAR and hyperspectral data. *Remote Sens.* 9, 1–14. doi:10.3390/rs9060589.

Wang, X., Wang, M., Wang, S., and Wu, Y. (2015). Extraction of vegetation information from visible unmanned aerial vehicle images. *Trans. Chinese Soc. Agric. Eng.* 31, 152–159. doi:10.3969/j.issn.1002-6819.2015.05.022.

Watson, E. B., Oczkowski, A. J., Wigand, C., Hanson, A. R., Davey, E. W., Crosby,

S. C., et al. (2014). Nutrient enrichment and precipitation changes do not enhance resiliency of salt marshes to sea level rise in the Northeastern U.S. *Clim. Change* 125, 501–509. doi:10.1007/s10584-014-1189-x.

Webster, P. J., Holland, G. J., Curry, J. A., Chang, H.-R., Michener, W. K., Blood, E. R., et al. (2005). Changes in Tropical Cyclone Number, Duration, and Intensity in a Warming Environment. *Science (80-.).* 309, 1844–1846. doi:10.1890/1051-0761(1997)007[0770:CCHATS]2.0.CO;2.

White, D. S., and Howes, B. L. (1994). Translocation, Remineralization, and Turnover of Nitrogen in the Roots and Rhizomes of Spartina alterniflora (Gramineae). *Am. J. Bot.* 81, 1225. doi:10.2307/2445397.

Whiting, G. J., and Chanton, J. P. (2001). Greenhouse carbon balance of wetlands: Methane emission versus carbon sequestration. *Tellus, Ser. B Chem. Phys. Meteorol.* 53, 521–528. doi:10.1034/j.1600-0889.2001.530501.x.

Wigand, C., Davey, E., Johnson, R., Sundberg, K., Morris, J., Kenny, P., et al. (2015). Nutrient Effects on Belowground Organic Matter in a Minerogenic Salt Marsh, North Inlet, SC. *Estuaries and Coasts* 38, 1838–1853. doi:10.1007/s12237-014-9937-8.

Willis, D. B., and Straka, T. J. (2017). The Economic Contribution of Natural Resources to a State Economy: A South Carolina Case Study. *Nat. Resour.* 08, 115–129. doi:10.4236/nr.2017.83009.

Willmott, C. J. (1982). Some Comments on the Evaluation of Model Performance. *Bull. Am. Meteorol. Soc.* 63, 1309–1313. doi:10.1175/1520-

0477(1982)063<1309:SCOTEO>2.0.CO;2.

Yebra, M., and Chuvieco, E. (2009). Linking ecological information and radiative transfer models to estimate fuel moisture content in the Mediterranean region of Spain: Solving the ill-posed inverse problem. *Remote Sens. Environ.* 113, 2403–2411. doi:10.1016/J.RSE.2009.07.001.

Zambrano-Bigiarini, M. (2017). hydroGOF: Goodness-of-fit functions for comparison of simulated and observed hydrological time series. doi:10.5281/ZENODO.840087.

APPENDIX A

PYTHON CODE FOR THE MARSH EQUILIBRIUM MODEL

```
#gdal needs to be installed on the computer
import time
import os
import subprocess
import gdal
import rasterio
import numpy as np

os.chdir(r"E:\Gwen\CISA\Beaufort\HUC11_3m")
outputDirectory = 'DEM2\extend'
#make a folder in the current directory called output if the folder doesnt already exist
if not os.path.exists(outputDirectory) : os.makedirs(outputDirectory)
#Variables
gDEM = "DEMZone2.tif" #elevation in meters relative to navd88
#Mean sea level at 2.230 m (local datum) Fort Pulaski, GA
#nadv88 2.301 relative to station
#Calculated the MSL and range based on the average in the area
MSL = -0.004757 #in meters in relation to nad88
AmpM = 2.34231/2 #tidal amplitude in meters
MHW = 1.166398 #relative to navd88
MHWcm = MHW * 100  #cm
MLW = -1.1759119 #relative to NAD88
MLWcm = MLW *100  #cm
MinE = MSL- 0.10 #minimum elevation in m
MaxE = MHW + 0.3 # max elevation in m
fE = MaxE + 1  #representing the maximum elevation needed for model simulation, was
calculated as the maximum vegetated elevation plus the total SLR
Trange = MHWcm - MLWcm #Tidal Range
gSLR = 100 #global SLR in cm
Amp= Trange/2  #tidal amplitude
T = 100 #time to run model in years
A = 0.317 #local rate of SLR in cm/yr (Fort Pulaski Georgia Tide Gauge)
sB = (gSLR - A*T)/T**2 #accelerating term for SLR
aa =2224.70489470017*0.0001 #biomass coefficient (changing to cm if mult by 0.0001)
ab =-2268.55839707401*0.0001#biomass coefficient
ac =854.575218904821*0.0001 #biomass coefficient
q = 2.8 # g/g  #proportional to the rate of sediment loading (trapping efficiency)
```

```
kr = 0.1 # g/g  refractory fraction of OM
#Calculated suspended sediment based on average in area
m= 31.8698e-6 #suspended sediment concentration g/cm3
f = 704 #the frequency of semi-diurnal tides per year
k1 = 0.085 #pure organic g/cm3 packing density
k2 = 1.99 #pure inorganic g/cm3
BGTR = 1 #belowground turnover rate
RSR = 2 #root-shoot ratio
outtime = 100 #years
t_int = 1

#Dictionaries

def PlatDepth(Zr, yslr, Output_File):
   #Open raster in both gdal and rasterio
   raster= rasterio.open(Zr)
   raster1= gdal.Open(Zr)
   #Create empty array with same shape as input raster, file1, and fill with 0s
   Array= np.zeros(shape=(raster.height, raster.width))
   #For each pixel, if pixel has a value, apply depth eq

   x=0
   for line in raster.read(1):
      List=list()
      #ListB=list()
                  #first find NA pixels or pixels than the min elevation for alterniflora.
Then find pixels suitable for alterniflora growth
      for pixel in line:
         if str(pixel)== "-32768":
            List.append("-9999")
            #ListB.append("-9999")
         elif str(pixel)== "-3.40282e+38":
            List.append("-9999")
            #ListB.append("-9999")
         elif str(pixel)== "-9999":
            List.append("-9999")
            #ListB.append("-9999")
         elif pixel > fE:
            List.append("-9999")
            #ListB.append("-9999")
         elif pixel <= MinE:
            ZZ = float(pixel)
            Z =  ZZ*100 #change units to centimeters
            ZZamp = AmpM-ZZ #meters
            Zamp  = Amp - Z #cm
            D = min(1, ((MHWcm) - Z)/Trange) #Dimensionless depth in cm values
between 0 and 1
```

```
            D = max(0, D)
            absD = round(max(MHWcm - Z, 0), 2)  #use this when using elevation relative
to MSL
            #B = (aa*Z + ab*Z**2 + ac)
            B = 0 #g/m2 to g/cm2
            DEDT = 0    #    #v5.4=(q*m*f*(Dreal/2) + kr*B)*(LOI/k1+(1-LOI)/k2)
            #print DEDT
            #Forcing elevation into meters
            Z = (Z + ((DEDT*10)- yslr))
            ZZZ = Z/100              #put elevation output back into meters
            List.append(ZZZ) #append the depth into the list
          elif pixel > MinE:
            ZZ = float(pixel)
            Z =  ZZ*100 #change units to centimeters
            ZZamp = AmpM-ZZ #meters
            Zamp  = Amp - Z #cm
            D = min(1, ((MHWcm) - Z)/Trange) #Dimensionless depth in cm values
between 0 and 1
            D = max(0, D)
            absD = round(max(MHWcm - Z, 0), 2)  #use this when using elevation relative
to MSL
            B = max((aa*Zamp + ab*Zamp**2 + ac), 0)*0.0001 #g/m2 to g/cm2  # when
using elevation to calculate biomass convert g/m2 to g/cm2
            DEDT = (((1/k2)*(q*m*f*absD*0.5*D))+((1/k1)*(kr*RSR*BGTR*B)))     #
            Z = (Z + ((DEDT*10)- yslr))
            ZZZ = Z/100              #put elevation output back into meters
            List.append(ZZZ) #append the depth into the list
        Array[x]=List
        x=x+1
#make arrays and then multiply or subtract the arrays. Then create a final array
    #Once equation is applied, create new raster
    array_to_raster(Array, Output_File, raster, raster1)
    raster = None
    raster1 = None

#########################
#Create raster from array
#########################

def array_to_raster(array, Output_file, raster, raster1):
    dst_filename = Output_file

    #Get values
    #Number of rows. In this case I'm taking the information from my input raster.
    x_pixels = raster.width
    #Number of columns. Also taking the information from my input raster.
    y_pixels = raster.height
```

```
    #Size of the pixels, pretty sure the default unit is meters. Also taking this info from
input raster.
    PIXEL_SIZE = raster1.GetGeoTransform()[1]
    #x_min and y_max are the longitude and latitude values of the top left corner of the
image. The "GetGeoTransform" tool gets longitude and latitude
    #information for each corner of the image.
    x_min = raster1.GetGeoTransform()[0]
    y_max = raster1.GetGeoTransform()[3]
    #This is the projection information. WKT stands for "Well-known text". If you input
the projection manually you need the WKT name for the projection.
    wkt_projection = raster1.GetProjection()

    #This is the type of output file you want. Probably always going to be geotiff.
    driver = gdal.GetDriverByName('GTiff')

    #This is setting the variable "dataset" to the driver.Create command, which creates
new rasters based on your input info.
    dataset = driver.Create(
        dst_filename,
        x_pixels,
        y_pixels,
        1,
        gdal.GDT_Float32, )

    #Setting the pixel size in the output raster.
    dataset.SetGeoTransform((
        x_min,    # 0
        PIXEL_SIZE,  # 1
        0,                  # 2
        y_max,    # 3
        0,                  # 4
        -PIXEL_SIZE))

    #This sets the projection info for the output raster.
    dataset.SetProjection(wkt_projection)
   #set no data value
    NoData_value = -9999
    dataset.GetRasterBand(1).WriteArray(array)
    dataset.FlushCache()  # Write to disk.
    return dataset, dataset.GetRasterBand(1)
    #assign no data value
    dataset.SetNoDataValue(NoData_value)

#Setting sea levels
SL = range(0, T+1)
#SL[0]=A#Sea level at time 0 is referenced to the current 0cm, not 0.32cm above it as sea
level has not risen yet. This happens in year 1
```

```
for i in range(0, T+1):
   SL[i] = A*i + sB * i**2
ySLR = range(0, T+1)
for i in range(1, T+1):
   ySLR[i] = round(SL[i] - SL[i - 1],5)
print ("sea levels finished")

namel = list()
namel.append(gDEM)
#namel.append('year_0.tif')

#create output names for files
xx=0
for i in range(t_int, T+t_int, t_int):
   name_i = str(i)
   dem_input = namel[xx]
   outputFileName = outputDirectory + '\\' + 'year_' + name_i + '.tif'
   #outputFileName2 = outputDirectory + '\\' + 'year_' + 'D' + '.tif'
   PlatDepth(dem_input, ySLR[i], outputFileName)
   print (name_i)
   namel.append(outputFileName)
   xx=xx+1
```

APPENDIX B

COPYRIGHT PERMISSION

Chapter 5

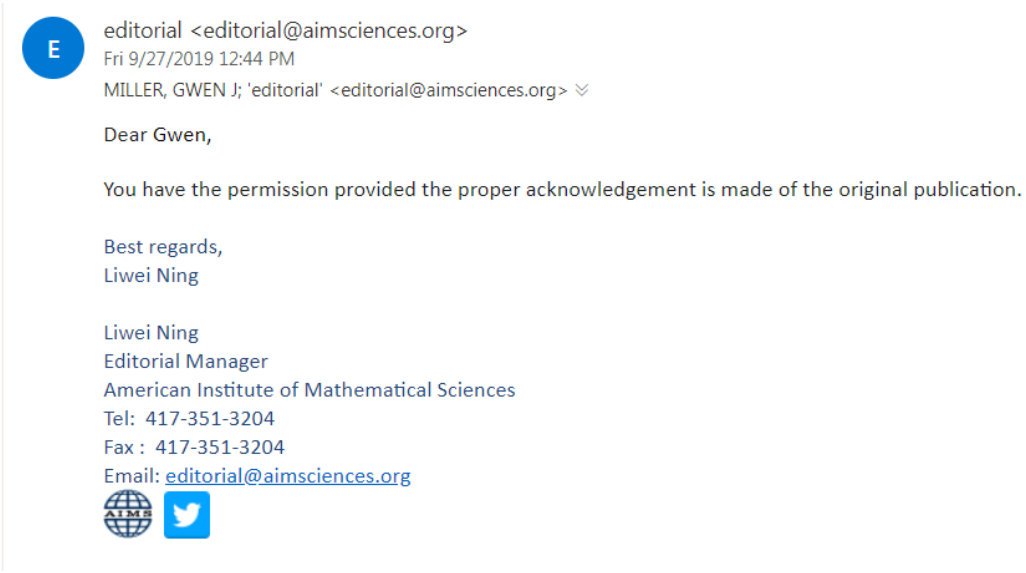

editorial <editorial@aimsciences.org>
Fri 9/27/2019 12:44 PM
MILLER, GWEN J; 'editorial' <editorial@aimsciences.org>

Dear Gwen,

You have the permission provided the proper acknowledgement is made of the original publication.

Best regards,
Liwei Ning

Liwei Ning
Editorial Manager
American Institute of Mathematical Sciences
Tel: 417-351-3204
Fax : 417-351-3204
Email: editorial@aimsciences.org

Chapter 3

MDPI Open Access Information and Policy

All articles published by MDPI are made immediately available worldwide under an open access license. This means:

- everyone has free and unlimited access to the full-text of *all* articles published in MDPI journals;
- everyone is free to re-use the published material if proper accreditation/citation of the original publication is given;
- open access publication is supported by the authors' institutes or research funding agencies by payment of a comparatively low **Article Processing Charge (APC)** for accepted articles.

External Open Access Resources

MDPI is a RoMEO **green publisher** — RoMEO is a database of Publishers' copyright and self-archiving policies hosted by the **University of Nottingham**

Those who are new to the concept of open access might find the following websites or 'Open Access 101' video informative:

Wikipedia article on 'Open Access'
Peter Suber's 'Open Access Overview'
Information Platform Open Access [in **English**, in **German**]
SHERPA's 'Authors and Open Access'

Meaning of Open Access

In accordance with major definitions of open access in scientific literature (namely the Budapest, Berlin, and Bethesda declarations), MDPI defines *open access* by the following conditions:

- peer-reviewed literature is freely available without subscription or price barriers,
- literature is immediately released in open access format (no embargo period), and
- published material can be re-used without obtaining permission as long as a correct citation to the original publication is given.

Open Access Explained!

Until 2008, most articles published by MDPI contained the note: "© *year* by MDPI (http://www.mdpi.org). Reproduction is permitted for noncommercial purposes". During 2008, MDPI journals started to publish articles under the **Creative Commons Attribution License** and are now using the latest version of the CC BY license, which grants authors the most extensive rights. All articles published by MDPI before and during 2008 should now be considered as having been released under the post-2008 Creative Commons Attribution License.

This means that all articles published in MDPI journals, including data, graphics, and supplements, can be linked from external sources, scanned by search engines, re-used by text mining applications or websites, blogs, *etc.* free of charge under the sole condition of proper accreditation of the source and original publisher. MDPI believes that open access publishing fosters the exchange of research results amongst scientists from different disciplines, thus facilitating interdisciplinary research. Open access publishing also provides access to research results to researchers worldwide, including those from developing countries, and to an interested general public. Although MDPI publishes all of its journals under the open access model, we believe that open access is an enriching part of the scholarly communication process that can and should co-exist with other forms of communication and publication, such as society-based publishing and conferencing activities.